2-p (MIX)

[redacted]

ELECTRO-OPTICAL SYSTEMS

A XEROX COMPANY

PASADENA, CALIFORNIA 91107 · 213/351-2351

Reproduced by
NATIONAL TECHNICAL
INFORMATION SERVICE
Springfield, Va. 22151

FACILITY FORM 602

N71-25965 (ACCESSION NUMBER)	(THRU)
185 (PAGES)	G3 (CODE)
CR-118632 (NASA CR OR TMX OR AD NUMBER)	30 (CATEGORY)

RECEIVED
JUN 1971
NASA STI FACILITY
INPUT BRANCH

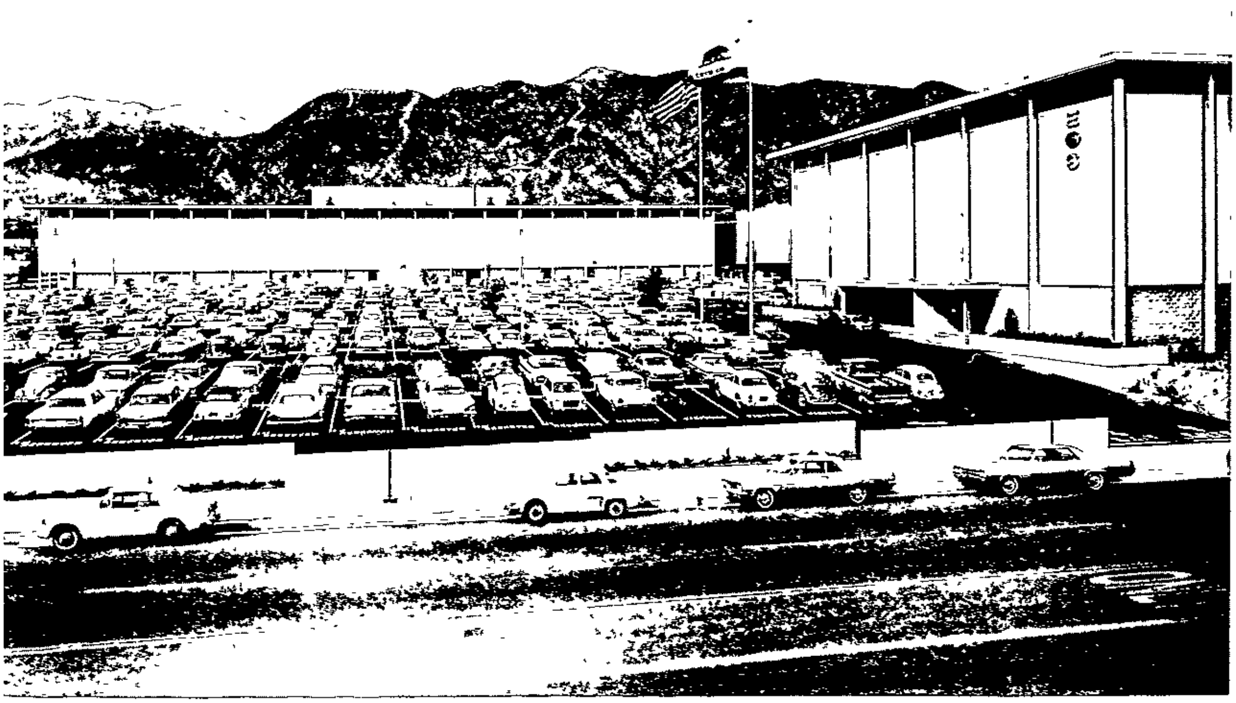

7003-Final

FINAL REPORT

FOR

THE REFLECTOMETER EXPERIMENT

FOR

APPLICATION TECHNOLOGY SATELLITE

PHASE II

1 JANUARY 1971

CONTRACT NO: NAS5-9669

PREPARED BY

ELECTRO-OPTICAL SYSTEMS
PASADENA, CALIFORNIA

FOR

GODDARD SPACE FLIGHT CENTER
GREENBELT, MARYLAND

7003-Final

FINAL REPORT

FOR

THE REFLECTOMETER EXPERIMENT

FOR

APPLICATION TECHNOLOGY SATELLITE

PHASE II

1 JANUARY 1971

CONTRACT NO: NAS5-9669

PREPARED BY

ELECTRO-OPTICAL SYSTEMS
PASADENA, CALIFORNIA

FOR

GODDARD SPACE FLIGHT CENTER
GREENBELT, MARYLAND

SUMMARY

This report contains a description of the reflectometer instrument, the measurement techniques involved in determining the sample degradation, and reduced flight data obtained during the period of operation.

Reflective surface degradation data gathered from 18 test samples flown on the Applications Technology Satellite (ATS-3) are presented. The reflectometer instrument measured specular sample reflectivity in four spectral bands plus one broadband. The measurements covered a spectral range of 0.3 to 3 microns.

The primary objective of this instrument was to test, in actual space environment, the durability of selected specularly reflective surface materials in order to obtain directly applicable data for use in equipment design. A secondary aim of the experiment was to obtain data of scientific value relating to the degradation process.

TABLE OF CONTENTS

TABLE OF CONTENTS (contd)

LIST OF ILLUSTRATIONS

LIST OF ILLUSTRATIONS (contd)

LIST OF TABLES

SECTION 1

EXPERIMENT OBJECTIVES

The objective of this experiment was to test in space, for an extended period, the durability of specularly reflective surface materials. The experiment was designed primarily for obtaining engineering data necessary for the design of solar energy converters, optical communications systems, spacecraft thermal coatings, and other reflective optical instruments or systems. The data obtained from this experiment is directly and immediately applicable for use in designing or evaluating such items.

A secondary objective of the experiment was to obtain data of scientific value relating to the causes of the degradation process. This objective was pursued only to the extent that the primary objective was not compromised. To this end, no direct systematic measurement of the environment was performed.

1.1 HISTORY

The present reflectometer contract represents a continuation of work performed under the following three NASA contracts.

1.1.1 STUDY OF A FLIGHT EXPERIMENT OF SOLAR-CONCENTRATOR REFLECTIVE SURFACES (NAS1-2880)

This contract was comprised of a study program to define a flight experiment for determining the effects of the space environment on the performance of solar concentrator reflective surfaces. The program included definition of the factors in space that will affect concentrator surfaces, the selection of concentrator surface samples for evaluation, and the analysis and prediction of the effects of various space environmental factors on concentrator surfaces. The program included consideration of the simulation of the space environment in ground tests. The main portion of the program consisted of the design of two satellite systems for testing concentrator samples in space, including consideration of launch vehicles, orbits, on-board power, telemetry, command, and attitude control. The basic concept of the rotating arm reflectometer was originated in this program.

1.1.2 EVALUATION OF CRITICAL FACTORS RELATED TO A FLIGHT EXPERIMENT FOR REFLECTIVE SURFACE SAMPLES (NAS1-2850)

This follow-on program consisted of three basic task items:

a. Design and fabrication of a breadboard model of the reflectometer system
b. Analytical study of bearings and seals in the space environment
c. Study of separation of effects

The reflectometer breadboard built under this program demonstrated the validity of the rotating arm approach. The breadboard included two light sources: a tungsten lamp and a virtual image solar source. Some difficulties were encountered with the solar source; however, the tungsten lamp source performed satisfactorily. The task items b and c also demonstrated the basic validity of the flight experiment approach conceived in the previous program.

1.1.3 DESIGN, DEVELOPMENT, AND FABRICATION OF A SECOND-GENERATION PROTOTYPE REFLECTOMETER FOR A SPACE EXPERIMENT FOR RELATIVE SURFACE SAMPLES (NAS1-4660)

This program included the design, fabrication, and evaluation of an improved reflectometer system. The second-generation reflectometer breadboard was similar to that built under the previous program except for the following particulars:

a. The optical system design was modified to minimize the effects of sample misalignment and lack of flatness.
b. The system was modified to use a-c (chopped) light to minimize the effect of stray light in the system.

The program also included a detailed experimental study of bearings and seals.

1.2 SPACE ENVIRONMENTAL FACTORS

The mechanisms by which reflective surfaces are degraded in space are reasonably easy to define in general terms. They involve such things as micrometeroids causing pitting, erosion, and roughening of the surface; charged particles causing surface sputtering; ultraviolet radiation causing degradation of dielectric coatings; temperature effects causing structural stress and changes in material properties; and vacuum causing evaporation of surface material. The difficulty in estimating specular reflectance loss stems from the following conditions:

a. The mechanism and environmental influences which could cause reflectance loss are only understood hypothetically.
b. Flux levels of possible degrading factors in space have generally not been determined directly but have only been estimated by extrapolation of other measurements.
c. Because of the uncertainties in degrading mechanisms and the character of the space environment, it has not been practical to simulate reflective surface degradation in the laboratory.

As an example of the unknowns in this area, consider the problem of reflective surface degradation caused by micrometeroids. Most of the space measurements made to date have been concerned with the penetration of pressure vessels, such as space power system radiators and pressurized space vehicles, by the larger particles. Therefore, most of the micrometeoroid instrumentation has been designed to detect encounters with these larger particles. The problem with reflective surfaces, however, is not penetration but the gradual erosion and roughening of the surface layer by small particles which cause no structural damage. In extreme cases, the entire reflective surface coating could be worn away exposing the reflective substrate material. The effect is particularly pronounced for samples having interference-type surface coatings which are especially sensitive to thickness changes.

Many attempts have been made to simulate certain of the space environmental factors on the ground. The difficulty is both in knowing what to simulate and in providing an adequate simulation of suspected factors. The micrometeoroid problem again provides a convenient example. The suspected conditions in space involve large flux levels of micron-sized particles moving at speeds of 20 to 70 kilometers per second relative to the spacecraft surface. In the laboratory, it has not been possible to match these conditions simultaneously. Obtainable velocities are much lower. Consequently, the same kinetic energy per particle can only be achieved using larger particles. However, the effect of slow-moving large particles is probably not the same as rapidly-moving small particles having the same kinetic energy. The way in which these parameters should be scaled to simulate the overall effect in space is the subject of controversy and has not yet been adequately solved.

Much the same sort of argument applies to the other suspected degrading influences in space. An area of uncertainty even greater than that associated with the individual effects of these factors, however, is their combined effect. All these uncertainties taken together weighed heavily in favor of a direct measure of reflectance degradation in space.

1.3 REFLECTIVE SURFACE APPLICATIONS

The use of reflective surfaces in space has been limited by the unknown degradation effects of the space environment on the reflective surfaces plus the structural problems involved in building and maintaining a large, stable, lightweight base for the reflective surface. Some of the major applications of reflective surfaces in space are in areas such as solar energy conversion; optical communications systems; optical instruments; space telescopes; and surface thermal control.

The use of solar energy in space is at the present time primarily limited to direct conversion of solar energy to electrical energy using large solar panel arrays to provide enough energy to operate a space vehicle. With the advent of larger and more complicated space vehicles as well as space-based systems the use of solar panels may become less desirable.

The use of solar concentrators in conjunction with thermal to electrical energy converters provides another form of solar to electrical energy conversion. This type of system would be capable of providing another "free" source of usable energy under space conditions.

Optical communications is another rapidly growing area of interest. Experiments have been performed in laser beam communication which indicate that this type of communication may become very important as a method of communicating in space. This would require the use of optical collectors to be used in the space environment. The information gained from the reflectometer experiment has provided a basis for selection of space-qualified reflective surfaces for this purpose as well as others.

SECTION 2

EXPERIMENT DESIGN

2.1 MEASUREMENT METHOD

Through the development programs preceding the building of flight hardware, many of the presently used concepts were devised, such as the use of the rotating scanner arm and the use of the incandescent tungsten lamp as a light source. In general the instrument operates in the following manner:

The samples to be measured and the reference samples are mounted in a circular array (figure 1). An arm pivoted at the center of the array rotates above the samples, scanning each one in turn. The arm projects a beam of light from a tungsten lamp onto the samples being tested and receives the reflected portion of the light. The reflected light passes through the arm down into the body of the reflectometer to the detectors and electronics.

Within the instrument the return beam is spectrally analyzed by a low resolution spectrometer. The spectrometer is an integrating sphere using filters and detector response bands to provide spectral resolution. The spectrometer analyzes the return radiation in each of four spectral bands, 0.3 to 0.4 micron, 0.3 to 0.65 micron, 0.65 to 1.2 microns and 1.2 to 3.0 microns plus one broad band covering approximately 0.3 to 3.0 microns. Two lead sulfide detectors, one silicon detector, and two photomultiplier (PM) tubes are used to detect the various spectral bands. The detector outputs are amplified and delivered to the spacecraft telemetry as analog signals.

76719

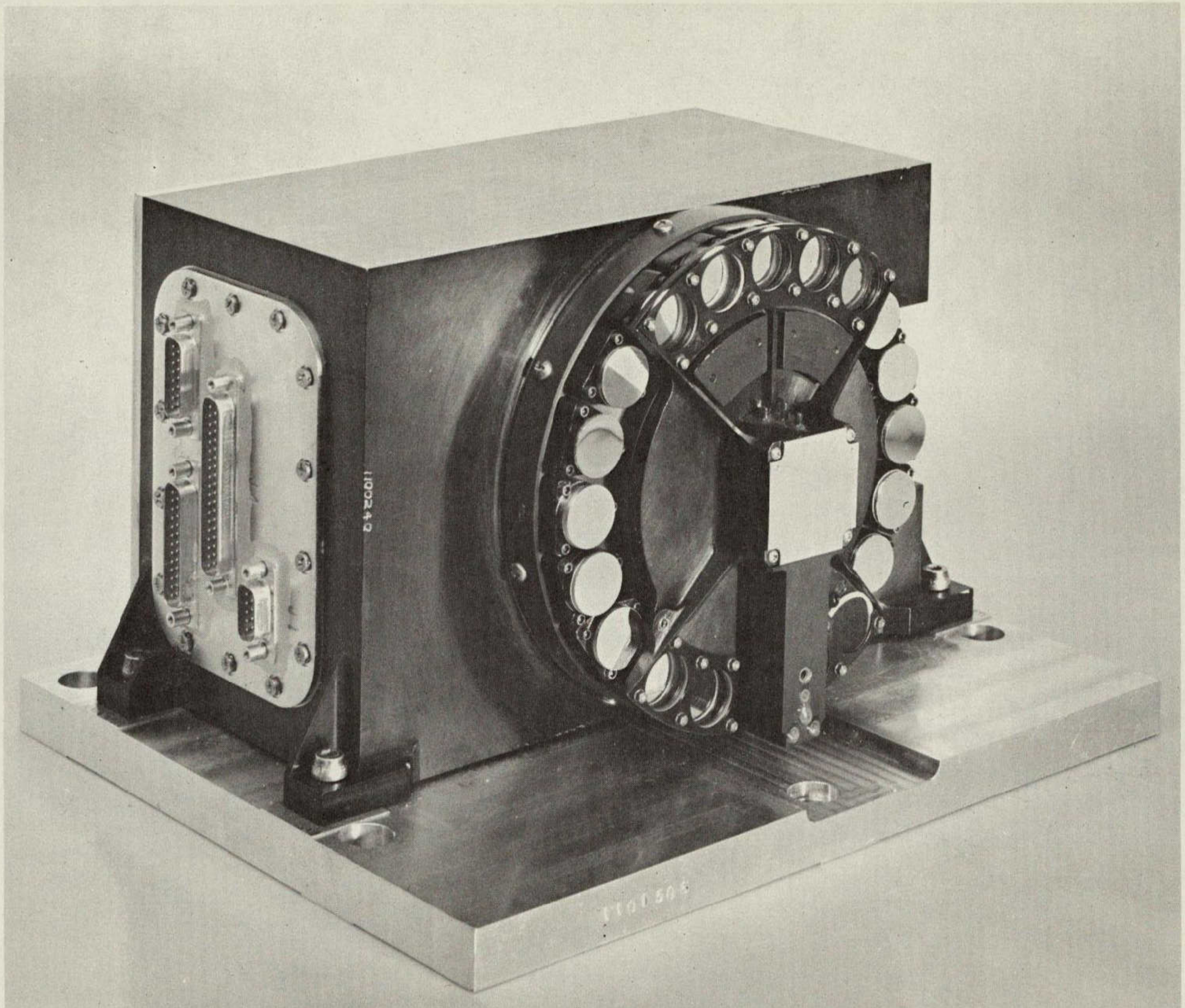

Figure 1. Reflectometer Instrument

2.2 SEPARATION OF EFFECTS

Degradation of the reflective samples in the space environment may occur from a variety of causes. The primary causes of degradation which have been identified include micrometeorite bombardment, ultraviolet radiation, and bombardment by energetic particles.

While degradation of reflectance caused by the gross environment is the basic question, still more information is available from the experiment by separating the degradation effects. This allows extrapolation of the data to calculate expected degradation under other environmental conditions such as different orbits or space locations. This also aids in the design of better reflective surfaces by identifying the most potent degradation factors.

Complete separation of causes is implausible in a spaceborne experiment of manageable complexity and duration. Nevertheless, considerable additional information can be obtained by shielding some of the samples from some of the environmental effects. In orbit the arm was stationary except when measurements were actually being made and was "stationed" over the 100 percent reference sample. A solid metal shield was mounted on a shield assembly above the zero percent sample, and fused silica shields were mounted on the shield assembly above other selected samples in such a way as to protect them from particle bombardment. The fused silica shields were transparent to much of the ultraviolet as well as the visible and infrared portions of the spectrum. Protecting these samples from particle bombardment provided at least partial separation of the degradation effects.

The shield assembly was an integral part of the rotating arm assembly As a result, the shielded samples were exposed to all space environments during rotation of the arm assembly, but only for a short period of time.

2.3 TEST SAMPLE SELECTION

Because of the limited number of surfaces which could be flown on an instrument of this nature, considerable effort was devoted to the selection of the sample materials. The materials selected were the result of discussions between NASA personnel, private industrial researchers and ATS program management personnel. The selection of the samples (see Table 1) was based on their expected ability to withstand the degradation effects encountered in the space environment.

The samples are circular discs 0.75 inch in diameter. These discs were mounted in a circular array around the outward looking face of the reflectometer. The reflective surfaces vary from materials which are plated directly on a substrate material to reflective materials which are bonded to the substrate material with no plating process involved. Each test sample substrate was bonded to a sample mount which, in turn, was bolted to the outward looking face of the reflectometer and aligned to provide the proper optical path.

2.4 ALIGNMENT REQUIREMENTS

It was critical that the entire optical portion of the reflectometer be properly aligned and continue to remain aligned throughout the mission. The arm mirrors, test samples, beam splitter, lamps, integrating sphere mirror and diagonal mirror were aligned through use of a Penn optical bench. This alignment equipment consisted of a microscope adjustable along three axes, two optical rails with a pulley for moving the equipment under test, and a holding fixture.

It was also important for the test samples to be properly aligned. A sample misaligned by more than ±1 degree could cause the reflected beam to follow an improper optical path and could result in a vignetted light beam when passed through the lenses, and an improperly placed beam at the spectrometer.

2.5 SPACECRAFT CONSIDERATIONS

The reflectometer was designed so that it imposed little demand on the spacecraft systems. At the same time, the reflectometer was not greatly affected by spacecraft parameters.

The use of the reflectometer on a spinning vehicle did not detract from the value of the experiment. The only effect of the spinning vehicle was to reduce exposure of the samples to sun light. It was calculated that the solar exposure would be 24 percent of that of a solar-oriented concentrator. Degradation on the order of 3 to 10 percent in 2 months have been obtained from measurements and estimates of ultraviolet-produced degradation. An equivalent exposure would be obtained on the ATS vehicle in approximately 8 months.

It should be emphasized that the experiment was designed and built to utilize the full 3-year lifetime of the spacecraft with a minimum life time of one year. The actual experimental lifetime was slightly over two years with portions of the instrument remaining operational into and probably through the third year.

SECTION 3

INSTRUMENT DESIGN AND PERFORMANCE

The reflectometer was designed to operate in the following manner:

A command from the ground turned on the spacecraft voltage regulator. Since stable voltages were necessary for proper operation of the detectors and PM tubes, a warm-up period was required to permit stabilization of the dc-to-dc converters. Following this period and prior to operation of the drive motor, telemetry was activated to verify scanner arm position and critical temperature and voltage parameters.

The lamp and the drive motor were then turned on, in that order, by separate ground commands. For approximately 8 minutes the scanner arm rotated, scanning each of the 20 samples in turn.

The scanner arm guided a beam of light from a tungsten lamp onto the sample being tested. The portion of the light that was reflected returned through the arm to the detectors. This return beam was analyzed by a low resolution spectrometer which analyzed the beam in each of four spectral bands and one broad band. Throughout the period of operation, critical system parameters were also being monitored

At the completion of a revolution, the scanner arm rotation automatically stopped.. A ground command was then sent to turn off the spacecraft voltage regulator and thus remove power from the reflectometer.

3.1 OPTICAL SUBSYSTEM

The Reflectometer optical subsystem operates as follows: (Refer to figure 2 for a schematic representation of the subsystem.)

Radiant energy from one of two redundant incandescent tungsten lamps was passed through or reflected from (depending upon the lamp used) a mechanical chopper rotating nominally at 2400 rpm. The light beam which passed the chopper to the beam splitter was limited by an aperture stop to 0.2 inch. Thirty percent of the light beam was then transmitted into the telecentric optical system. The remaining light was reflected out of the system.

The optical path from the beam splitter lens to the reflectometer sample consisted of two 1.2-inch-diameter lens elements and two mirrors. The two mirrors were located in the rotating arm and were used to focus the light onto the sample surface. The sample reflected a portion of the light back along the same path to the beam splitter. The amount of reflected light depended, of course, on the properties of the reflective sample.

Approximately thirty percent of the reflected light from the sample passed through the beam splitter and into an integrating sphere spectrometer. Two lead sulfide photodetectors, two PM tubes, and one silicon photodetector were mounted at apertures on the integrating sphere.

By using filters and the inherent spectral cutoff limits of the detecting devices the reflected light was spectrally detected. The spectrum from 0.3 to 0.65 micron was detected by two PM tubes (0.3 to 0.4 micron and 0.3 to 0.65 micron). The 0.65 to 1.2 micron spectral area was detected by the silicon detector. The lead sulfide detectors were used for the 1.2 to 3.0 micron portion of the spectrum and for the broadband spectrum.

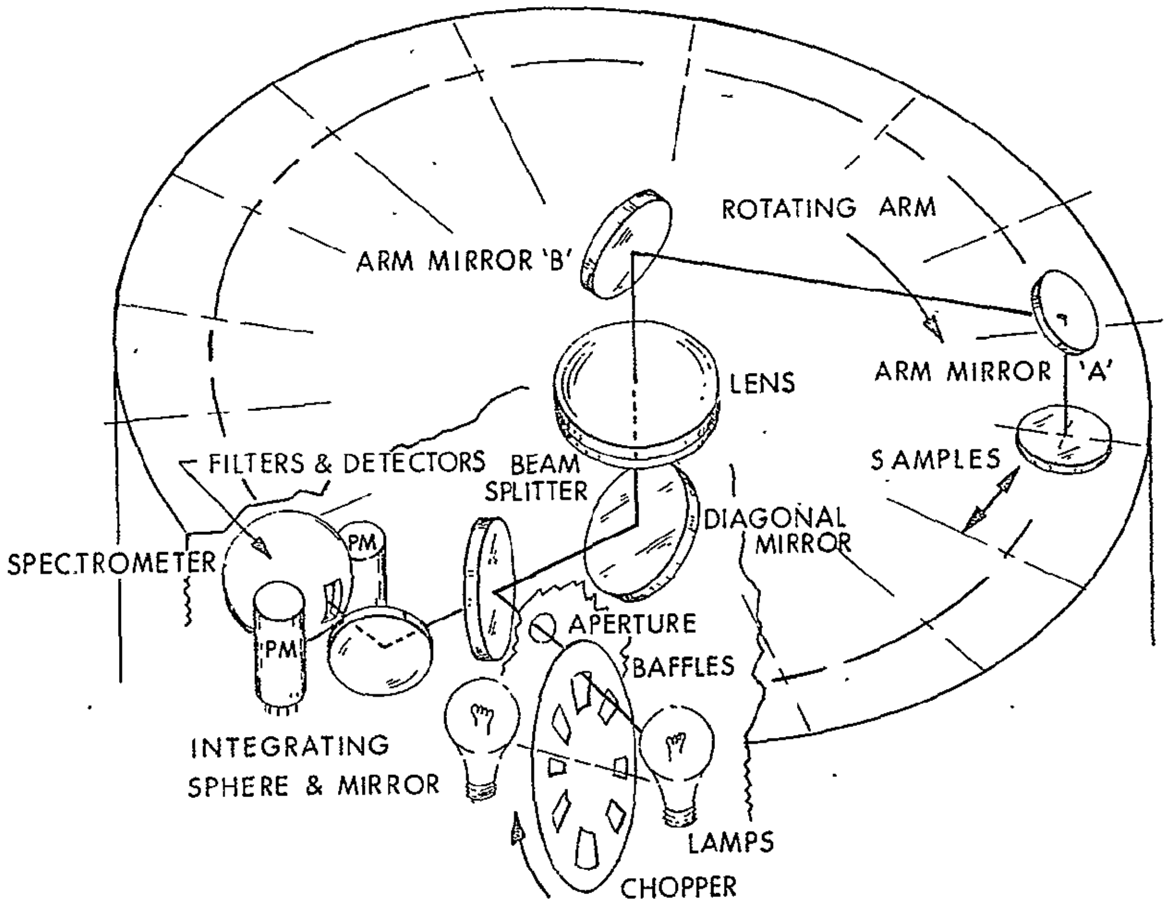

Figure 2. Reflectometer Optical Schematic

73628659

The experiment included 20 samples: 10 unshielded, 8 shielded with quartz inserts, and 2 shielded reference samples (one full scale and one zero). To determine the cause of surface deterioration on the samples, all but two test samples were mounted in matched pairs, one of which was unshielded while the other was shielded by a clear quartz shield (except during arm rotation). The two unmatched test samples were continuously exposed to the space environment. The quartz shield blocked passage of all micrometeorites and most charged particles, but permitted passage of ultraviolet radiation. The unshielded sample of each pair was exposed to all elements of the space environment. The reference samples (full scale and zero percent) were continuously shielded except during arm rotation.

The rotating arm, which contained two mirrors to direct the light beam to the sample under test was rotated at a rate of about 1/8 revolution per minute. During one revolution all 20 reflective surfaces were observed. The reflectometer data rate was slow compared to the telemetry rate and was completely independent of the spacecraft spin rate. Thus, synchanization of the arm rotation with the rate of the spacecraft telemetry system or the spin rate was not necessary.

3.1.1 LIGHT SOURCE

The desirable properties of a light source for use in the reflectometer could be stated in fairly broad terms. The source should have relatively uniform output in the spectral region of interest, sufficient output to allow the use of simple detectors and amplifiers, long life, good efficiency, simple operating procedures, and stable output in all respects. There are few sources that satisfy the above requirements. Even fewer are suitable for prolonged, unattended operation in a hostile environment.

It would be most desirable to use the sun as the light source, however this could only be done by maintaining the reflectometer in a fixed and predetermined orientation relative to the sun or by using a servo-controlled tracker. The former was not practical because of satellite attitude considerations and the latter approach was unattractive because of complexity and potentially poor reliability.

Considering all factors, the incandescent tungsten filament lamp was considered the most suitable source. Other possible selections such as fluorescent, luminescent or arc types have poor spectral output, short life or difficult starting characteristics. The incandescent tungsten lamp, however, has reasonable efficiency and brightness and is easily operated. With conservative design and application, the tungsten lamp can also have a long lifetime. The life of a tungsten lamp is proportional to the inverse of the 13th power of the applied voltage while the power output, in the area of interest to this experiment, is proportional to the 1.5 power of the applied voltage. The major disadvantage of a tungsten source is its relatively low output in the spectral regions below 0.4 micron. Figure 3 illustrates this point. Also, tungsten does not radiate as a blackbody. The output is relatively high in the visible portion of the spectrum because of increasing emissivity at the shorter wavelengths.

Because of the above considerations, a tungsten filament lamp was selected for the light source. The specific lamp that was selected was a Chicago Miniature Lamp, part number CM8-1626, a special version of the CM8-903. Several other lamp types were considered before the CM8-1626 was selected.

The spectral range of the experiment was limited by the power spectrum of the light source used for measurements. The tungsten lamp, operating below rated voltage, was a tradeoff between reliability, lamp lifetime

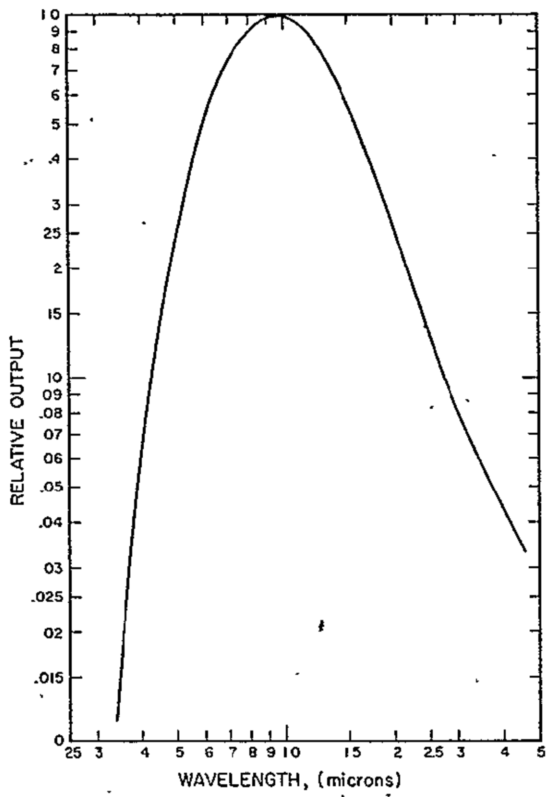

Figure 3. Relative Output of Tungsten at 2800°K as a Function of Wavelength

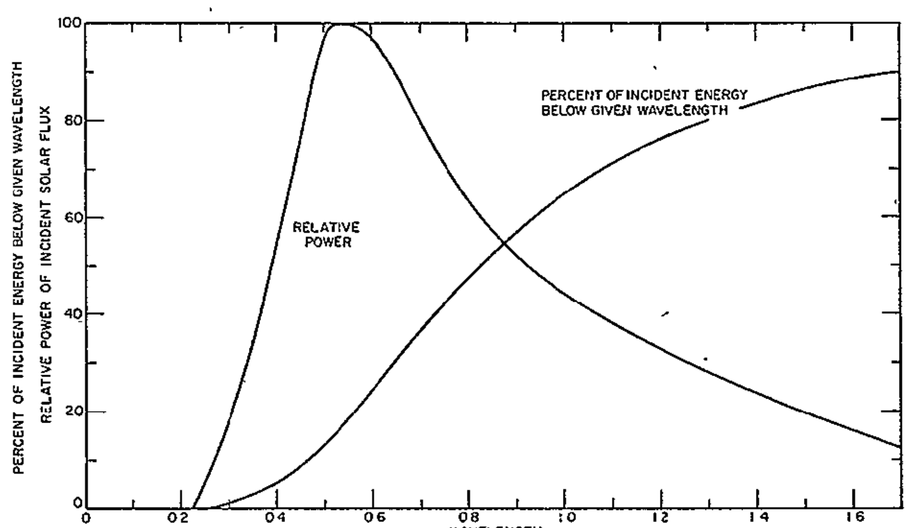

Figure 4. Solar Spectrum

and the desired lamp response in the ultraviolet region. The consequence of low output below 0.4 and above 3 microns is not especially great, since approximately 85 percent of the solar energy falls in this region. The integrated distribution of solar energy is illustrated in figure 4.

Figure 5 represents the electromagnetic spectrum of the tungsten lamp in relation to the solar spectrum. As illustrated, an incandescent tungsten filament lamp provides a satisfactory spectral range. Approximately 98 percent of the solar energy is found within the range of 0.3 to 3 microns. The solar spectrum extends somewhat beyond that of a tungsten lamp operating at 2800°K.

At the lower end of the spectrum, 9 percent of the solar energy is below 0.4 micron and 1.2 percent of the energy is below 0.3 micron. The tungsten lamp exhibits less than 0.08 percent of its total energy at wavelengths less that 0.4 micron when operated at 2800°K.

The problem of tungsten lamp reliability was solved by using two especially rugged lamps and operating them below rated voltage. The lamps are low-voltage high-intensity devices which operate with approximately 0.6 amperes at 3.2 volts.

3.1.2 MATERIALS FOR REFLECTOMETER OPTICAL ELEMENTS

The transmission elements (lenses, windows, and beam splitters) used in the reflectometer were made of materials that have good transmission in the spectral range from 0.3 to 3 microns and are as stable as possible in the space environment. Fused quartz fit these requirements quite well. The low index of refraction of quartz (approximately 1.46) resulted in low surface reflection losses. From Fresnel's equations for normal incidence of light, the reflection loss per surface is given by

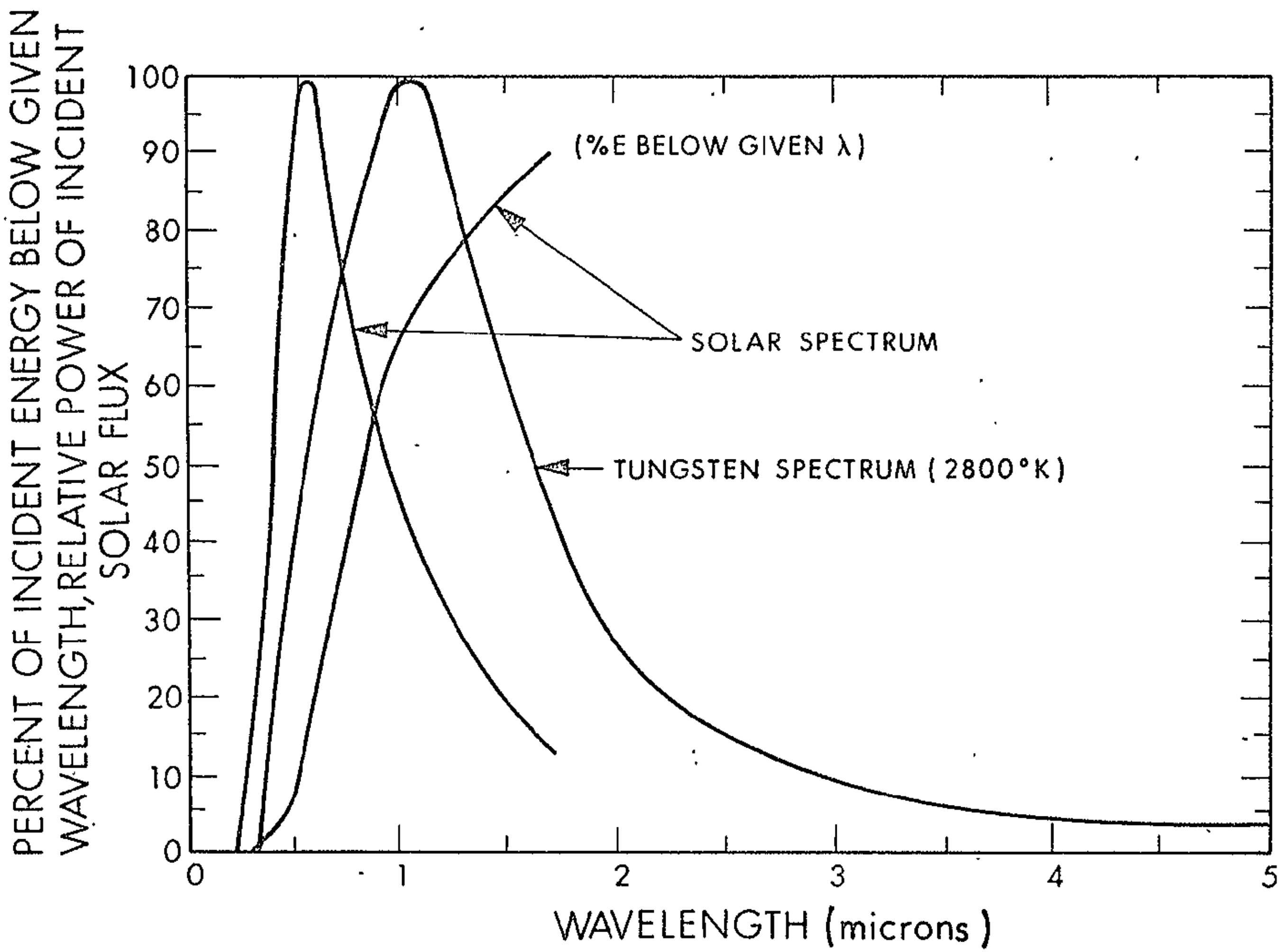

Figure 5. Electromagnetic Spectrum of Tungsten Lamp

$$\text{Loss} = \left(\frac{n - 1}{n + 1}\right)^2$$

$$= \left(\frac{1.46 - 1}{1.46 + 1}\right)^2 = \left(\frac{0.46}{2.46}\right) = 0.035 = 3.5 \text{ percent}$$

Thus, the total reflection loss for four uncoated surfaces is 14 percent. The average transmission of quartz from 0.3 to 3 microns should exceed 97 percent ignoring reflection losses. The overall efficiency of an uncoated lens doublet is thus estimated to be 83 percent.

The lens doublet system used in the reflectometer consisted of one fused quartz lens coated on one side for improved transmission and one light flint lens coated on both sides. This system was used to correct for aberrations. The overall efficiency of this lens system is 90 to 93 percent, depending on the wavelength.

3.1.3 REFLECTOMETER OPTICAL PATH

Figure 2 illustrates the reflectometer optical schematic. As was discussed previously, radiant energy from one of the two incandescent tungsten lamps is mechanically chopped producing a pulse rate of 480 Hz. The light beam passing to the beam splitter lens is limited by an aperture to 0.2 inch. The beam splitter reflects about 30 percent of the beam energy into the telecentric optical system. The remaining light is transmitted out of the system or absorbed in the beam splitter. The beam splitter has a partial Inconel coating on a Vycor 7900 substrate for near neutral reflectance-transmittance characteristics.

The optical path to the reflective sample consists of two 1.2-inch-diameter lens elements inside the housing, and two mirrors which form an integral part of the rotating arm. The mirror arrangement focuses the light onto the sample surface. The light is then reflected off the sample surface and returned along the same mirror and lens system to the beam splitter. Again, 70 percent of the light is reflected or is dissipated and the remaining 30 percent is transmitted via another mirror into an integrating sphere spectrometer.

After penetrating the integrating sphere aperture, the beam strikes a diffusely reflecting MgO interior surface. This results in an infinite number of reflections producing a constant power density and spectral content on any internal point. Photodetectors and PM tubes, with their respective filters, are located on the surface of the integrating sphere spectrometer.

Two sets of ghosts are formed by the beam splitter. One set is formed by the outgoing bundle and the other set by the return bundle. The ghosts formed by the outgoing rays are mostly vignetted by the optical system, and the ghosts formed by the return rays are formed near the primary image at the integrating sphere entrance window.

The uncertainties of optical component alignment caused by changing thermal and 'g' force conditions greatly affected the reflectometer optical design. An image of the incandescent filament is optically projected on the surface of the reflective samples, and reimaged at the entrance window of the integrating sphere after reprojection back through the same, nearly telecentric, optical system. The initial cone angle of the bundle of energy is restricted by the mechanical aperture. All other optical component apertures are very much greater so as to allow the return bundle a wide latitude of position within the return envelope. Therefore, within the limits of component aperture diameters the reflectometer effectiveness is relatively insensitive to sample tilting, warping, or other internal optical misalignment.

The acceptance angle of the instrument optics was tested using the engineering model unit. One sample was tilted through an angle of -5 degrees to +5 degrees off of the optimum allignment position. Figure 6 illustrates the percentage of relative reflectance reduction resulting from the misallignment.

3.1.4 INTEGRATING SPHERE

The integrating sphere is approximately 1 inch in diameter and is internally coated with MgO by a process developed by EOS. (This coating was developed for use in pulsed laser cavities.)

The integrating sphere spectrometer efficiency is a function of the reflectance of the interior coating and the ratio of the detector area to the total surface area of the coating. The spectrometer's relatively low power efficiency required high input power and sensitive photodetectors.

3.1.5 DETECTORS AND FILTERS

Two lead sulfide photodetectors, one silicon photodetector, and two PM tubes are mounted at apertures on the integrating sphere. The reflected light is spectrally detected by using filters and the inherent spectral cutoff limits of the detecting devices.

The spectrum from 0.3 to 0.65 micron is detected by two PM tubes (0.3 to 0.4 micron and 0.3 to 0.65 micron). The 0.65 to 1.2 micron spectral area is detected by a silicon detector. Lead sulfide detectors are used to detect the 1.2 to 3.0 micron sector of the spectrum and the total 0.3 to 3.0 micron spectrum.

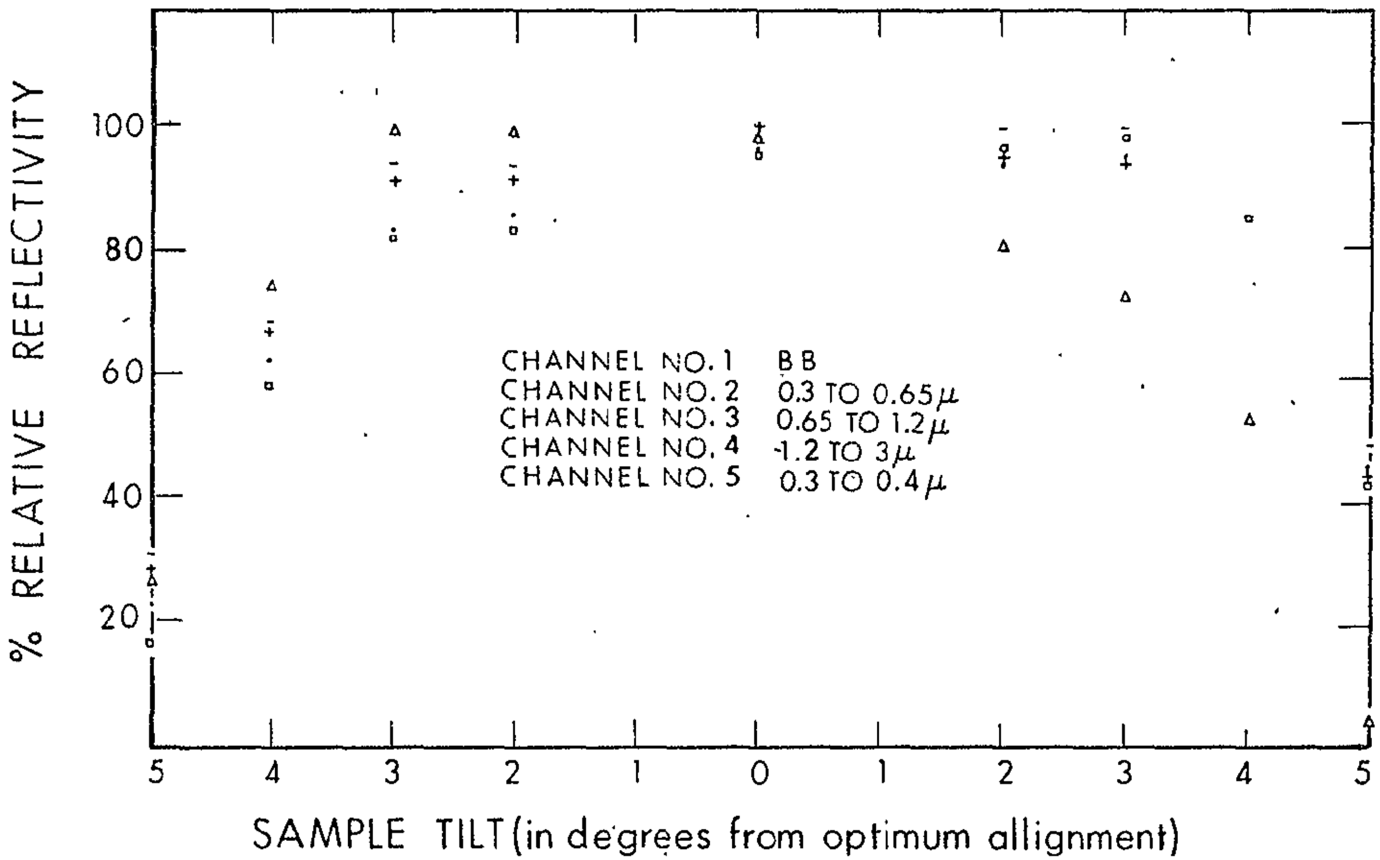

Figure 6. Optical System Acceptance Angle

3.1.5.1 Light Detectors

The system used three types of light detectors as mentioned above. One type was a lead sulfide photoconductive device whose electrical resistance is inversely proportional to the impinging light level. Lead sulfide detectors have a broad response spectrum extending from ultraviolet to about 3.0 microns (see figure 7). The response falls off rapidly at the near-ultraviolet wavelengths. The lead sulfide detector responsivity, on the order of 100 microvolts per microwatt, is an order of magnitude better than other solid-state or photoconductive devices. The lead sulfide detectors also operate at a fairly low voltage dc bias.

Lead sulfide photodetectors are extremely temperature-sensitive, having a dc resistivity temperature change on the order of 4 percent per degree centrigrade. Another characteristic of lead sulfide is that its responsivity diminishes with age. To compensate for this and changes due to temperature the signal conditioning electronics included ground-controlled range switching.

The second type of light detector was a silicon photodetector whose output current is proportional to the impinging light level. The silicon photodiode responsivity is on the order of 0.5 microampere per microwatt. This type photodetector has a broad response spectrum from approximately 0.32 micron to 1.2 microns. By combining the spectral output of the tungsten source and the spectral response of the silicon photodetector the capability to detect the 0.65 to 1.2 micron spectrum was established.

In a manner similar to that of the lead sulfide detector the silicon photodetector operates at a relatively low dc bias level. The silicon diode is not as temperature sensitive as the lead sulfide detectors; however, ground-controlled range switching was also provided in this channel.

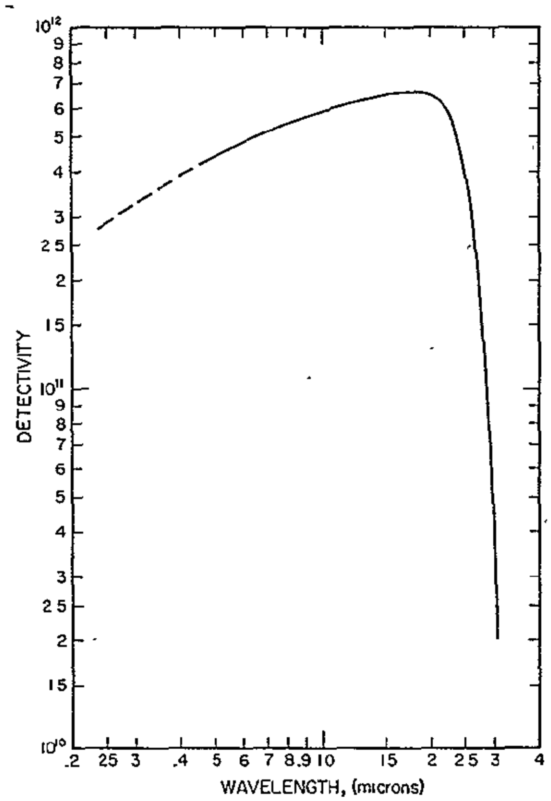

Figure 7. Detectivity as a Function of Wavelength for Lead Sulfide with a Cutoff of 2.5 Microns at 25°C

The third type of light detector, a PM tube, RCA8571, was used to monitor the near-ultraviolet end of the reflected spectrum. Its responsivity is on the order of 10^5 microamps per microwatt. The PM tube overall spectral response is much narrower than that of the lead sulfide detectors, but high in the near-ultraviolet region. PM tubes were used to detect the 0.3 to 0.4 micron spectral band and the 0.3 to 0.65 micron spectral band. A Schott UG-1 filter was used for the 0.3 to 0.4 micron band and an unfiltered tube was used for the 0.3 to 0.65 micron band. The tube required a high-voltage bias for between 500 and 1000 volts.

3.1.5.2 Optical Efficiencies

The effective optical efficiencies of the five spectral areas of the reflectometer are primarily determined by the operating temperature of the lamp, beam splitter efficiency, glass transmission, mirror reflectance, chromatic vignetting, and cutoff and/or bandpass of the filter/detector combinations. The lamp is operated at approximately 2700°K with approximately 2 watts input.

The effects from chromatic and other optical aberrations as well as alignment uncertainties are taken into account by making the integrating sphere entrance window large compared to the energy beam.

The uv spectral band was limited by the interrelated effects of the PM tube and the transmittance of light flint at a cuton of approximately 0.3 micron and a Schott UG-1 cutoff filter at approximately 0.4 micron. The effective optical efficiency of the uv channel is depicted in figure 8.

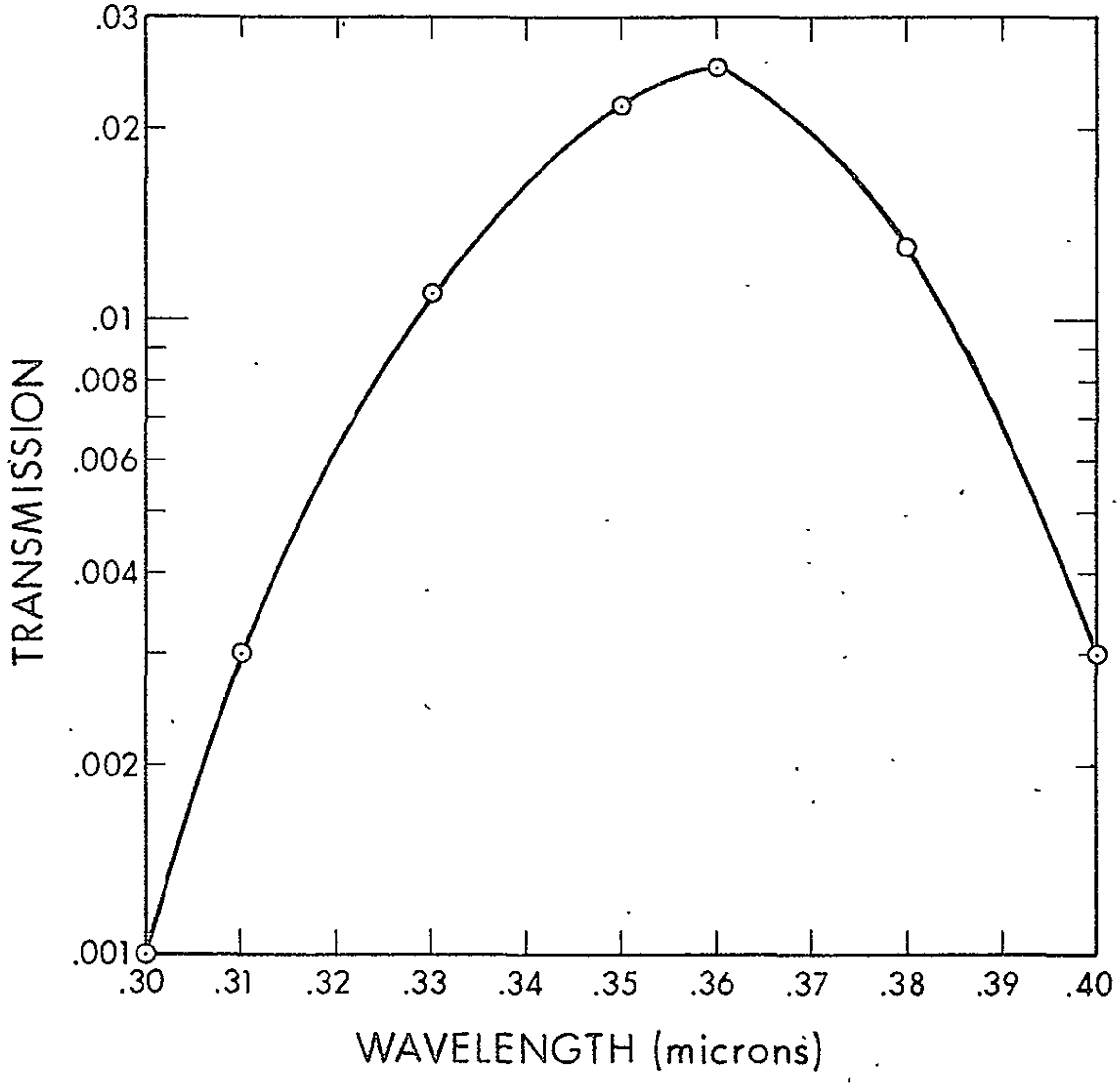

Figure 8. System Transmission for Region: 0.30 to 0.40 micron

73628660

The visible light spectral band was bounded by the 0.3 micron cuton and 0.65 micron cutoff of the PM tube alone. The effective optical efficiency of the visible channel from 0.3 to 0.65 micron is presented in figure 9.

The 0.65 to 1.2 micron spectral band used the spectral response of an unfiltered silicon photodetector in conjunction with the spectral output of the tungsten light source to provide the spectral limits. The 0.65 micron cuton was provided primarily by the light source spectral output, and the 1.2 micron cutoff was provided by the spectral response of the silicon detector. Figure 10 depicts the relative optical efficiency of the 0.65 to 1.2 micron channel.

The medium IR spectral band was bounded by a silicon cuton filter at approximately 1.2 microns and by the lead sulfide detector cutoff at approximately 3 microns. Figure 11 depicts the optical efficiency of the 1.2 to 3 micron channel.

The white light band, approximately 0.3 to 3 microns, consisted of an unfiltered lead sulfide detector. This detector operates over the entire experimental range of interest for this instrument and provides redundancy for the other four channels.

The detector sampling and entrance apertures of the integrating sphere subtended a relatively large angle with their respective normals; therefore, the efficiency of the integrating sphere was approximately the ratio of aperture area to sphere area. Laboratory tests indicated an integrating sphere efficiency of approximately 0.2 percent.

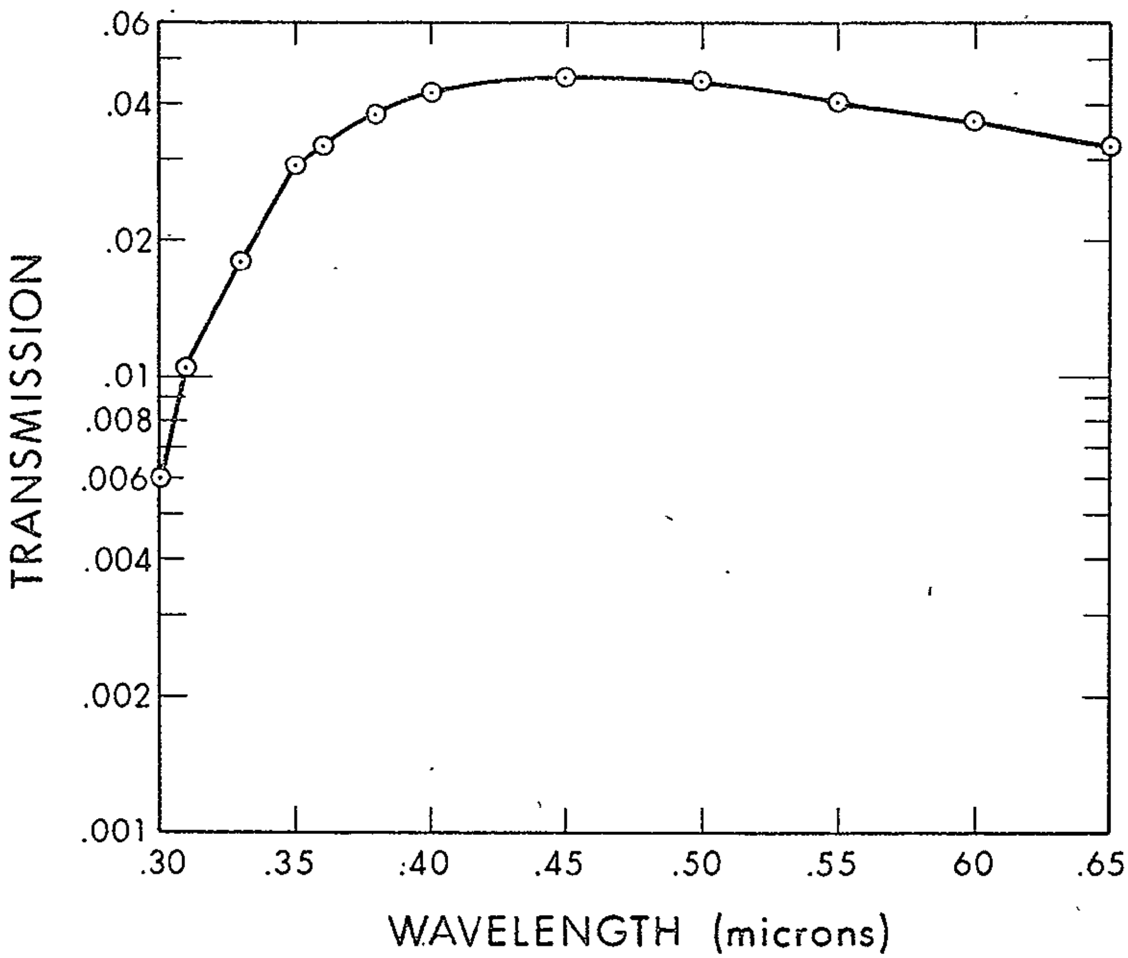

Figure 9. System Transmission for Region: 0.30 to 0.65 micron

73628661

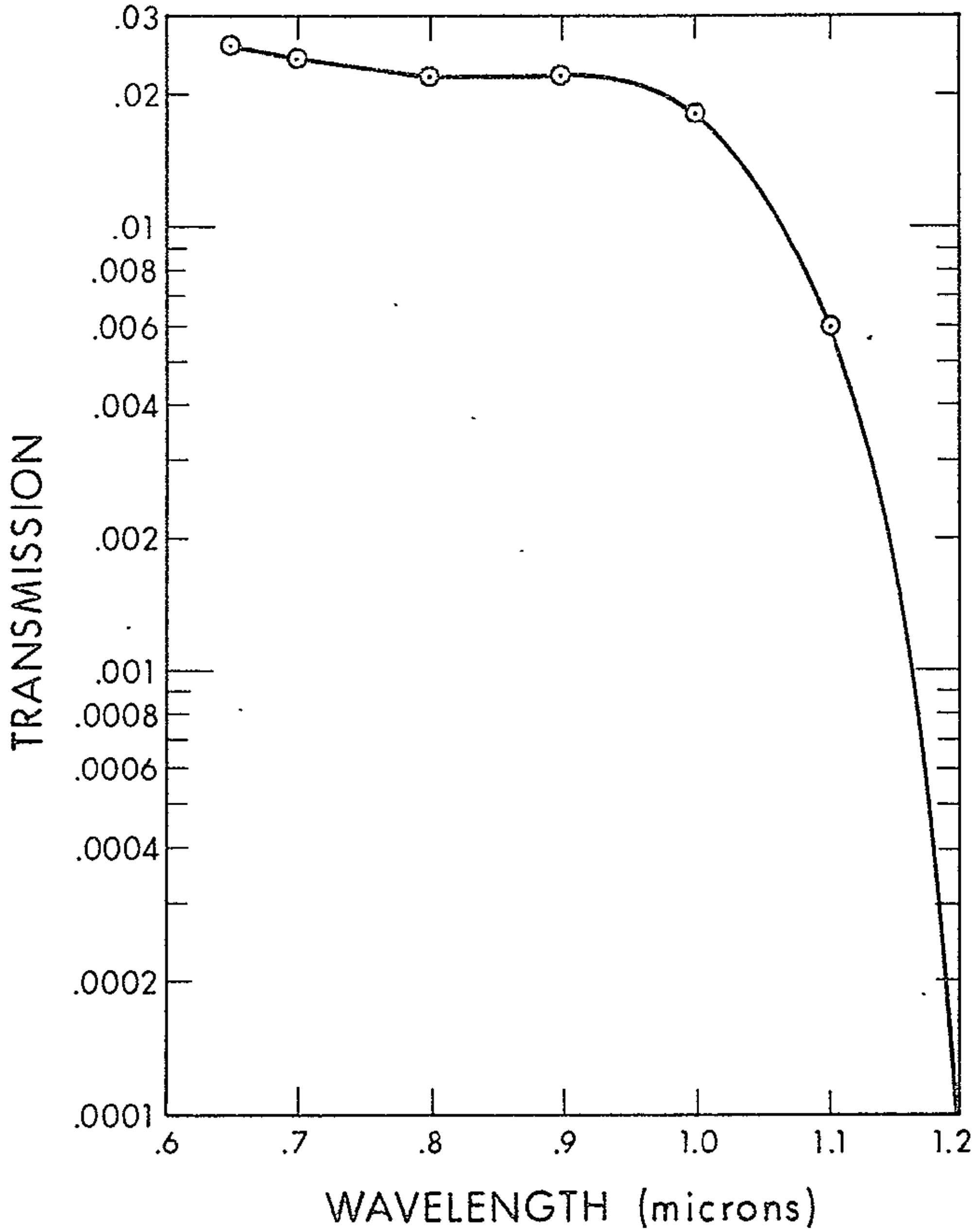

Figure 10. System Transmission for Region: 0.65 to 1.20 microns

73628662

7362D663

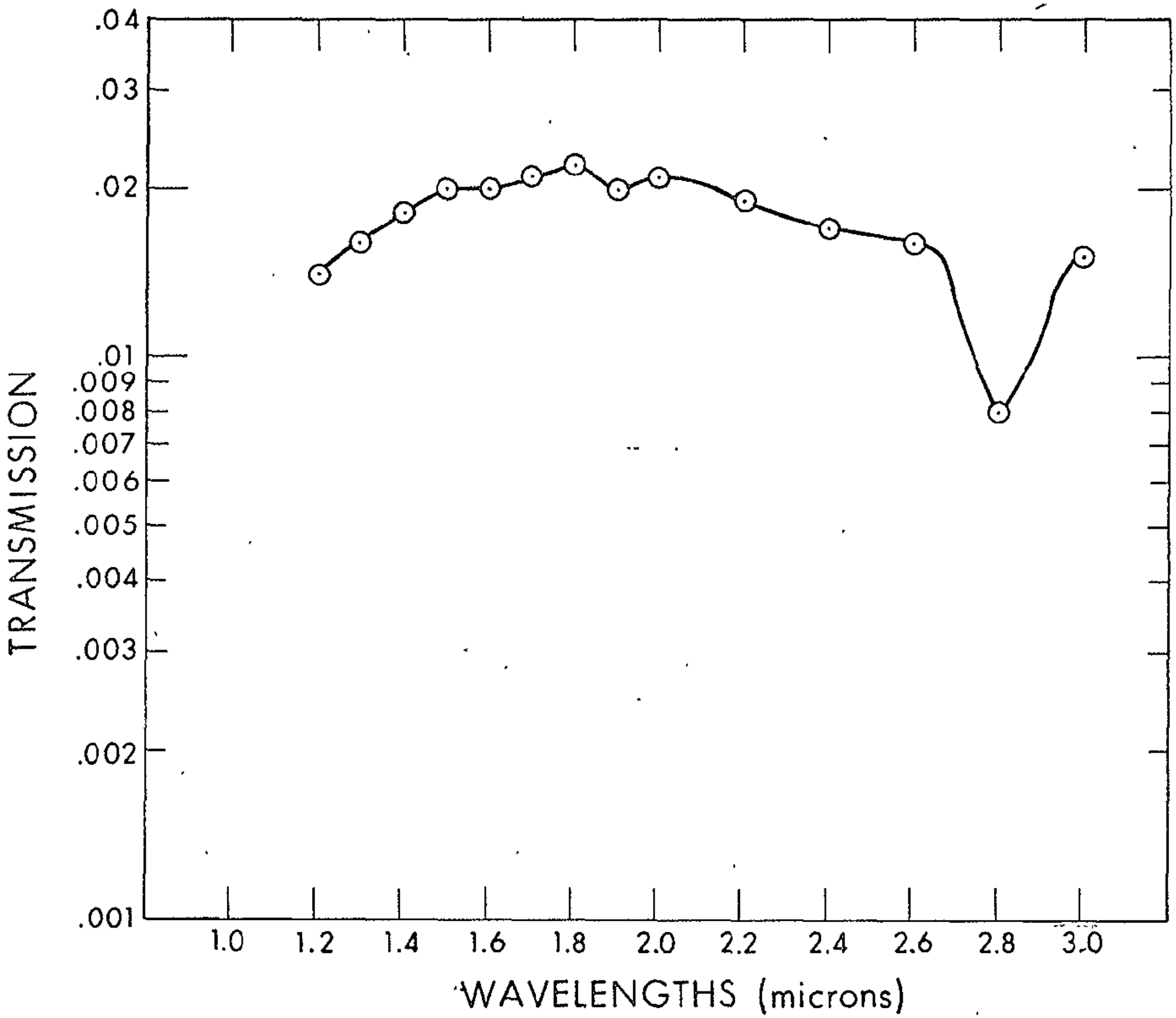

Figure 11. System Transmission for Region: 1.2 to 3.0 microns

3.1.6 TEST SAMPLES

Conferences between NASA experimenters, private industrial researchers, and ATS program management personnel resulted in selection of materials currently of interest to the space environment experimenters and also materials which offered the best promise of resisting the erosion forces encountered in a space environment.

Table 1 lists the number and kind of materials selected for reflectometer test surfaces. The reflective materials had as substrates either nickel, quartz, aluminum or epoxy. The reflective test surfaces were either Alzak, Mylar, aluminum, or silver. The various over-and-under coatings were in general, derivatives of the silicon oxide family. The samples themselves are approximately 3/4 inch in diameter.

Certain geometrical reactions are to be expected from thermally induced structural stresses. To reduce the number of uncontrolled variables and increase the reliability of the instrument and the validity of the data, every effort was made to prevent geometrical changes in the samples being tested. To accomplish mechanical sample stability the mounts were fabricated from a material with high conductivity. The sample mount had a spherical recess at the center, such that it could be adjusted in any direction. The plate upon which the test samples were mounted was designed such that it was a rigid section.

3.1.7 REFERENCE SAMPLES

For the reflectometer experiment two standards were selected, a full scale reference standard and a zero percent reference standard. The full scale reference standard was a second surface mirror of fused silica,

TABLE 1

LIST OF REFERENCES AND SAMPLES

Sample Number	Coating	Reflecting Surface	Undercoat	Substrate	Source[a]
1	(100% reference) Second Surface mirror				
3	(0% reference) Black anodized grooved Al				
7, 12*	SiO_2, 12λ/4[b]	Al	Cr/SiO	Ni	C
17,20*	SiO_2, 12λ/4[b]	Al	SiO	Quartz	C
16	Al_2O_3, 12λ/4[b]	Al	SiO	Al	C
2*,4	SiO_x (0.17μ)	Al	Cr/SiO	Ni	A
18A, 19A*	SiO_x (0.17μ)	Al	SiO	Al	A
9*,15	$(Si_2O_3)_x$ (1.2μ)	Al	SiO	Mg + epoxy	E
13*,14	Alzak	Al	None	Al	D
6	none	Al	1/2 mil Mylar	Al	B
5, 11*	none	Al	Cr/SiO	Ni	A
18B, 19B*	none	Al	SiO	Al	A
8, 10*	MgF_2, 2λ/4[b]	Ag	Cr	Ni	D

* Indicates those samples that are shielded.
[a] Lettering indicates laboratory that supplied the sample.
[b] Coating thickness expressed in terms of quarter waves at 550 nm.
A - Electro-Optical Systems, Pasadena, Calif.
B - NASA-Langley Research Center, Langley Station, Hampton, Va.
C - Night Vision Laboratory, Ft. Belvoir, Va.
D - NASA-Goddard Space Flight Center, Greenbelt, Md.
E - NASA-Lewis Research Center, Cleveland, Ohio.

optical grade A, with an aluminum layer overcoated by evaporating nickel to an opaque layer. The zero percent reference standard was a black anodized metal sample machined to act as a scatter plate.

3.1.8 SEPARATION OF EFFECTS

Quartz windows, which act as test sample shields for separation of effects, were mounted on the rotary arm assembly. With the arm in the "home" position, the quartz shields cover eight test samples and solid shields cover the two reference samples. This provides protection from micrometeoroids and most charged particles. The remaining ten test samples were exposed to the total space environment. The protected samples were left unshielded for only a fraction of each revolution of the rotating arm assembly since the shields rotate with the arm.

3.2 ELECTRONICS SUBSYSTEM

The electronic system performed three basic functions in the reflectometer instrument. The first major function was that of processing the signals which result from light reflected from the reflective samples. This function was performed by electrically detecting the light output at the integrating sphere, amplifying the detector output signals, and supplying the amplified output signals to the spacecraft telemetry subsystem.

The second major task of the electronic system was to control the operation of the instrument. The control circuits served as an interface between the spacecraft command subsystem and the items in the reflectometer which were to be controlled. The three items to be controlled in the reflectometer were the motor, lamps, and amplifier gains.

The third major function of the electronic system was to take environmental measurements. This included temperature sensors and a pressure transducer which monitored the internal pressure of the reflectometer enclosure.

3.2.1 SIGNAL PROCESSING CIRCUITS

Five channels of reflectivity data were processed by the signal processing circuits. However, only two different types of signal processing circuits were used.

The circuitry to process each output of the solid-state detectors consisted of a preamplifier, a multirange amplifier, and a bandpass amplifier. The signals from the solid-state detectors were processed as follows: The low level, high output impedance signals from the solid-state detectors were connected to the preamplifier inputs. The preamplifiers incorporated a field effect transistor to provide a high input impedance. The output level of the preamplifiers were in the low millivolt range with an output impedance of approximately 100 ohms. This signal was connected directly into the input of the multirange amplifier. The gain of the multirange amplifier was controlled by commands from the spacecraft command subsystem to provide an output of approximately 1 volt peak-to-peak. The 1-volt output signal was ac-coupled into the bandpass amplifier where it was amplified to approximately 10 volts peak-to-peak and detected by a peak detector. The peak detected dc voltage was filtered and sent to the spacecraft telemetry subsystem.

The signal processing for the PM tube channels was similar to that used for the solid-state detector channels except that the multirange amplifier was not used. The output current of the PM tube was applied to a high input impedance preamplifier and converted to an ac voltage. The preamplifier feedback resistor was adjusted to provide an output voltage of approximately 1 volt peak-to-peak. The output of the preamplifier was applied directly to the input to the bandpass amplifier. The bandpass amplifier used in the PM tube channels was identical with that used in the solid-state detector channels and supplied an output voltage directly to the spacecraft telemetry subsystem.

3.2.1.1 Photomultiplier Tube Preamplifier

The PM tube preamplifier consisted of a dual field effect transistor differential amplifier, a dual transistor differential amplifier, and a transistor emitter follower. The field effect transistor differential amplifier provided an immunity to power supply noise and provided high input impedance, allowing current flow through the feedback resistor. The second differential stage combined the two output signals from the field effect transistor to provide a single input to the emitter follower stage.

The PM tube current output was converted to a voltage at the field effect transistor amplifier input by passing the current through a feedback resistor. The value of the resistor was selected during testing to provide a preamplifier output of approximately 1 volt peak-to-peak.

3.2.1.2 Detector Preamplifier

The detector preamplifier was basically a two-stage emitter follower circuit. The first stage used a field effect transistor to provide high input impedance. The second stage, a transistor emitter follower, served as a buffer between the field effect transistor and the output signal to provide a low output impedance. The preamplifier voltage gain was approximately 0.85 with an output impedance of approximately 100 ohms. The detector preamplifier operated from the +15V power supply and was protected from power supply noise by an r-c decoupling circuit.

3.2.1.3 Multirange Amplifiers

The multirange amplifiers, present only in the three solid-state detector channels (lead sulfide and silicon), were integrated circuit operational amplifiers with switchable feedback resistors. The switchable feedback resistors provided a wide amplification range to offset the change in detector signal output due to temperature variations and degradation with age.

The gain of each amplifier was matched to the signal output of the detector by selecting a gain-setting resistor, separate from the switchable feedback resistors, for each amplifier. This resistor was selected, during preassembly system operation, to provide a usable output signal at room temperature with the gain 25X feedback resistor selected. This provided an adequate range of selectable gains to compensate for a wide range of detector signal outputs.

Field effect transistors were used in the amplifier feedback circuit to provide for feedback resistor switching. The field effect transistors were controlled by gate voltages applied from the gain control logic circuit. Each detector channel multirange amplifier was at the same gain state and simultaneously switched to the next state upon command.

3.2.1.4 Bandpass Amplifiers

The bandpass amplifiers, located at the output of each of the five reflectivity channels, served as bandpass filters, amplifiers, and ac-to-dc signal converters to provide a 0 to 5 volt dc output voltage to the spacecraft telemetry subsystem.

The filter and amplifier sections of the bandpass amplifier were made up of an operational amplifier with associated frequency sensitive feedback circuitry. This module provided a voltage gain of 10 with a bandpass centered at approximately 500 Hz. Following the bandpass amplifier section of this module was a peak detector which rectified and filtered the amplifier output signal to provide a 0 to 5 volt dc output voltage to the spacecraft telemetry subsystem.

3.2.2 CONTROL CIRCUITS

The control circuits were used as an interface between the spacecraft command subsystem and the items in the reflectometer which were to be controlled. All of the control circuits in the reflectometer were similar; however, because of different power handling requirements, the design of some of the control circuits was extended beyond the basic interface circuit. More detailed explanation of the control circuits is provided in the following subsections.

3.2.2.1. Motor Control

The motor control circuit consisted of three basic sections. The first section, up to point A (see figure 12), is the basic interface circuit. The second section of the circuit, point A to point B, was used in conjunction with the first circuit to provide more power handling capability. The third section of this circuit consisted of Q5 and Q6 which generated a "turn-off" pulse for the motor control module when the scanner arm reached the "home" position.

The first section of the circuit shown in figure 12 is a bistable circuit which is triggered into both its high and low states by a positive going step voltage applied to either of its inputs by the spacecraft telemetry

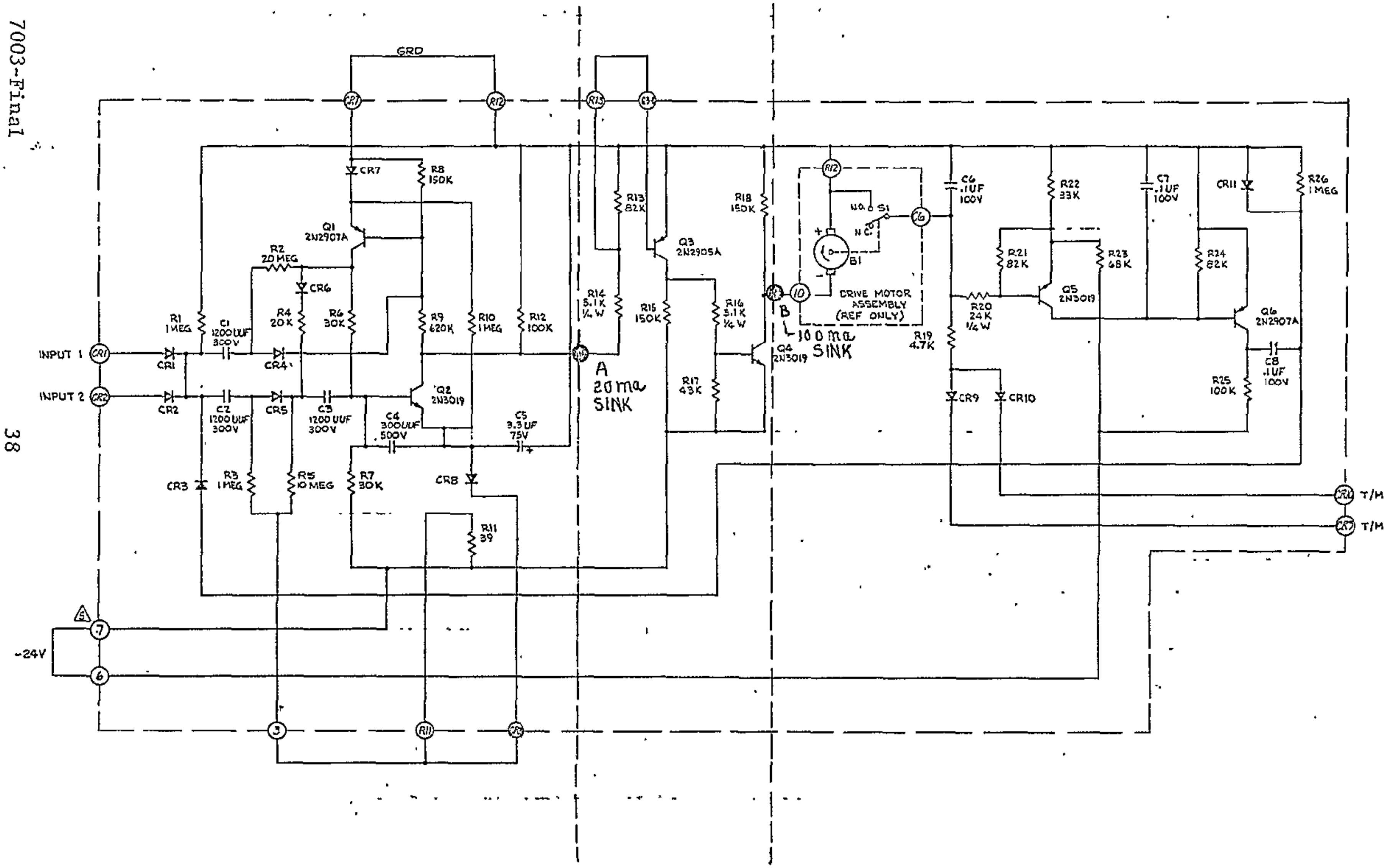

Figure 12. Motor Control Circuit

subsystem. When power was initially applied to the module the output voltage was approximately zero and all transistors were in the "off" condition, therefore consuming a very low amount of power.

The circuit operation, up to point A, is as follows: The voltage at inputs 1 and 2 are held at -5.5V by the telemetry subsystem. When power is applied to the module the filter formed by C5 and R11 assures that the motor control circuit will be in the "off" state by forcing the emitter of Q2 to fall toward -24 volts more slowly than does the base of Q2. After capacitor C5 has reached the fully charged condition the voltage drops across R7 and R8 will be less than the voltage drops across CR7 and CR8 so that the base emitter junctions of Q1 and Q2 will be reverse biased. Under these conditions point A is near zero volts. When a positive pulse is applied to either input 1 or input 2 the pulse will be coupled through CR1 or CR2 (depending on which input received the positive pulse) then through C2, CR5 and C3 into the base of Q2. When Q2 is turned "on", a minus voltage is applied to the base of Q1 causing regenerative feedback to the base of Q2. Both Q1 and Q2 will saturate, causing point A, the basic output of this circuit, to be capable of supplying approximately 20 milliamperes of current at -24 volts. After the initial transients die down, inputs 1 and 2 will again return to -5.5V. This will back bias CR1 and CR2, thus isolating the -5.5V from the remainder of the circuit.

When the next positive command pulse is applied to either input 1 or input 2 the pulse will be coupled through CR1 or CR2, C1 and CR4 to the base of Q1. This positive pulse will hold the base emitter junction of Q1 reverse biased long enough to turn both Q1 and Q2 off. This returns the circuit to its original condition with approximately zero volts at point A. When the voltage at the input returns to -5.5V, CR1 and CR2 will both be back biased causing the -5.5V to be isolated from the rest of the circuit.

This is the operation through one cycle of the circuit. At the end of one cycle the circuit is in the initial "power on" condition and will recycle in the same manner as described above.

To provide greater power handling capabilities, a two-transistor stage was added to the first section. At point B, the output of the second section, the circuit is capable of providing approximately 100 milliamperes of current at -24 volts. Point B was the output point which was used to drive the motor in the motor control circuit.

The motor control module contained an additional two-transistor circuit to provide an "off" command to the motor control circuit when the scanner arm reached the home position. This circuit operated as follows:

Switch S1 is open during the time the scanner arm is rotating. This causes the voltage at the base and emitter of Q5 to be equal, biasing Q5 and Q6 off. When the scanner arm reaches the home position, switch S1 is momentarily closed and applies a higher voltage to the base of Q5 than is on the emitter. This causes Q5 to conduct, which, in turn, causes Q6 to conduct. The collector of Q6 was initially at approximately -24 volts. When Q6 is turn on the voltage at the collector of Q6 goes to approximately zero volts causing a positive pulse to be applied through C8 and CR3 to the input of the motor control circuit. This pulse commands the motor "off" and reduces the voltage at point B to approximately zero volts.

3.2.2.2 Amplifier Gain Control

Selection of the multirange amplifier gain states was provided by a two-stage command conditioning system. The first stage consisted of the scale factor select module which provided an interface between the spacecraft command subsystem and the second stage, the reflectometer gain control logic circuitry.

The scale factor select circuit is basically a bistable flip-flop circuit. The circuit has redundant inputs in order to best utilize the redundancy built into the spacecraft command subsystem. When power is initially applied, the circuit has an output of approximately zero volts. A spacecraft command (positive pulse) applied to either of the circuit inputs will change the state of the circuit and provide a -24V dc output. The next spacecraft command applied to the circuit will return it to the initial turn-on state with approximately zero volts at the output. This circuit is identical with the first section of the motor control circuit. Refer to Subsection 3.2.2.1 for a detailed discussion of the circuit.

The output of the scale factor select circuit was applied directly to the gain control logic circuitry. The gain control logic circuit consisted of two inverter circuits, one flip-flop circuit, one AND gate, and four driver circuits. The two-state output of the scale factor select circuit was conditioned, through the inverters and the flip-flop, to provide four inputs to the AND gate. Four outputs of the AND gate were generated and applied directly to the four driver circuits which control the gain switches of the multirange amplifiers. The output of the driver circuit was approximately -15 volts when its gain state was selected and approximately zero volts when it was not selected.

The scale factor select circuit and the flip-flop in the gain control logic circuit were both designed to provide zero volt outputs when power was initially applied. This provided an initial "turn-on" gain state of gain X. The first telemetry gain switch command switched both the scale factor select circuit and the flip-flop. This selected a gain state of 5X. The next telemetry command changed the state of the scale factor select circuit. (The flip-flop changes state only on negative voltage changes.) This selected a gain state of 25X. Gain 125X was selected by the next telemetry command. The circuit recycled to gain X on the command following the gain 125X state.

A telemetry output circuit was also provided in the gain control logic circuit to provide telemetry monitoring of the gain state condition.

3.2.2.3 Lamp Control

There were two lamp control circuits in the reflectometer instrument: the lamp select circuit and the lamp on/off circuit. Both circuits were electrically and mechanically identical.

Each lamp control circuit was basically a bistable flip-flop circuit. When power was initially applied to the circuit it had an output of approximately zero volts. The circuit was triggered to the opposite condition, -24 volts at the output, by a positive pulse from the spacecraft command subsystem. This circuit is identical to the motor control circuit, up to point B (see figure 12).

The lamp select module supplied control current to relays K2 and K4 in the low voltage power supply. With no current supplied to the relays the initial turn-on condition, lamp A, was automatically selected. When a "lamp select" command was received from the command subsystem -24 volts appeared at the output of the lamp select module. This energized relays K2 and K4 causing lamp B to be selected. When another "lamp select" command was received, current was removed and lamp A was again selected.

The lamp on-off module supplied control current to relays K1 and K3 in the low voltage power supply. With no current supplied to the relays the lamp voltage circuit was interrupted and neither of the lamps were powered. When a lamp "on-off" command was received, -24 volts appeared at the output of the lamp on-off module. This energized relays K1 and K3 and applied power to the selected lamp. When another "lamp on-off" command was received, current was removed from the relays, which in turn removed power from the lamp.

3.2.3 POWER CONVERTERS

Two basic power conversion modules were used in the reflectometer instrument. The low voltage power converter supplied power to all of the signal processing circuitry, the lamps, and the environmental measurements circuitry. The two high voltage power converters provided output voltages to the two photomultiplier tubes. Both of the high voltage power converters were housed in the high voltage power supply enclosure. Two high voltage converters were used to provide greater redundancy for the two photomultiplier tube channels.

3.2.3.1 Low Voltage Power Converter

The low voltage power converter was a dc-to-dc converter with multiple output voltages. The converter supplied ±15 volts, unregulated, for operation of signal conditioning and logic circuitry. In addition to the unregulated output voltages, two voltage outputs, regulated to 0.1 percent, were provided. One was a -20 volt bus to provide detector bias voltage. This bus had a -8 volt zener regulated tap to provide operating voltage for the temperature detectors. The second regulated voltage supply was adjustable from 2.9 volts to 3.5 volts. This voltage supply provided power to operate the lamps.

The converter oscillator operated directly from the -24 volt bus. No feedback regulation was provided on the -24 volt power to control the oscillator. The regulated voltage buses were controlled individually by a feedback controlled series transistor in each of the regulated output voltage lines.

The +15 volt bus voltage was obtained by rectifying and filtering the ac output voltage of the 15 volt secondary winding of the oscillator transformer. The analog telemetry output for the +15 volt bus was achieved by using a voltage divider from the +15 volt bus to the -24 volt supply bus. This allowed the telemetry output to be negative with respect to ground and still reflect the changes in the +15 volt bus voltage. Figure 13 shows the +15 volt bus voltage versus the analog telemetry output voltage. The dashed lines indicate the limits of the telemetry output voltages due to variations in the -24 volt (±0.48V) bus.

The -15 volt bus voltage was obtained by rectifying and filtering the ac output voltage of the second 15 volt secondary winding of the oscillator transformer. The analog telemetry output for the -15 volt bus was achieved by using a voltage divider between the -15 volt bus and ground. Figure 14 shows -15 volt bus voltage versus the analog telemetry output voltage.

The regulated -20 volt bus used the unregulated voltage from the 20 volt secondary winding of the oscillator transformer. This voltage, after being rectified and filtered, was regulated by a series transistor regulator in the -20 volt bus line. The series transistor was controlled by an operational amplifier which sensed the -20 volt bus voltage at the output and by a transistor driver which was controlled by the operational amplifier.

One input of the operational amplifier sensed the -20 volt bus voltage through a voltage divider network. The other input to the operational amplifier was held at a constant reference voltage by a zener diode referenced to ground. A "select at test" resistor was provided in the sensing voltage divider to provide for adjustment of the -20 volt output bus voltage. The output of the operational amplifier drove a control transistor which in turn controlled the voltage at the base of the series regulating transistor.

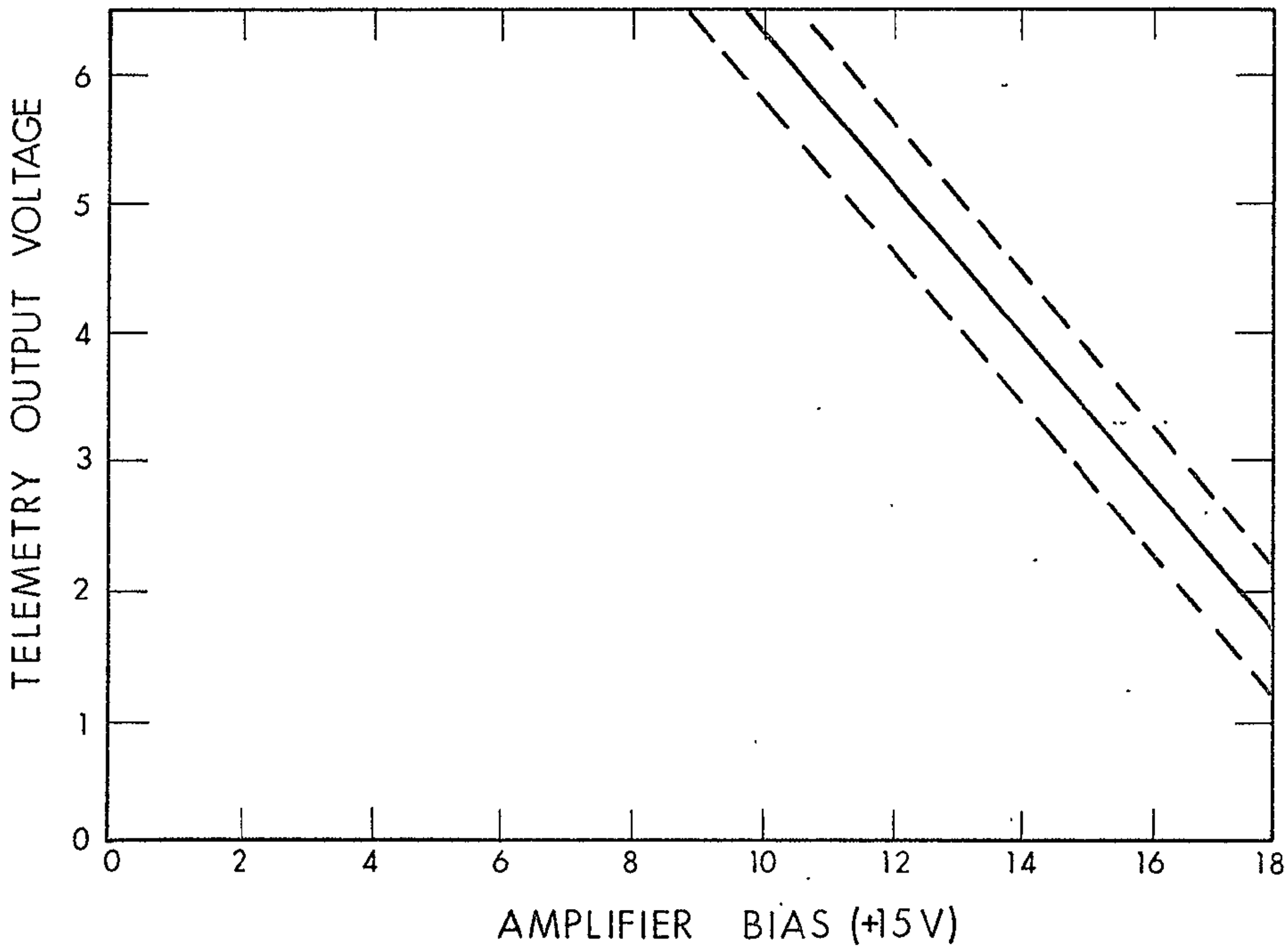

Figure 13. Amplifier Bias (+15V) versus Telemetry Output Voltage (telemetry channel L-16)

73628819

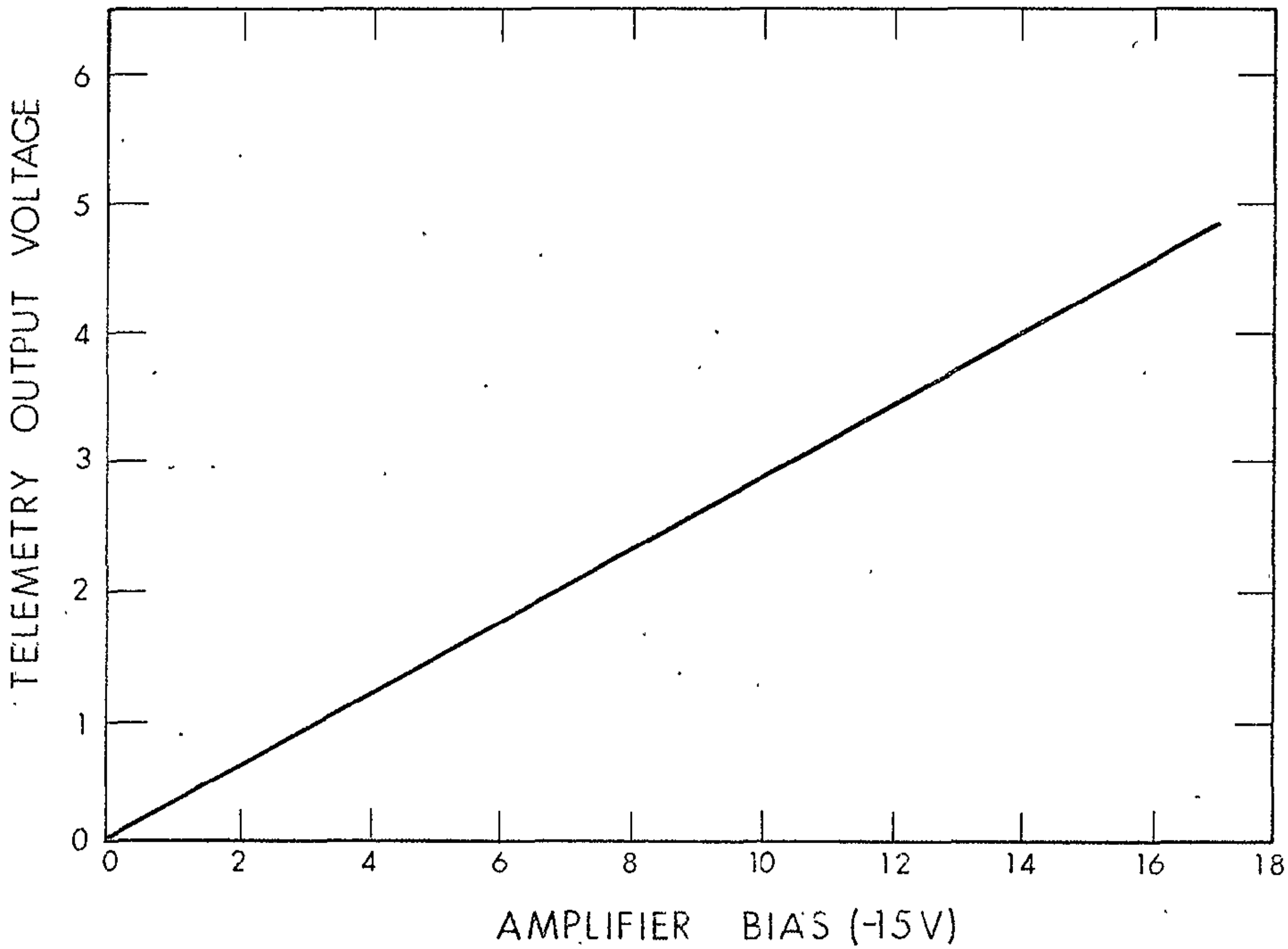

Figure 14. Amplifier Bias (-15V) versus Telemetry Output Voltage (telemetry channel L-17)

The -20 volt bus was also current limited. This was achieved by placing a low value resistor in series with the emitter of the regulating transistor and by referencing the base of the transistor, through two forward biased diodes, to the side of the resistor not attached to the emitter. If the current output at the -20 volt bus plus the current at the -8 volt bus exceeded approximately 40 mA the voltage on the buses would drop. This was the result of excess current flow through the resistor which would bias the series regulating transistor into a cutoff condition.

The -8 volt bus was used to provide power to the temperature sensors and was achieved by zenering of the -20 volt bus voltage.

The -20 volt bus analog telemetry output was obtained by using a voltage divider from the -8 volt bus to ground. This was possible since the -8 volt bus voltage was directly proportional to the -20 volt bus voltage. Figure 15 shows the -20 volt bus voltage versus the analog telemetry output voltage.

The regulated lamp voltage bus used the unregulated voltage from the 3.5 volt secondary winding of the oscillator transformer. This voltage, after being rectified and filtered, was regulated in exactly the same manner as that described above for the -20 volt bus voltage. However, two functional differences did exist in the circuit. The output voltage of the lamp supply was adjustable by adjusting a potentiometer. This potentiometer was part of the voltage divider which sensed the output voltage and supplied the error signal to the operational amplifier. The second difference was that the lamp voltage output was current limited at approximately 1 ampere. This current limiting function was achieved in exactly the same manner as was described for the -20 volt bus above except that the series resistor value was different.

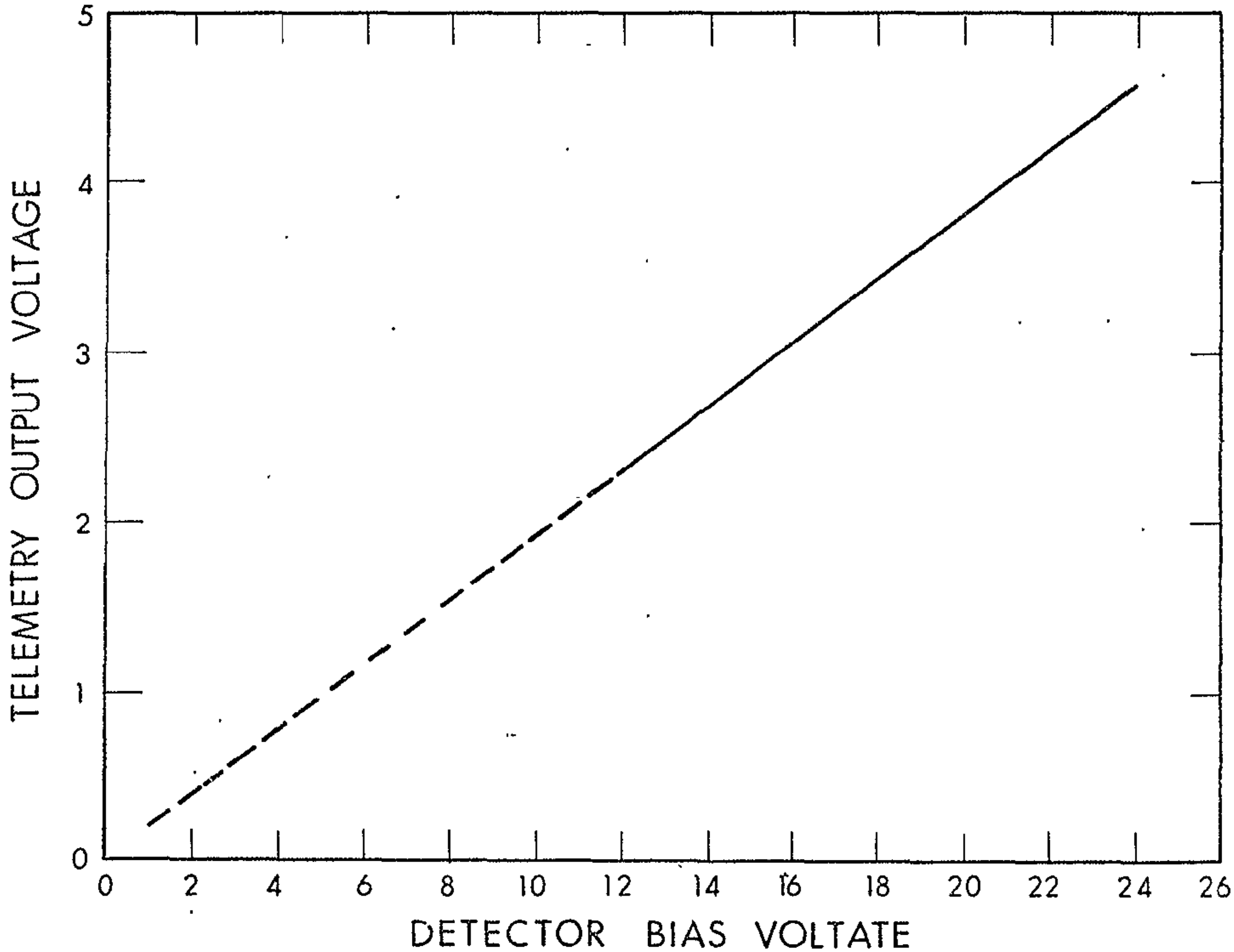

Figure 15. Detector Bias Voltage versus Telemetry Output Voltage (telemetry channel L-14)

The lamp voltage analog telemetry output was supplied directly from the lamp voltage bus. This voltage is within the limits of the telemtry subsystem without further processing. Figure 16 shows the telemetry output voltage versus the voltage delivered to the lamps. As seen from the graph the lamp bus voltage is not the same as the voltage applied to the lamps. This difference was caused by voltage drops in the relay contacts and in the cable carrying the relatively high lamp current.

Control of the lamps was achieved by using relays to direct power to the lamps. The relays were activated by the lamp control modules, lamp on-off and lamp select, discussed above. The lamp bus voltage was applied to the lamps through a redundant relay system. When the spacecraft regulator was initially turned on, the relays were in a nonenergized condition with lamp A selected and no power applied to the lamps.

When a "lamp on-off" command was transmitted to the lamp on-off control module, the module supplied current to two relays in the low voltage power converter. Each of the two relays had two operating contacts. When the initial "lamp on-off" command was given, both relays were activated and power was applied through four contacts, to the "lamp select" relays in the low voltage power converter

In the initial turn-on condition lamp A was selected. This is the condition with no "lamp select" current being supplied by the lamp select module. Under these conditions power is supplied to lamp A through the two redundant "lamp select" relays with four conducting contacts.

When a "lamp select" command was transmitted, after initial power was applied to the reflectometer, the lamp select module would supply current to energize the two redundant "lamp select" relays. This caused the lamp voltage to be removed from lamp A and supplied to lamp B.

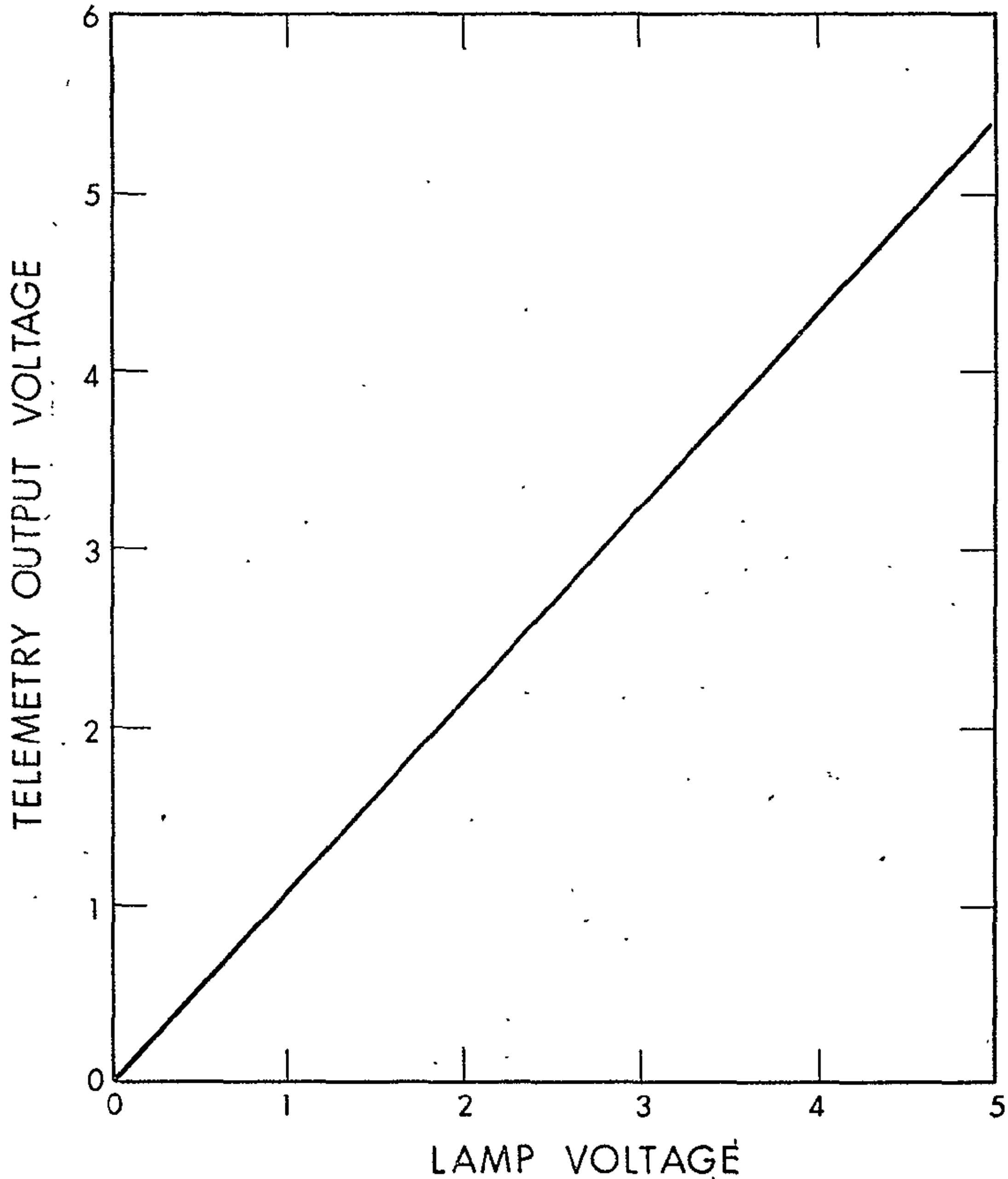

Figure 16. Lamp Voltage versus Telemetry Output Voltage (telemetry channel L-19)

The multiple redundancy in both the "lamp on-off" relays and the "lamp select" relays provided reliability and also distributed the lamp current through a larger number of contacts.

3.2.3.2 High Voltage Power Converter

The reflectometer instrument contained two high voltage power converters. Each power converter supplied voltage to one PM tube. The high voltage power supply outputs were adjusted during postassembly system operation to provide a proper gain for the associated PM tube. The high voltage power converter was a dc-to-dc converter with current limiting and an adjustable voltage control feedback circuit. The power supply was adjustable from approximately 500 volts to 1000 volts with a static load regulation of ±0.1 percent and a temperature regulation of ±0.5 percent over a range of +14 to +122°F. The output was current limited at approximately 600 microamperes.

Voltage adjustment and regulation control of the high voltage output was achieved by monitoring the output through a voltage divider and applying the divider output, as a feedback voltage, to one input of an operational amplifier. A potentiometer was included in the voltage divider with the wiper arm of the potentiometer supplying the feedback voltage to the operational amplifier. The potentiometer could be adjusted to provide an output between approximately 500 and 1000 volts. The other input point of the operational amplifier was connected to a stable zener voltage reference.

The output of the operational amplifier controlled one of two series transistors used to control the supply voltage to the converter oscillator. When the high voltage output of the power converter started to increase, the increase was sensed by the operational amplifier which in turn controlled the input series transistor to reduce the voltage at the oscillator.

A similar control mechanism was used to achieve the current limiting capability. The second series transistor in the oscillator voltage supply line was used as a current limiter control. The base of the transistor was biased with a stable voltage supply. A current sensing resistor in series with the emitter of the transistor biased the transistor toward cutoff when the output current exceeded 600 microamperes. This reduced the input voltage to the oscillator and lowered the output voltage.

The high voltage telemetry output was obtained by rectifying the output voltage of a secondary winding on the oscillator transformer. This voltage is a function of the high voltage output of the power converter. Figures 17 and 18 show the high voltage output versus telemetry analog output for each of the converters.

The two high voltage power supplies were enclosed in one housing. The primary purpose of this housing was to shield the signal electronics from the power supply switching spikes.

3.2.4 ENVIRONMENTAL MEASUREMENTS

To monitor the environmental conditions existing in and around the reflectometer enclosure the temperature at various points in the instrument and the internal instrument pressure was monitored. Temperature sensor units were mounted in positions to monitor the case temperature and also to monitor the temperature of the integrating sphere which in turn was a measure of the solid-state detector temperatures. A pressure transducer monitored the internal pressure of the enclosure.

73628822

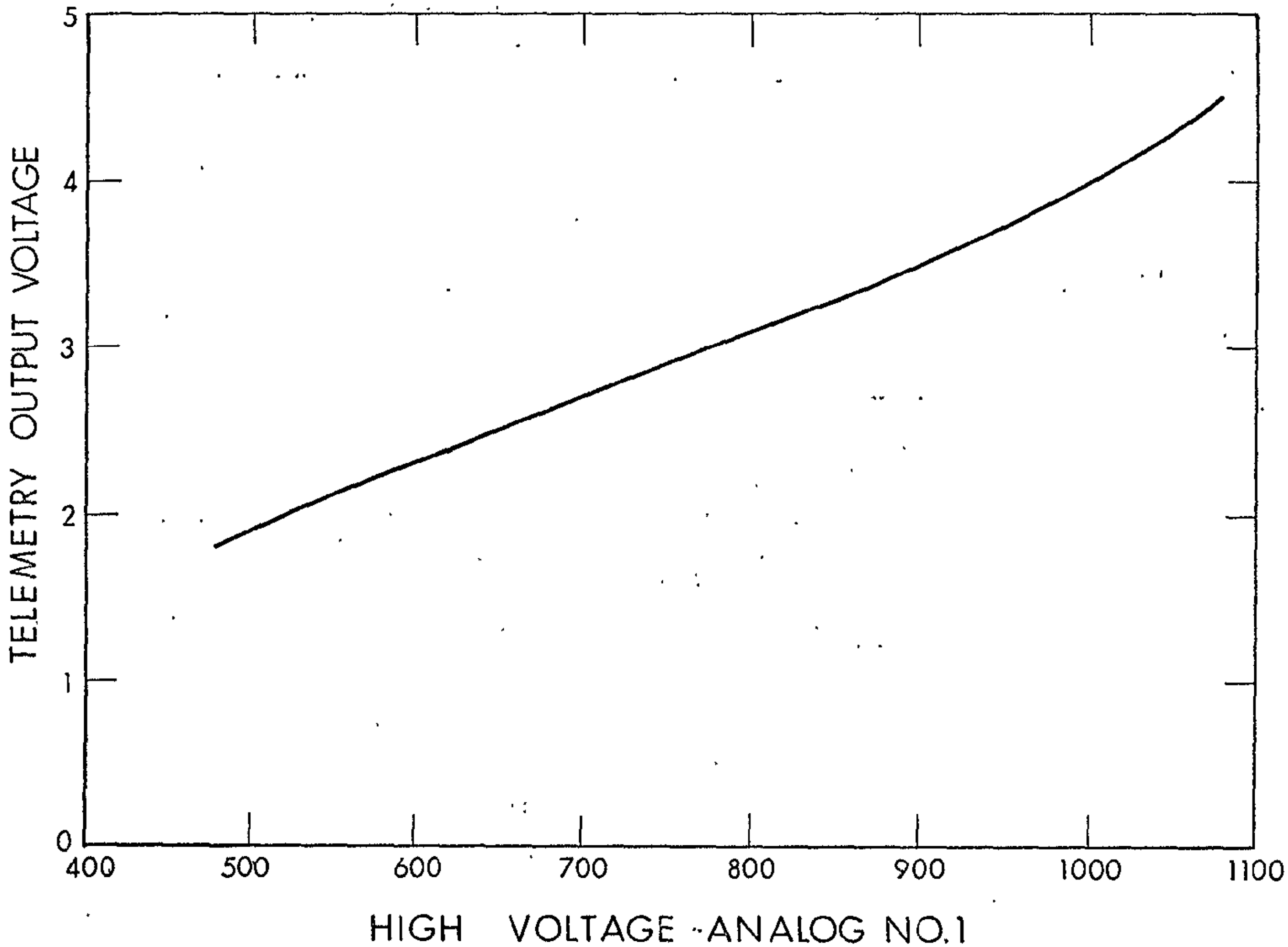

Figure 17. High Voltage Analog No. 1 (0.3 to 0.65 micron channel) versus Telemetry Output Voltage (telemetry channel L-15)

73628823

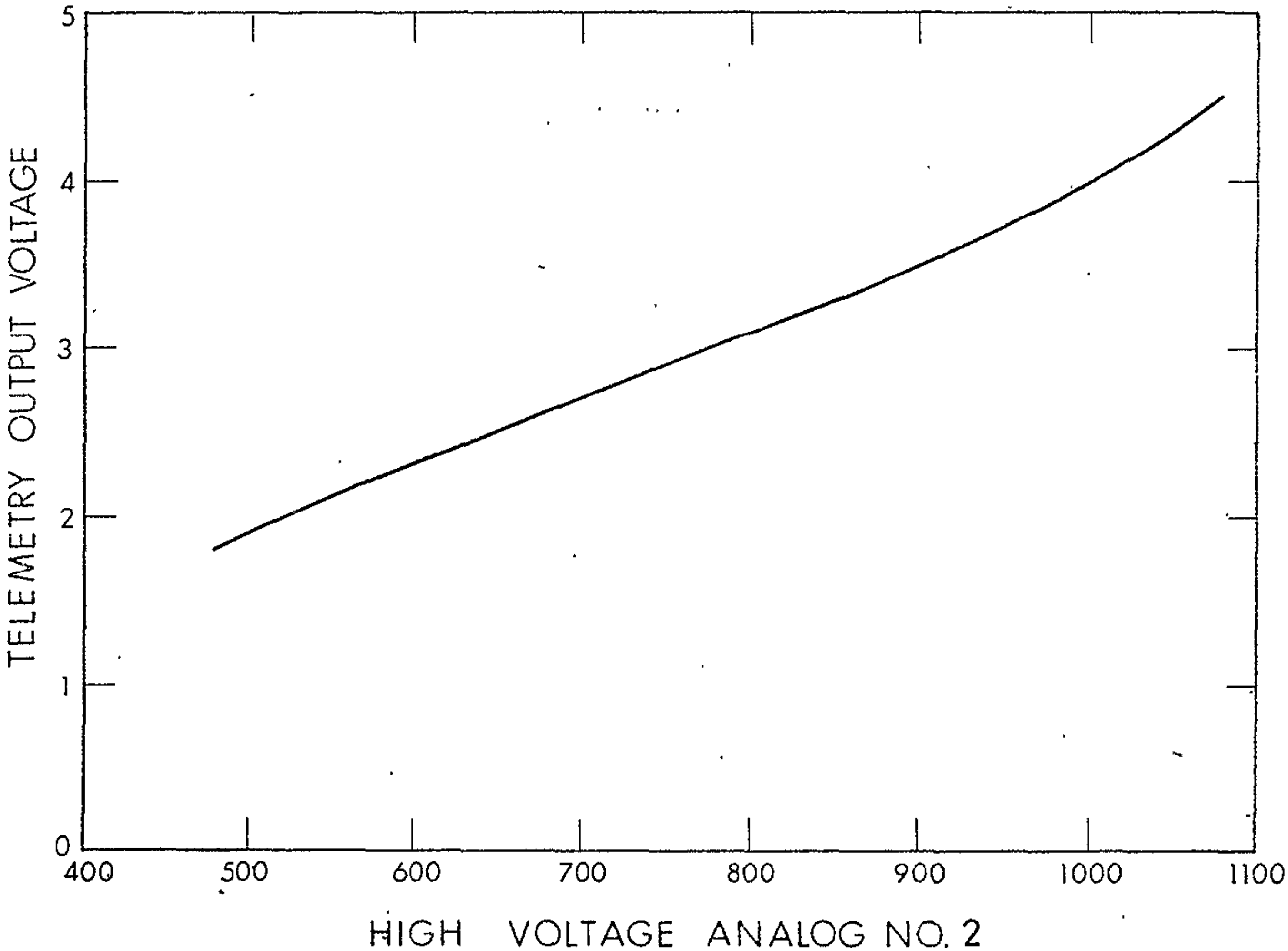

Figure 18. High Voltage Analog No. 2 (0.3 to 0.4 micron channel) versus Telemetry Output Voltage (telemetry channel L-20)

3.2.4.1 Temperature Sensors

Three temperature sensors were used in the reflectometer instrument. Two of the sensors were used on the integrating sphere to monitor the temperature of the solid-state detectors. The third temperature sensor was mounted to the inside surface of the enclosure near the sample mounting points. This temperature sensor was used to monitor the approximate enclosure temperature.

The temperature sensors were thermistors and were used in conjunction with a series resistor to form a voltage divider network. The bias voltage, -8 volts, was supplied to the network from the low voltage power converter. The resistance of the thermistor changed with temperature to control the current flow through the network.

The analog telemetry output voltage was the voltage across the resistor of the network. Figures 19, 20, and 21 show the temperature versus the analog telemetry output voltage for the three thermistors.

3.2.4.2 Pressure Transducer

One pressure transducer was present in the reflectometer package. This unit was provided in order to monitor the internal pressure of the reflectometer enclosure.

An absolute measuring pressure transducer was used as the basic pressure sensing element. This element is a diaphragm type transducer using solid-state strain gauges as the electromechanical interface between diaphragm deflection and electronic signal.

The outputs of the pressure transducer were connected in a bridge network to supply two inputs of a differential operational amplifier. A

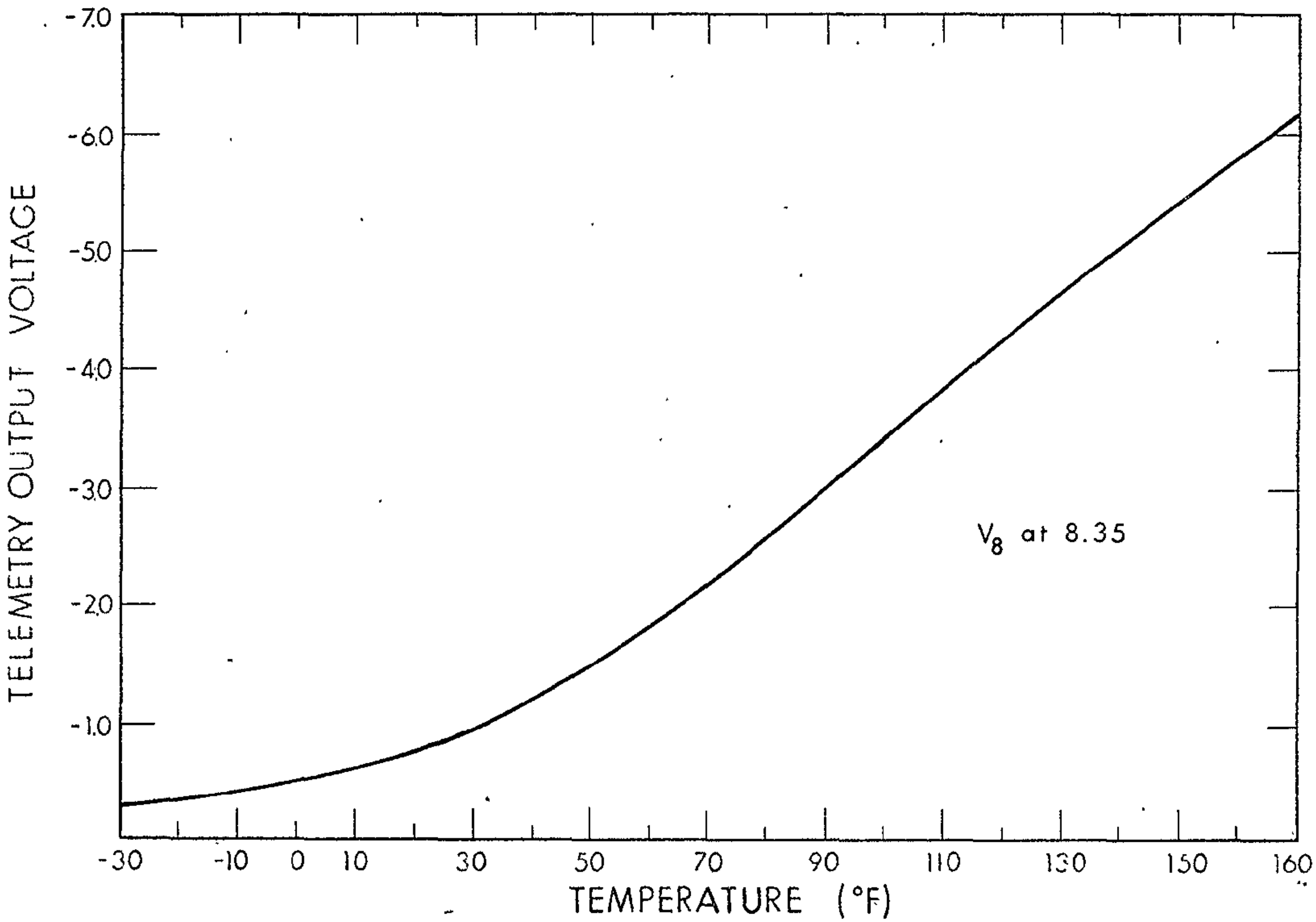

Figure 19. Temperature Sensor VS, Detector Temperature Primary versus Telemetry Output Voltage (telemetry channel L-13)

73628825

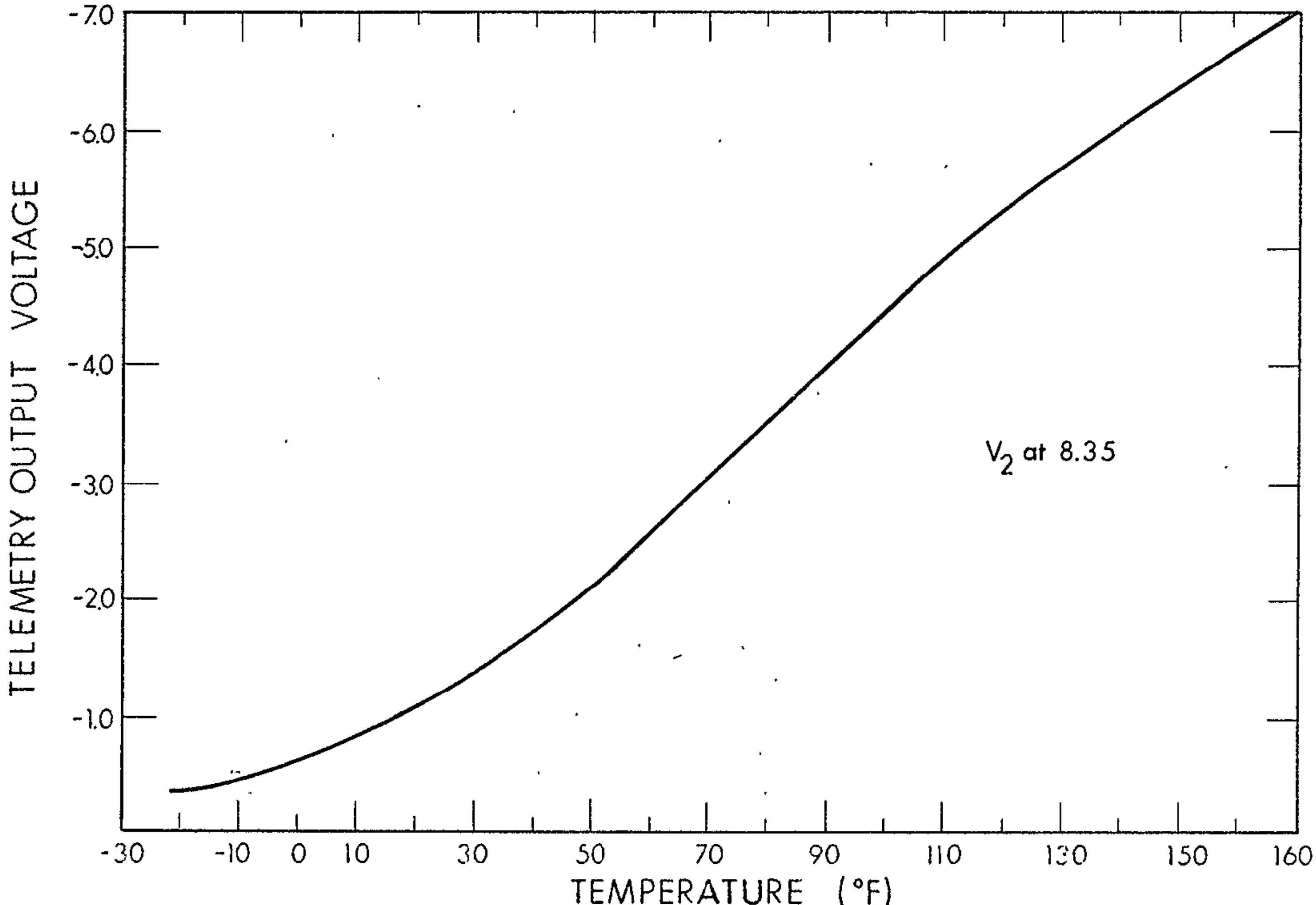

Figure 20. Temperature Sensor V2, Detector Temperature Secondary versus Telemetry Output Voltage (telemetry channel L-9)

73628826

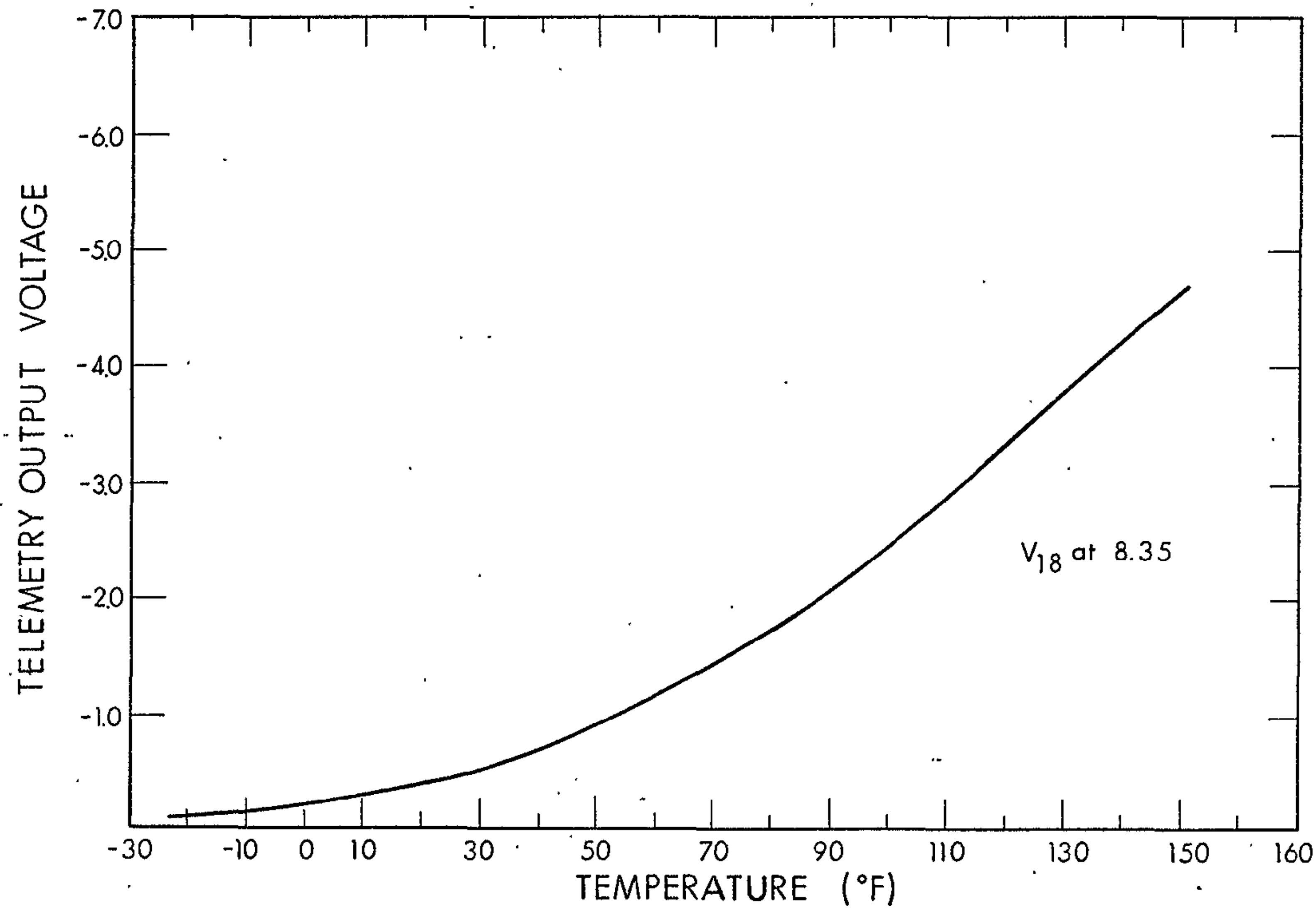

Figure 21. Temperature Sensor V18, Case Temperature versus Telemetry Output Voltage (telemetry channel L-11)

potentiometer was included as part of the bridge to adjust the limits of the pressure transducer output during postassembly system operation.

The output of the operational amplifier supplied pressure transducer analog telemetry data directly to the spacecraft telemetry subsystem. Figure 22 shows the pressure versus telemetry output voltage for the flight unit. Temperature compensation was not used in this circuit; therefore, a family of temperature dependent curves was generated.

3.3 MECHANICAL SUBSYSTEM

The mechanical subsystem was designed to house the optical subsystem and electronics subsystem, to support the reflective samples, and to provide the drive system which rotated the chopper, encoder, and scanner arm.

The housing, machined from a solid block of aluminum alloy, provided the structure to support the various components. Most of the reflectometer elements were inside the hermetically sealed enclosure with the exception of two gears, a pair of bearings, the scanner arm, and the samples and sample mounts. The housing also acted as a heat exchanger between the scanner arm, samples, and spacecraft to maintain a minimum temperature gradient.

The source of power for the drive system was a brushless 24-volt dc motor, operating at 2400 rpm. Power was transferred through a gear train to a harmonic drive assembly which provided an effective dynamic coupling through the hermetically sealed housing enclosure. The output of the harmonic drive drove the reflectometer rotary scanner arm through a spur gear train.

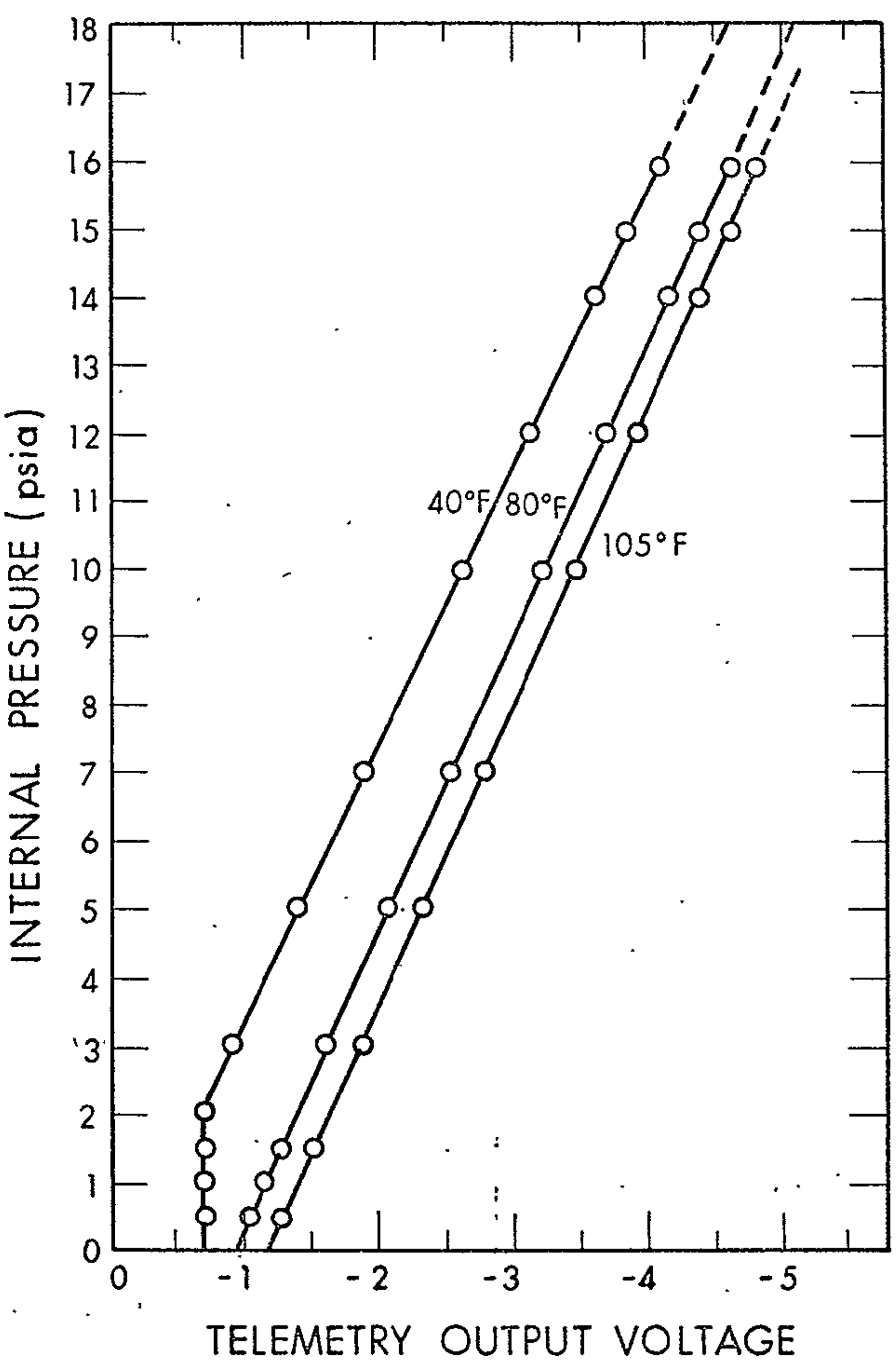

Figure 22. Internal Pressure versus Telemetry Output Voltage (telemetry channel L-18)

73628827

Possibly the most critical portion of the reflectometer instrument design was that of the bearing assembly, drive motor, and rotating arm torque seal. The drive motor and associated bearings were located inside the body of the reflectometer and were thus protected from the space environment. The reflectometer enclosure was sealed to maintain a low leak rate and an internal pressure, during the life of the mission. The internal pressure was maintained at a high enough level to allow the use of conventional lubricants on internal gears and on the motor without contaminating the optics.

The arm bearing system exposed to the space environment consisted of two ball bearing supports mounted sufficiently far apart to provide stability for the rotating arm and to maintain optical alignment. Dry lubricants were provided to prevent damage to the external gears and bearings.

To produce chopping frequency as high as practicable the chopper wheel was driven, through a gear train, at the motor speed of 2400 rpm. Spacecraft inertial properties and gyroscopic couple specification considerations forced a chopper wheel design of essentially a flat disc with 12 equally spaced sharp-edged slots.

Sufficient care was taken in the design of the high speed components and in other moving portions of the system to assure that no spacecraft interface difficulties would arise in the area of applied torques or magnetic fields. When the scanner arm was rotating the spacecraft was subjected to a torque of 13.2 inch-ounces perpendicular to its spin axis and a torque of 0.0039 inch-ounce parallel to its spin axis. The scanner arm was statically balanced to provide a minimum disturbance to the spacecraft.

The weight of the reflectometer in its final flight configuration was 15.26 pounds.

An encoder, driven through a speed reducing gear train, translated the mechanical angular position of the scanner arm into a digital electrical signal. The digital encoder read out the position of the scanner arm with 8-bit resolution.

3.3.1 ENVIRONMENT

The reflectometer was designed and built to withstand all of the launch and space environments. The hermetically sealed enclosure provided maximum protection for all of the high speed mechanical parts, all electronics components and most of the optics. The enclosure also provided a highly conductive thermal path for heat transfer and protection against radiation damage for the electronics and other components. Gears and bearings which were exposed to the space environment were lubricated with solid lubricants and operated at slow speeds in order to eliminate the possibility of cold welding.

Each individual test sample was precisely aligned and mechanically secured at assembly, providing a firm metal-to-metal contact and thereby assuring that the adjustment would not change under vibration conditions. All optical components requiring alignment were adjusted with self-locking screws. The scanner arm bearings were preloaded using bellville washers and shims so that a uniform loading would be maintained during flight.

3.3.2 HERMETIC ENCLOSURE

Figure 23 shows the mechanical subsystem. Because of the complexity of the housing it was decided to machine the unit from a solid block,

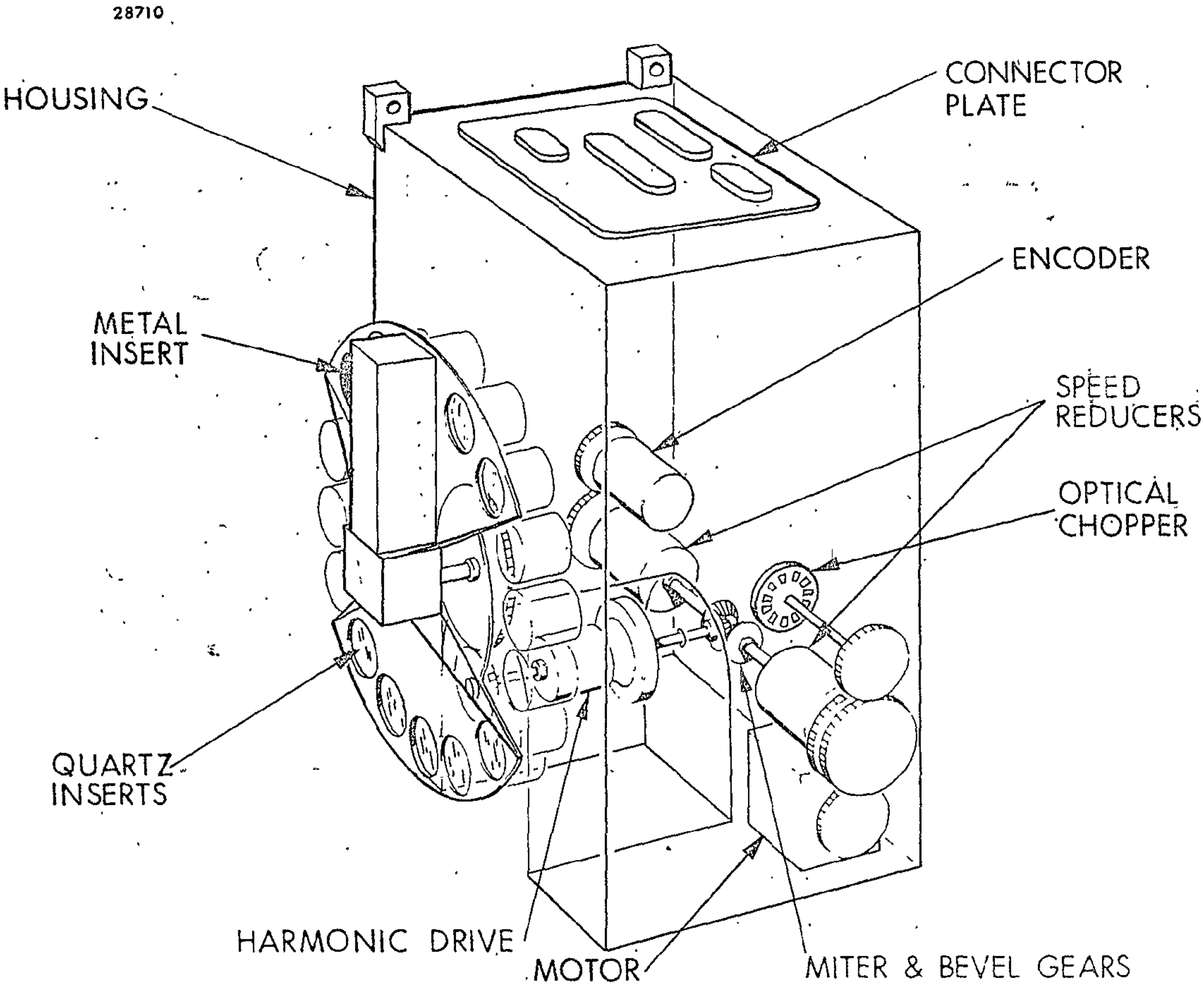

Figure 23. Mechanical Subsystem

thus eliminating welding, heat treating, and other problem areas. A high grade billet, X-rayed and ultrasonically tested for soundness, was machined to the required shape. The number of openings was reduced to a minimum to prevent leakage of the pressurized dry air from the sealed enclosure. Three major openings were required. One opening was used for the lens system, another opening was used for the harmonic reducer, and the third opening was used for the connector plate. The connector plate was sealed by a Teflon-covered metal O-ring and fastened with 14 screws to produce a uniform clamping force on the O-ring, assuring mechanical seal. In addition, a resilient silicon rubber material was used in the joint area and the area near the base of the connectors. Thus, if a leak developed, the silicon material would flow into the gap, closing the leak.

The large component access opening at the bottom was closed by welding the enclosure cover plate in place. Heat sinks were used to draw heat away during the welding process to protect the sensitive electronic components. The bottom cover plate was equipped with a pinch-off tube for final purging and pressurizing.

3.3.3 DRIVE SYSTEM

3.3.3.1 Motor

The source of power for the drive system was a Sperry-Farragut type 590-388 brushless dc motor with the following characteristics:

Volts: 24V dc
Speed: 2400 rpm at 0.1 in.-oz torque
Power: 1.0 watt at 0.1 in.-oz torque
Weight: 6.7 oz

The selection of this drive motor was primarily based upon reliability, speed, performance, and cost.

This motor had the following nonoperational survival characteristics:

Shock:	20g, 20 milliseconds, 3 axes
Acceleration:	20g, 1 minute, 3 axes (20 to 2000 Hz)
RFI:	Conforms to MIL-I-6181D

The unsealed brushless dc motor fit the reflectometer requirements with the exception of a proven reliability program. EOS evaluated the type 590-388 motor by operating it for 1000 hours in conjunction with the reflectometer harmonic drive unit. The operation of both the motor and the harmonic drive unit were found to be satisfactory over this period.

During further testing of the motors (5 tested) it was found that the motor speed had increased. The motors were returned to Sperry-Farragut where they were analyzed and repaired. The motors had apparently received an over-voltage pulse which had demagnetized the motor magnet. The minor hysteresis loop area was increased by improving the magnetization techniques. In addition, zener diode protection was added in the bench checkout equipment and in the instrument to protect the motor from further over-voltage pulses.

3.3.3.2 Gear Train

The brushless dc motor, mounted on the drive train platform, drove a 1:1 spur gear train (see figure 23). The drive spur gear was attached to the drive speed reducer input shaft. The speed reducer (100:1) output shaft drove a miter gear train. The in-line branch of the miter gear train drove the output shaft of a 180:1 speed reducer. This speed reducer drove an encoder through a 1:1 spur gear train. The 90° branch of the miter gear was directly coupled to the harmonic drive.

The harmonic drive provided the rotary interface between the space vacuum and the sealed enclosure. The output shaft of the harmonic drive (speed reduced 72:1) drove the reflectometer scanner arm through a spur gear train. The input end of the harmonic drive was bolted to the housing and a static seal was provided by a metal O-ring.

The scanner arm was suspended on two bearings, enabling scanning of the test samples. A complete description of the various components is provided in the following sections.

Also mounted on the drive speed reducer input shaft with the drive spur gear was a larger spur gear. This larger spur gear drove the optical chopper wheel through a 1:1 spur gear train. The chopper wheel was supported by the drive-train platform.

The chopper wheel was essentially a flat disc with 12 equally spaced sharp-edged slots. To produce as high as practicable chopping frequency for the electronics the chopper wheel was driven at the motor speed of 2400 rpm. However, its inertial properties were kept low so that the total gyroscopic couple was below that specified in the ATS specifications.

As mentioned above, the in-line branch of the miter gear train drove a 180:1 speed reducer which in turn drove the encoder. The encoder provided a means of translating mechanical angular position into a digital electrical signal. Precautions were made in this path as elsewhere to minimize backlash and to provide an accurate positioning device through 360° of rotation. The digital encoder read out the position of the scanner arm with 8-bit resolution providing precise scanner arm position data.

3.3.3.2.1 Solid-Film Lubricant Gears

Chrome-plated, MoS_2-burnished gears have been successfully used on the EGO-POGO for low-speed, moderately loaded gears. In other applications the use of a Duroid idler gear to supply transfer films has been employed. Gears coated with MoS_2 films in a sodium silicate binder worked well on the Mariner IV television camera.

One failing of solid-film lubricants is that should they wear through, welding of the metals might occur. If the Duroid idler gear method is used this failure mode is minimized since the lubrication film is constantly replenished as the gears revolve. If the gears are not revolving during launch, vibration may cause two mating teeth to wear through the film and weld before the film can be replenished. Locking the gears and providing extremely rigid mounts (static deflections of less than 2.5 micro-inches) can minimize the problem.

Through private correspondence with Mr. Charles Vest of Goddard Space Flight Center, it was found that he had operated one set of hard-coated aluminum gears of 48DP, 1-inch thick, 1-1/8 inches in diameter, transmitting a 20-inch-ounce torque load in a vacuum for 1500 hours at 1800 rpm using a Duroid idler for transfer film lubrication. If it were assumed that the reflectometer were operated 16 minutes per day for 3 years, the total required operating life of the gears would be 292 hours. At 1/8 rpm, the total revolutions would be 2190 in 3 years. When this is compared to Mr. Vest's single experiment, and applying a safety factor of 100 because of the inadequate statistical data (one sample), it may be seen that reflectometer gears made of this material would have an expected lifetime of over 100,000 years.

The actual gears used on the reflectometer were made of MoS_2 filled nylon material. These gears have properties similar to those of the Duroid gears. Therefore, approximately the same performance and lifetime would be projected.

3.3.3.2.2 Reflectometer Gears

The spur gears used in the various drive sections were:

a. Motor to 100:1 reducer
b. 100:1 reducer to chopper wheel
c. 180:1 reducer to encoder

These gears were fabricated by Pic Designs Corporation from 2024-T4 aluminum alloy and anodized to provide hard surfaces on the tooth flanks. In addition, these gears were run-in to insure correct mating and proper coating with MoS_2 film. The tolerance standard adopted was class 1 precision for the motor to harmonic drive train and harmonic drive to encoder. The gear attached to the chopper wheel shaft was made of AISI 303 CRES to class 2 precision. The gear attached to the encoder shaft was fabricated from 2024-T4 aluminum alloy to class 3 precision. Class 3 precision gears were also used in the portion of the gear train leading to the scanner arm. The gear train was run-in as a bench system and provided with a dry film lubricant coating of MoS_2 on the internal train and MoS_2-Teflon for the external train.

The speed reducers used in the reflectometer were standard Pic units U2-13 (100:1) and U2-14 (180:1). Their characteristics were:

Rated output torque	65 oz.-in.
Max. output torque	90 oz.-in.
Backlash	30 minutes (max)
Gears	Precision Class 2
Lubricated	Per unit Spec MIL-L-6085 MIL-G-3278
Ball bearings	Per ABEC-5

These assemblies were designed to retain their lubricant over the flight duration under pressurized conditions.

The miter gear used between the 100:1 and 180:1 speed reducers and the harmonic reducer was a type N1-7-A-P2 gear manufactured by Pic. This gear was made of 2024-T4 aluminum alloy to a class 2 precision. The 100:1 reducer shaft imparted the driving force to rotate the miter gear which in turn rotated the harmonic drive and the encoder (through the 180:1 reducer).

The harmonic reducer, Model HDUH100-72-2, was fabricated by United Shoe Machinery, and modified by EOS per EOS Drawing 1100219 to suit the particular application. The input side was bolted to the housing. The output side was supported by a set of precision bearings, enclosed in a housing bolted to the reducer flange. This support was needed to maintain alignment requirements of the unit. Engineering data for the HDUH100-72-2 unit are as follows:

Reduction:	72:1
Torque:	300 in.-oz.
Maximum input:	15,000 rpm
Operating temperature:	$-65^{o}F$ to $+200^{o}F$
Breakable temperature:	$750^{o}F$

The output section (elliptical gear train) of the harmonic reducer was run in a slurry of MoS_2 for 1 hour at a speed of 2400 rpm. The unit was then oven-dried to remove all outgassing products. The gear on the output shaft of the harmonic reducer was a standard Pic gear fabricated from aluminum alloy to precision class 3 tolerance limits.

3.3.3.3 Scanner Arm Assembly

The unsealed scanner arm system used on the reflectometer utilized bearings and a drive as shown in figure 23. The bearings were preloaded with a spring to eliminate play and to keep the reflectometer scanner arm rotating in a true plane. A MoS_2 solid-film lubricant was used in the gear train drive by separating the two aluminum gears with a filled nylon gear and used on the bearings by means of filled nylon separators. The solid-film lubricants have low outgassing characteristics which is an important consideration due to the close proximity of the reflecting surfaces and other optical elements.

3.3.3.3.1 Bearings

The main bearing system for the support of the scanner arm and harmonic drive consisted of four bearings: two for the scanner arm (type 3TWG 49-62 and 21-28), and two for the harmonic drive (type 3TWG 21-28). These items were standard parts manufactured by Miniature Precision Ball Bearing Company. To ensure optical alignment, ultra-precision grade (ABEC-3) bearings were used. In addition, MoS_2-filled Teflon was used as the ball separator and dry film lubricant source. The bearings were also shielded to maintain cleanliness.

The bearings were run in for 2 hours at 400 rpm maximum speed. This process produced a thin uniform layer of the solid lubricant on the raceways and balls.

3.3.3.3.2 Scanner Arm Gears

The gear on the scanner arm was fabricated from aluminum alloy to class 3 precision tolerances. The idler gear driving the scanner arm gear was a class 1 precision gear made from Nylatron GS material.

The MoS_2 filled nylon idler gear in mesh with the driver gear provided lubrication and transmitted the driving force. Correct engagement was determined by bench tests to reduce the backlash to minimal proportions.

3.3.4 INTERNAL ALIGNMENT

One of the prime requirements for a successful mission was to assure the accurate and continued alignment of the optical components. The basic design philosophy was to provide an absolute minimum of alignment adjustments. Alignment of most mechanical components was assured by "machining in" the required alignment. Where adjustments were required, they were provided by the use of adjustment screws.

A significant contribution to the success of the project depended upon the accurate alignment of the samples during the life of the experiment. It was imperative that the sample mounts be insensitive to distortion and temperature gradients. To accomplish the latter it was necessary to utilize a material with a maximum thermal conductivity and cross section. The optical design permitted ±1 degree of sample misalignment from the nominal position before vignetting occurred at the system lens. The sum of the two arm mirror errors was held to under 1/2 degree in any plane. However, sample adjustment could have been used to compensate for arm mirror misalignments.

The lower face of the sample mount had a spherical recess to provide a pivotal seat for a ball bearing at the center in order that the mount could be adjusted in any direction. Three small screws (2-52) locked the mount in position over the ball bearings as well as provided the adjustment device. By this method, alignment in the assembled condition was practical, and mechanical rigidity was maintained during all vibration and thermal environments.

The plate upon which the test samples were mounted was stiffened by a skirt for attachment on the outside, and the bearing wall on the inside, providing a rigid section. The plate or platform was riveted to the housing structure for additional stiffening.

3.4 INSTRUMENT MALFUNCTION

After slightly more than two years of operation in space the reflectometer instrument failed to respond to a Motor On command. This occurred on December 8, 1969. All of the other functions appeared to be operating including the voltage supplies, analog output channels, and temperature and pressure sensors. A similar malfunction had been noted in the engineering model unit which had been maintained at EOS for flight model support testing and storage. The first conclusion reached with each of these malfunctions was that a circuit failure had occured. However after the failure occured in the flight model the engineering model failure was further investigated. This investigation showed that all of the circuitry which controlled the voltage to the motor was operating properly. However, the motor was not responding to the voltage applied to its terminals. The failure in the engineering model took the form of an intermittence. The flight model failure however, was constant and the unit did not respond to further commands after the initial failure. Further investigation of the engineering model unit revealed that the motor was not capable of handling the initial startup conditions.

Investigation of the gears and gearing structure associated with this system did not indicate any unusual conditions. A small build up of dry film lubricant was noted surrounding the areas where the gears meshed; however, all of the mechanical transmission system appeared to operate smoothly and without a noticable increase in startup or operating torque. When the motor was commanded on and manually started the motor was capable of driving the system through one revolution without any noticable change in speed. The eight minute rotation period which was designed into the system was still within fifteen seconds of being accurate. This precluded any major malfunction in the system drive mechanism. The operating load had not increased sufficiently to reduce the speed of the motor and the gearing appeared to be free prior to the application of power to the motor. The problem appeared to be with the startup characteristics of the motor.

Sperry-Farragut type 9821 brushless d-c motors had been used successfully in various programs at Goddard Space Flight Center. The motor selected for use in the reflectometer was similar to the type 9821 and was considered to be a highly reliable motor. In addition to this, EOS evaluated the type 590-388 motor by operating it for 1000 hours in conjunction with the reflectometer harmonic drive unit. The operation of both the motor and the harmonic drive unit were found to be satisfactory over this period. Further evaluation of the motor, following the motor harmonic drive test resulted in a malfunction in each of the five motors which were being tested. This malfunction is discussed in paragraph 3.3.3.1. The evaluation of this malfunction indicated that all of the motors had been subjected to an over voltage which had partially demagnitized the motor magnet. This had caused the motor speed to increase. The motors were repaired by Sperry-Faragut and the magnitization technique was improved to reduce the susceptibility of the motors to this type of failure. EOS also incorporated protective devices in the electronic circuitry to prevent a reoccurance of this problem.

An investigation of the facts associated with each of the three failures, the origional magnetics failure, the engineering model failure, and the flight model failure would lead to two possible conclusions. The first, and I believe least likely, would be a failure of the magnetics of the motor. This failure mode only gains merit because of the origional magnetics failure. The time sequencing associated with the engineering model and the flight model failures lead to the suspicion that the failure was due to a time degradation of some component within the motor. Because of the apparent normal operation of the engineering model after startup the possibility of degradation of magnetics in the motor does not seem plausible. The only explanation which would explain both the failure of the flight model and the engineering model would be a degradation in the optical commutation section of the motors. The motor design utilizes a solid state light source and a phototransistor to provide the motor commutation. If one of these devices degraded with time it would impair the startup characteristics of the motor but would, under marginal conditions, continue to drive the motor at the designed speed and with sufficient output torque to maintain the system operation after startup.

Under normal conditions a motor failure of this nature would warrant further investigation to firmly establish the cause of the failure and to prevent a recurrence in the future. This does not seem warranted at this time however because this line of motor is no longer being manufactured by Sperry.

SECTION 4

TEST AND CHECKOUT

4.1 QUALIFICATION AND ACCEPTANCE TEST

A fully assembled prototype reflectometer was subjected to environments and tests similar to those specified in NASA document ATS S2-0101, "Environmental Qualification and Acceptance Test Specification, Spacecraft Testing." The actual testing performed is detailed in EOS Report 7003-TP-1, "Design Qualification Test Procedure." The humidity test was eliminated from the program, with NASA aaproval, because of the possible long term degradation effects on the test samples. Since the prototype was being utilized as a flight backup, such degradation would render it unsuitable for that purpose. All other tests were performed satisfactorily; only minor discrepancies were noted.

The flight unit was also subjected to environments and tests similar to those specified in NASA document ATS S2-0101. The actual testing performed is detailed in EOS Report 7003-TP-2, "Acceptance Test Procedure." All tests were satisfactorily completed by the flight unit before delivery to the spacecraft contractor.

Electronic testing of the reflectometer was performed with the use of specially designed bench checkout equipment (BCOE) (see figure 24). The BCOE is described in detail in Appendix I.

4.2 SPACECRAFT GROUND TEST

Long form and short form system performance tests were performed on the reflectometer after it had been installed on the ATS-C spacecraft. These

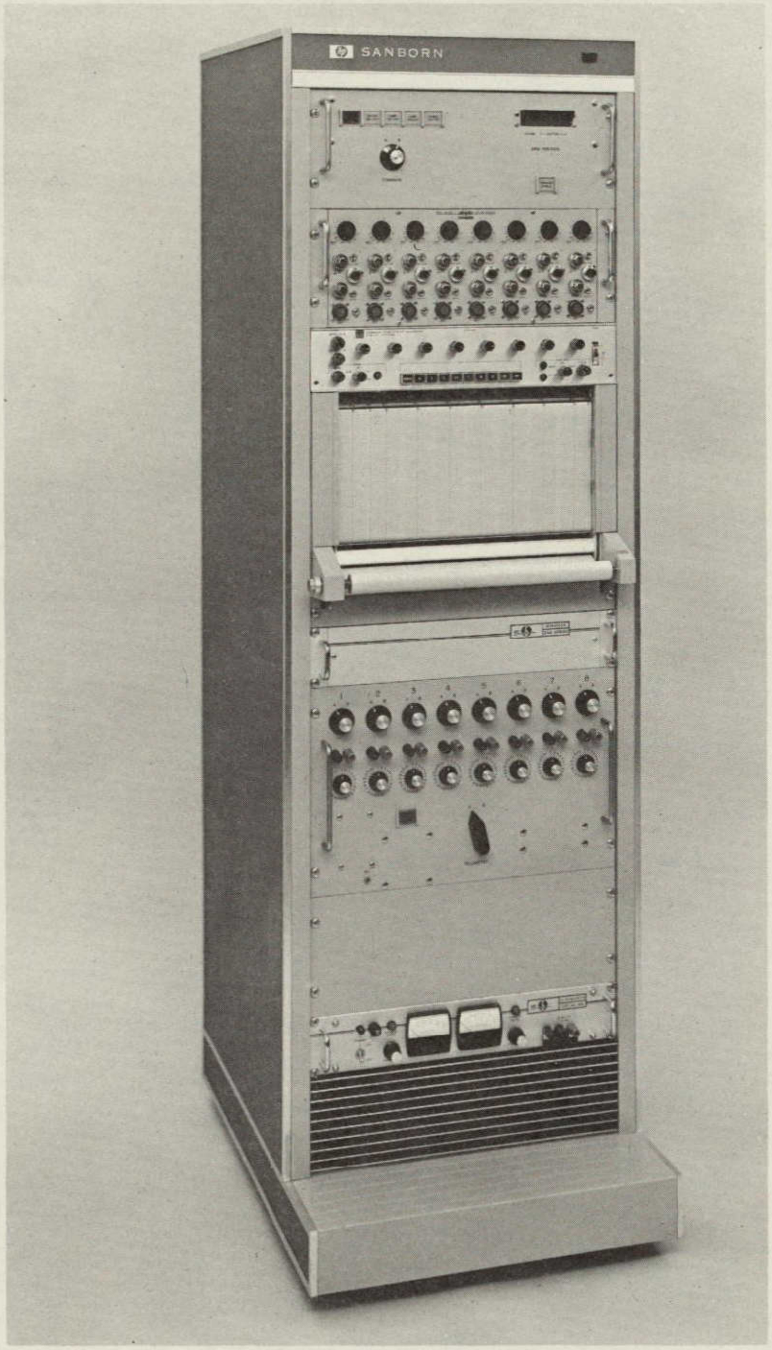

36756

Figure 24. Bench Checkout Equipment

tests were performed by Hughes Aircraft personnel using Hughes-generated test procedures. These procedures were based on EOS Reports 7003-TP-19, "Long Form System Performance Test Procedure," and 7003-TP-20, "Short Form System Performance Test Procedure." The long form tests were performed before and after spacecraft environmental tests, and short form tests were performed during environmental tests.

The short form test was designed to determine whether or not the reflectometer was acceptable for space flight. This was determined with one revolution of the scanning arm; all systems were checked during this one revolution. The two spacecraft command decoders and telemetry subsystems interfacing with the reflectometer were also tested during this period.

The long form test was also designed to determine that the reflectometer was acceptable for space flight. The primary difference was that the long form test required one complete revolution of the scanning arm to test lamp A, command decoder 1, and telemetry 1 and another complete revolution to test lamp B, command decoder 2, and telemetry 2.

4.3 FLIGHT OPERATIONAL TEST

The reflectometer was operated while in orbit in accordance with EOS Report 7003-TP-28, "Flight Operational Test Procedure" (see Appendix II). This procedure outlined the functional tests required prior to and during operation of the reflectometer. Data obtained during this phase was used to evaluate system performance and to provide scientific data regarding space environment effects on the reflective samples. The instrument operated for slightly over two years in space prior to a malfunction of the drive system.

SECTION 5

DATA REDUCTION AND CONCLUSIONS

The basic function of the reflectometer was to acquire data which, when analyzed, provided information on the extent and causes of specular surface degradation resulting from long-term exposure to the space environment. The data required for analysis of both extent and causes include not only reflectometer sample parameters, but supplementary information which includes real-time and reference data.

5.1 PRIMARY DATA ACQUISITION

The total reflectivity data consist of a single broadband (white light) reflectivity measurement, four spectral reflectivity measurements, and a scanner position readout (see Table 2). The bandwidth of the white light measurement is essentially that of the tungsten lamp source modified by the spectral response of the lead sulfide detector. The four spectral reflectivity measurements cover the range from 0.3 micron to 3.0 microns. In effect, the five reflectivity measurements are mutually redundant in that the loss of any one channel causes no significant loss in data.

The essential reflectivity data are contained in the broadband measurement which extends roughly from 0.3 micron to 3.0 microns. This measurement provides an indication of the overall reflectivity of a sample. The other four spectral reflectivity measurements supply additional information concerning the condition and mode of decay of the specular reflectance surface.

TABLE 2

REFLECTOMETER TELEMETRY DATA

Item	Function
L-1	Regulator ON/OFF
L-2	Broadband reflectivity
L-3	Spectral reflectivity (0.3-0.65 micron)
L-4	Spectral reflectivity (0.65-1.2 microns)
L-5	Spectral reflectivity (1.2-3.0 microns)
L-6	Spectral reflectivity (0.3-0.4 micron)
L-7	Scanner position
L-8	Home Switch Position
L-9	Detector temperature secondary
L-10	Amplifier range
L-11	Case Temperature
L-12	(not used)
L-13	Detector temperature primary
L-14	Detector bias voltage
L-15	High voltage analog No. 1
L-16	Bias voltage No. 1
L-17	Bias voltage No. 2
L-18	Pressure, internal
L-19	Lamp voltage
L-20	High voltage analog No. 2

End-to-end calibration of each of the reflectivity channels was accomplished once during each cycle of the scanner arm when the full scale and 0 percent reflectivity samples were measured. Thus the effects of dc drifts, such as long-term lamp intensity decay or transmissivity losses in the optics, were reduced to negligible levels.

Scanner position was measured with an 8-bit digital shaft position encoder which provided an angular resolution of 1.4 degrees ±0.25 degree. The ±0.25-degree tolerance (mainly attributable to the backlash in the drive system) is equivalent to an arc length of about 0.023 inch along the circumference of the scanned circle. The angular resolution, therefore, is less than 1/11 the width (1/4-inch) of the interrogating light beam and 1/33 the effective length (3/4-inch) of the reflective samples. This degree of angular resolution allowed observation of localized effects on the sample (e.g., the local effect of a collision with a relatively large micrometeoroid).

The five reflectance channels and the scanner position were each sampled by the telemetry main multiplexer once every frame (i.e., nominally 1 sample of each channel every 2.97 seconds). The scanner rotational rate was approximately 0.75 degree/second and the sample time (i.e., the time during which the telemetry multiplexer is actually reading in data) was nominally 46.26 milliseconds per word.

Hence, during the sample time, the scanner rotated through an angle of about 2.07 minutes of arc. Since the five reflectivity channels were connected to adjacent channels on the multiplexer, the total angular spread per data sample was 10.4 minutes of arc.

5.2 SUPPLEMENTARY DATA

To correlate causal factors with any adverse effects indicated by the reflectivity measurements, some description of the spacecraft environment was needed. Explicit real-time measurement of certain environmental parameters (e.g., charged particle dose rates, ultraviolet radiation, and micrometeoroid flux) was not considered feasible in the instrument because of cost, weight, and power considerations. Qualitative information was obtained, however, regarding the deleterious effects of environmental parameters through the selective shielding of samples.

To assure that the instrument was operating properly, several housekeeping measurements were made. These are specified in Table 2 and include principal voltages, internal pressure, and temperature.

5.3 DATA PROCESSING AND REDUCTION

The ultimate form of the reflectivity data is a graphic presentation of sample reflectivity versus time. The raw data taken from the reflectometer are nearly in the correct form for such a graph. A series of very simple arithmetic operations needed to be performed, but, because of the relatively large number of such calculations, they were performed on a digital computer.

The raw data from each of the reflectivity channels was a voltage (0 to -5 volts) which was proportional to the reflectivity of the surface being monitored. To eliminate the dc drift errors (caused by such factors as source lamp aging), the data from the experimental samples were compared with the data from the zero percent and full-scale standard samples. The specular reflectivity of each of the test samples was calculated from the following equation:

$$R_s = \frac{V_s - V_o}{V_{fs} - V_o} \quad (1)$$

where

R_s = test sample reflectivity

V_s = applicable test sample reflectivity signal voltage (volts)

V_{fs} = applicable full-scale sample reflectivity signal voltage (volts)

V_o = applicable zero sample reflectivity signal voltage (volts)

One of the computer computations, therefore, was the solution of Eq. 1 for every reflectivity data point recorded. With a nominal instrument scanning rate of 8 minutes per revolution and a telemetry frame rate of 1 sample every 3 seconds there were a total of 160 data samples per channel per revolution. Thus, for the five reflectivity channels there were 800 data samples per revolution. Equation 1 was solved for each data sample.

Not all of the recorded data points were from usable portions of the experimental samples. Some data include the nonreflective space between samples and the edges of the samples. Experimental samples exhibit some edge effects within approximately a 0.125-inch-wide ring around the edge of the sample.

Another computer operation was required to translate the output of the shaft position channel (gray code encoder) into a meaningful number in terms of experimental sample positions. The position channel, in digital format, was compared with a stored tabulation of scanner position relative to the sample positions. If a given data point was recorded while the scanner was within a useful region of a sample, all of the reflectivity measurements associated with that data frame were appropriately identified. The first level of data analysis was performed using these most significant measurements. Each experimental sample has five curves associated with it: the white light reflectivity and the four spectral reflectivities, all plotted against time.

The objective of data analysis is to determine, from the accumulated data, the extent and cause of any detected surface degradation and to develop appropriate conclusions regarding the utility of the tested materials in space system applications.

Table 3 describes each of the samples flown on the reflectometer. The prelaunch reflectance values of the samples are shown in Table 4 and are arranged in matched pairs where possible. Identical samples nominally have identical initial optical reflectance values; however, Table 4 illustrates several discrepancies between the sample reflectances prior to launch. These were apparently due to preparation differences and differences in prelaunch exposure.

Mechanical details of a typical sample and the relationship of the samples to the instrument are shown in EOS Drawing 1100241, Appendix III.

TABLE 3

LIST OF REFERENCES AND SAMPLES

Sample Number	Coating	Reflecting Surface	Undercoat	Substrate	Source[a]
1	(100% reference) Second Surface mirror				
3	(0% reference) Black anodized grooved Al				
7, 12*	SiO_2, 12λ/4[b]	Al	Cr/SiO	Ni	C
17,20*	SiO_2, 12λ/4[b]	Al	SiO	Quartz	C
16	Al_2O_3, 12λ/4[b]	Al	SiO	Al	C
2*,4	SiO_x (0.17μ)	Al	Cr/SiO	Ni	A
18A, 19A*	SiO_x (0.17μ)	Al	SiO	Al	A
9*,15	$(Si_2O_3)_x$ (1.2μ)	Al	SiO	Mg + epoxy	E
13*,14	Alzak	Al	None	Al	D
6	none	Al	1/2 mil Mylar	Al	B
5, 11*	none	Al	Cr/SiO	Ni	A
18B, 19B*	none	Al	SiO	Al	A
8, 10*	MgF_2, 2λ/4[b]	Ag	Cr	Ni	D

* Indicates those samples that are shielded.
[a] Lettering indicates laboratory that supplied the sample.
[b] Coating thickness expressed in terms of quarter waves at 550 nm.
A - Electro-Optical Systems, Pasadena, Calif.
B - NASA-Langley Research Center, Langley Station, Hampton, Va.
C - Night Vision Laboratory, Ft. Belvoir, Va.
D - NASA-Goddard Space Flight Center, Greenbelt, Md.
E - NASA-Lewis Research Center, Cleveland, Ohio.

TABLE 4

INITIAL VALUE OF RELATIVE REFLECTANCE R,
FOR EACH SAMPLE, ARRANGED IN PAIRS

Sample Number	Reflectivity Spectral Channels				
	0.3-0.4μ	0.3-0.65μ	0.65-1.2μ	1.2-3.0μ	0.3-3.0μ
2*	0.85	0.99	0.92	0.94	0.93
4	0.82	0.91	0.90	0.90	0.91
5	1.03	0.92	1.02	1.03	1.06
11*	1.03	0.99	1.02	1.03	1.04
6	1.03	0.89	1.06	1.10	1.11
7	1.04	0.87	1.07	1.05	1.06
12*	0.95	0.94	0.96	0.96	0.96
8	0.84	0.95	1.01	1.00	1.01
10*	0.77	1.00	1.02	1.03	1.05
13*	0.81	0.80	0.86	0.85	0.85
14	0.83	0.80	0.90	0.90	0.90
9*	0.45	0.63	0.82	0.91	0.90
15	0.45	0.63	0.91	1.06	1.06
16	0.95	0.85	1.03	1.09	1.10
17	1.08	0.93	1.04	1.07	1.08
20*	1.03	1.00	1.00	1.01	1.01
18A	1.12	0.98	0.98	0.98	0.99
19A*	1.09	1.00	0.96	0.95	0.96
18B	1.16	0.96	1.03	1.01	1.00
19B*	1.16	1.00	1.00	0.97	0.98

*Indicates samples that are shielded.

5.4 EXPERIMENT CONCLUSIONS

5.4.1 SUMMARY OF REFLECTANCE DATA

Curves of sample reflectance versus time in orbit are shown in figures 25 through 44. Many of the data points recorded during the first few weeks of flight have been omitted in order to improve the visual clarity. The order of listing is by pairs of samples, one shielded and one unshielded. The listing and description of the pairs are found in Table 3.

The sample pairs are grouped as follows:

Group I - Uncoated aluminum (various undercoats and substrates), Samples 6, 5, 11, 18B, and 19B

Group II - SiO_2 coated aluminum, Samples 7, 12, 17, and 20

Group III - SiO_x coated aluminum, Samples 2, 4, 18A, and 19A

Group IV - Alzak, Samples 13 and 14

Al_2O_3 coated aluminum, Sample 16

$(Si_2O_3)_x$ coated aluminum, Samples 9 and 15

MgF_2 coated Ag, Samples 8 and 10

A discontinuity in the reflectivity data for the 0.3 to 0.4 micron channel and the 0.3 to 0.65 micron channel was observed on approximately 20 November 1967. The discontinuity was very noticeable for samples with low reflectivity in the 0.3 to 0.65 micron range. A review of the data indicated that lamp B had been used through 20 November 1967 and that lamp A was primarily used thereafter with some noticeable exceptions. Low data points appear on the data plots on days when lamp B was used, which confirmed the correlation between lamp selected and data output. The lower reflectivity indication during lamp B operation was apparently caused by noise on the zero percentage sample output.

FOLDOUT FRAME 1

FOLDOUT FRAME 2

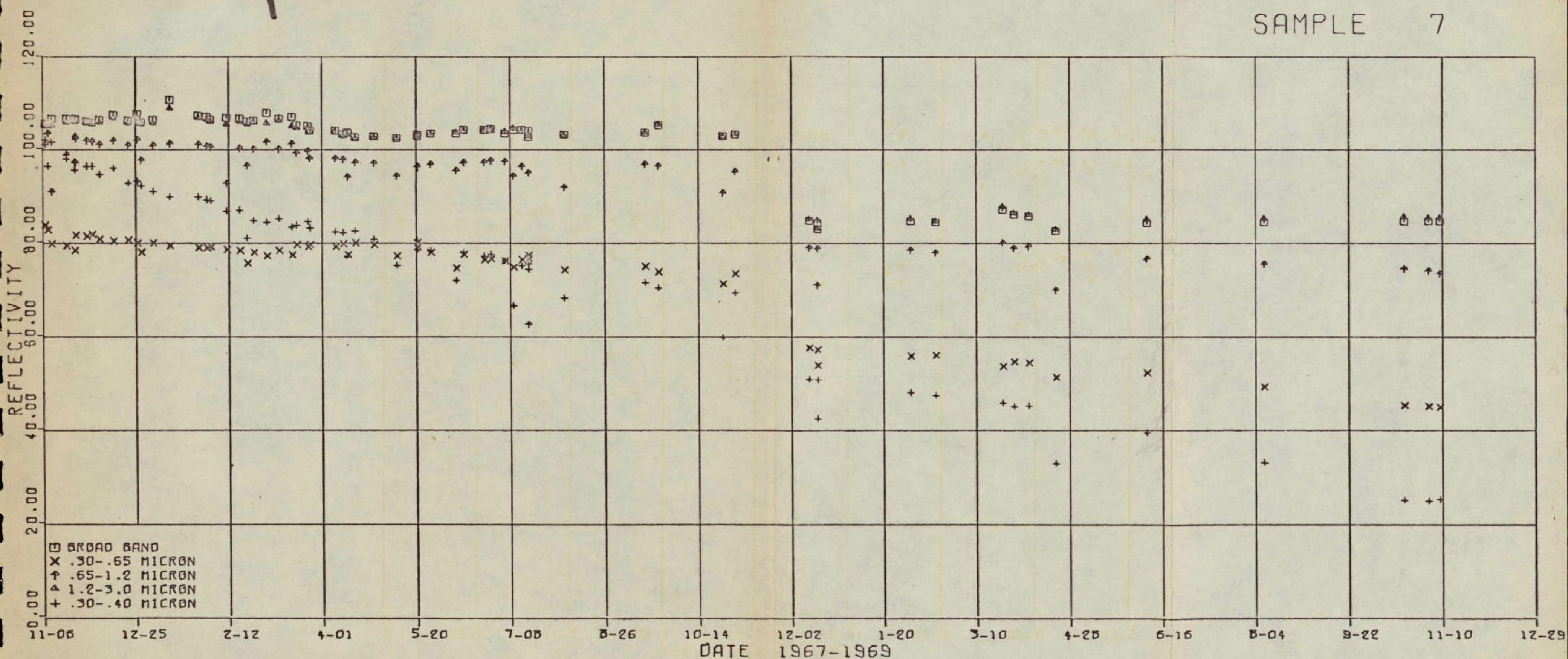

Figure 25. Sample 7, Unshielded

FOLDOUT FRAME 1

NOT REPRODUCIBLE

FOLDOUT FRAME 2

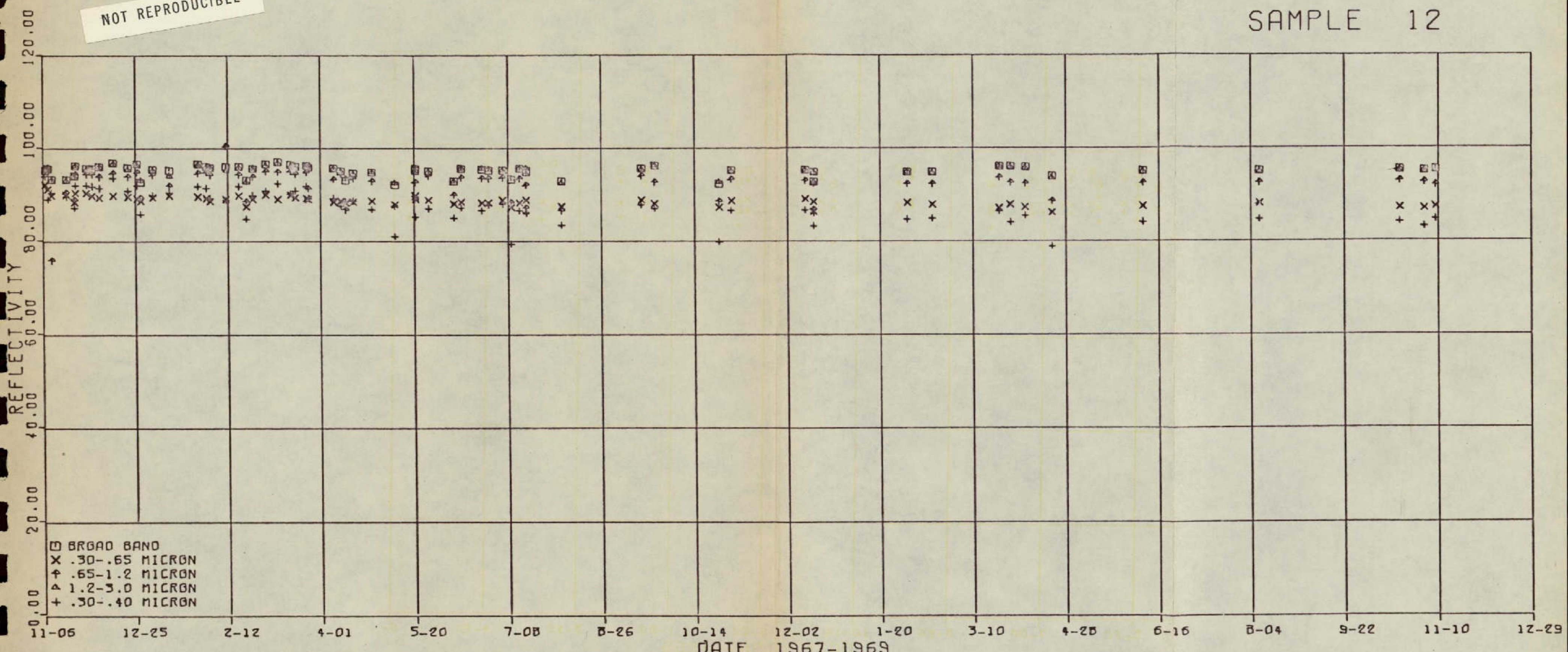

Figure 26. Sample 12, Shielded

FOLDOUT FRAME 1

FOLDOUT FRAME 2

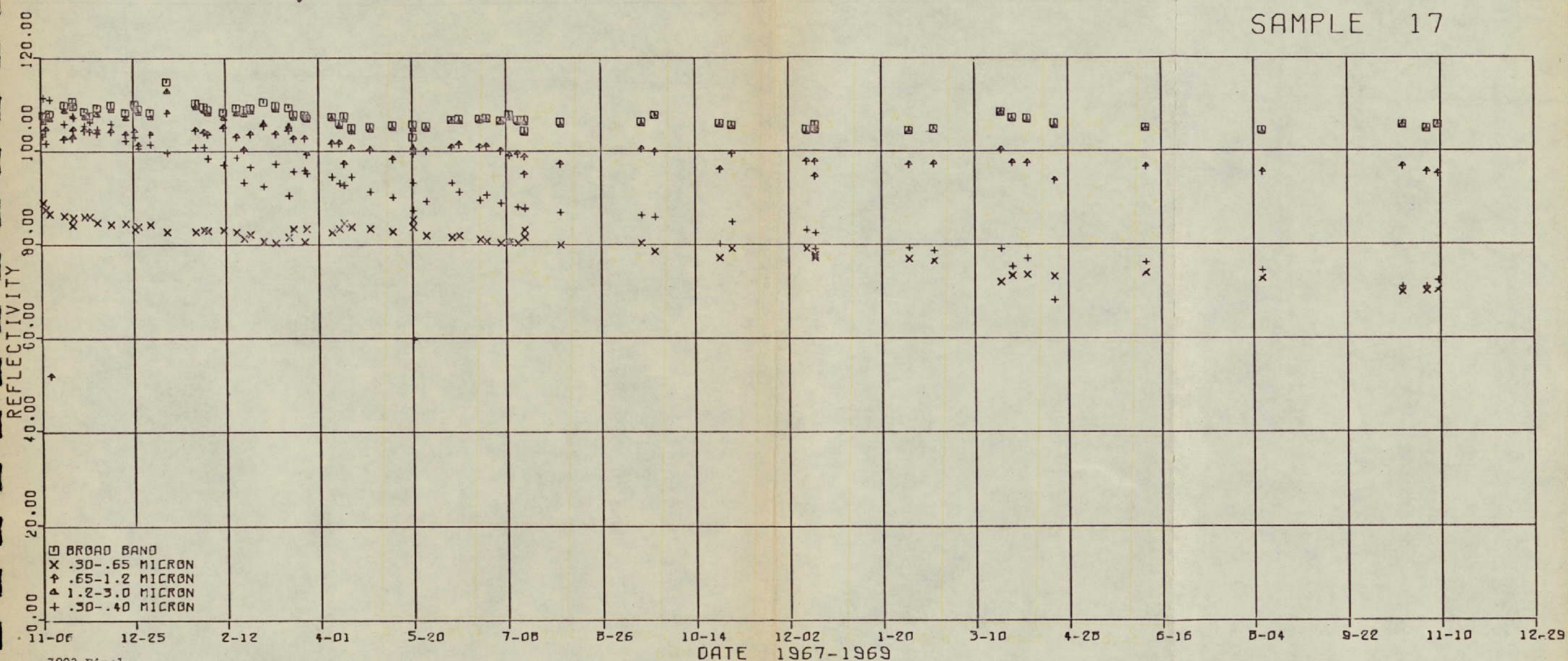

Figure 27. Sample 17, Unshielded

FOLDOUT FRAME 1

FOLDOUT FRAME 2

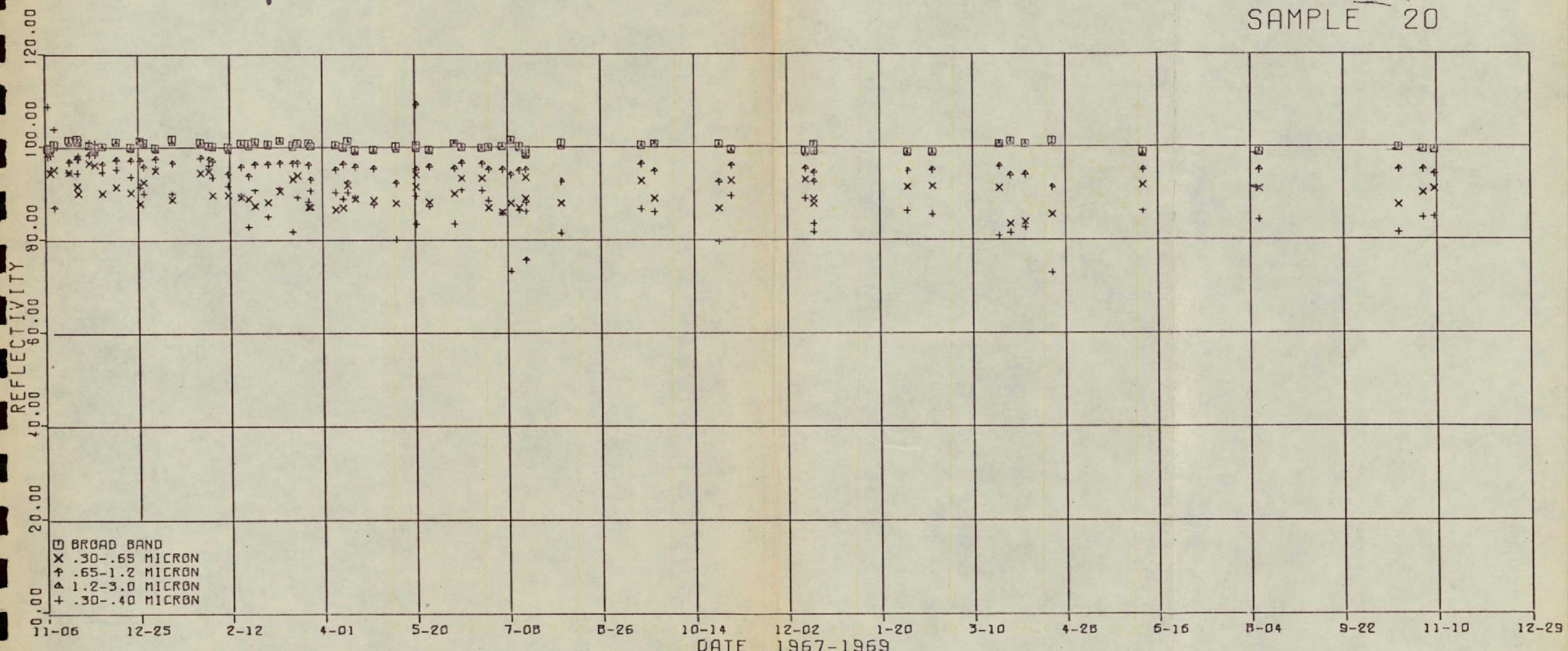

Figure 28. Sample 20, Shielded

FOLDOUT FRAME 1

FOLDOUT FRAME 2

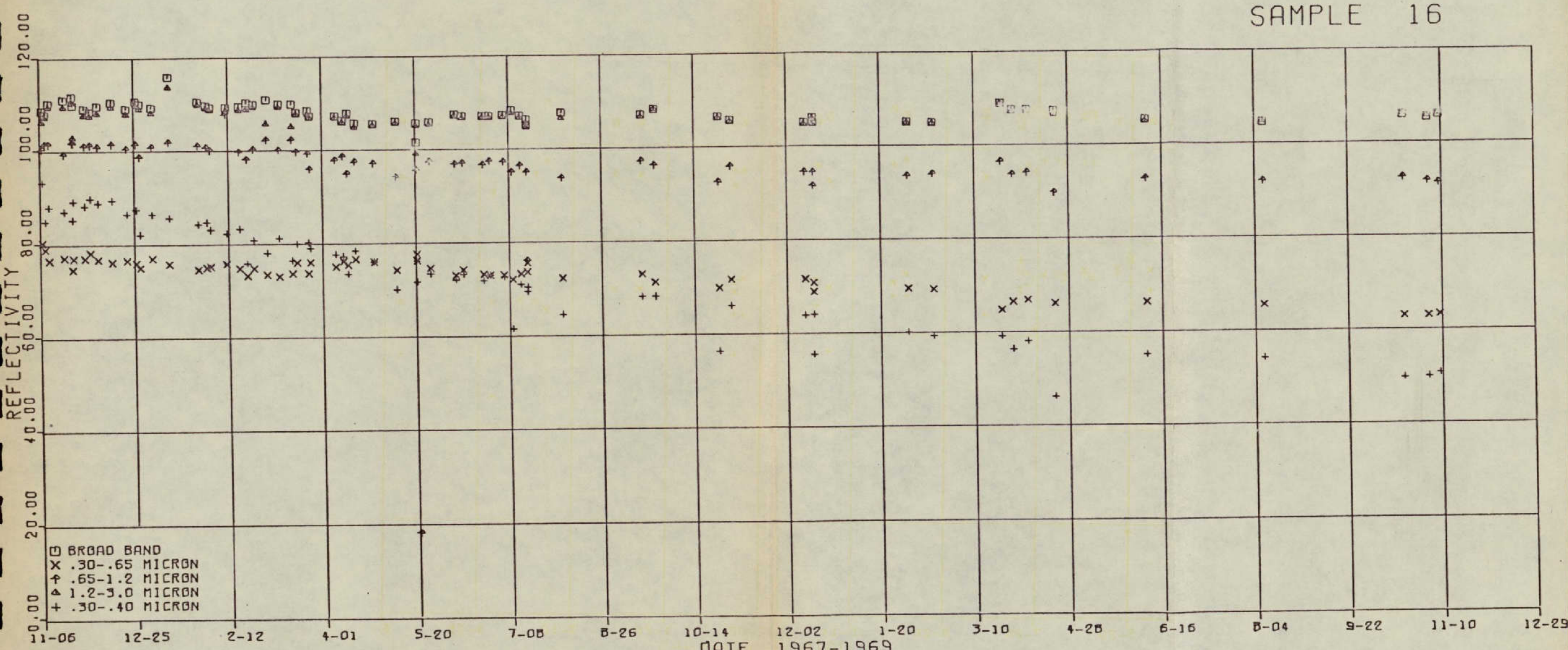

Figure 29. Sample 16, Unshielded

FOLDOUT FRAME 1

FOLDOUT FRAME 2

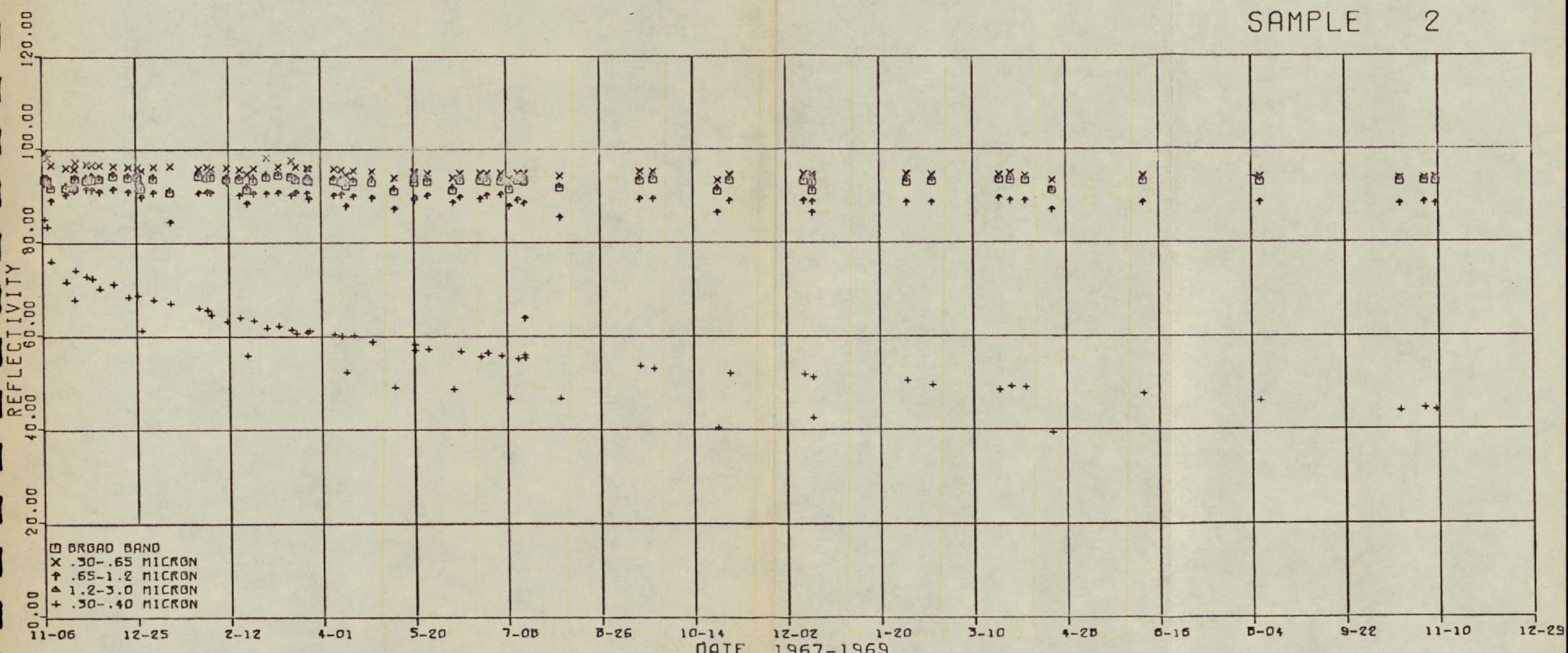

Figure 30. Sample 2, Shielded

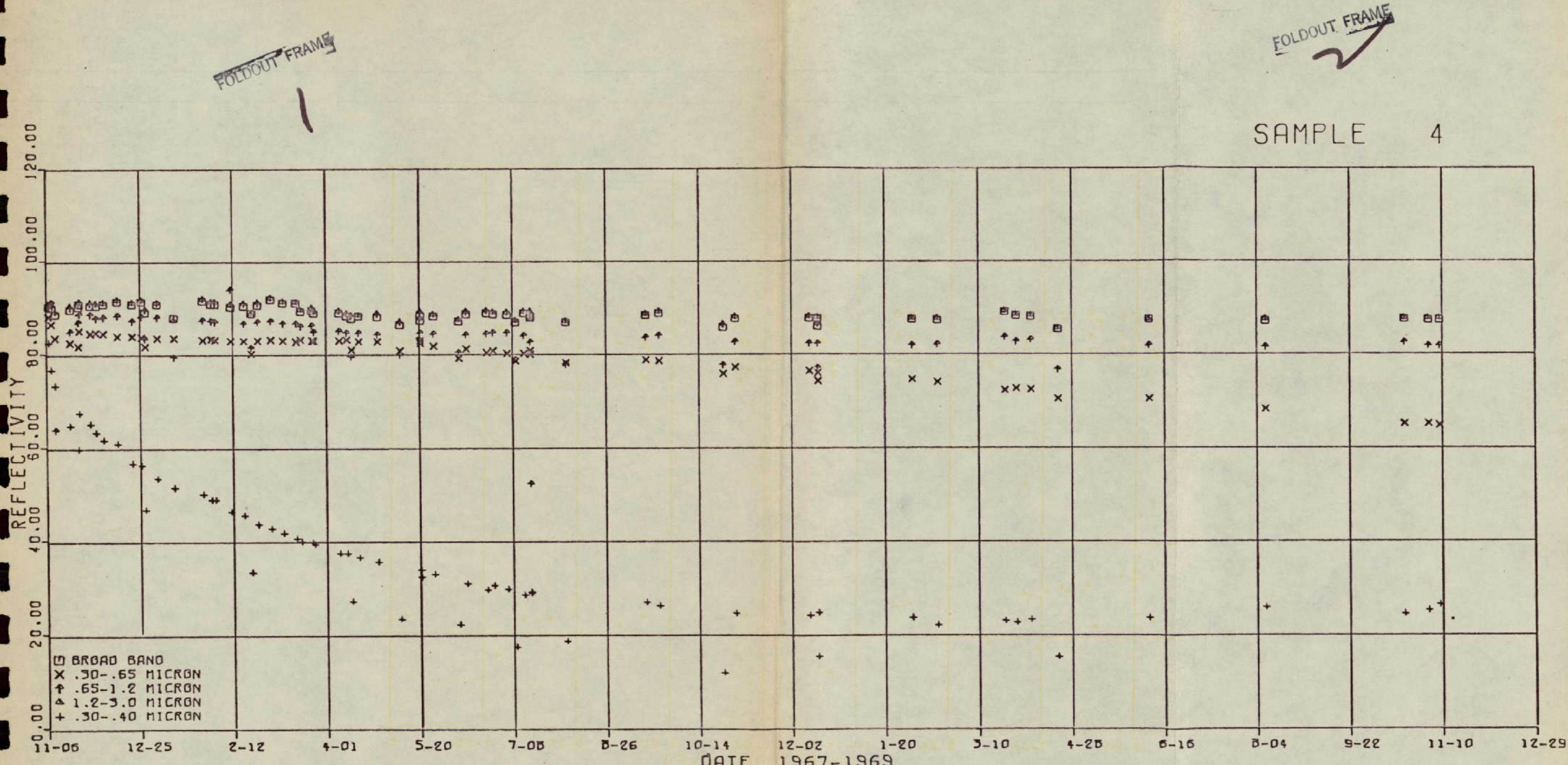

7003-Final

Figure 31. Sample 4, Unshielded

FOLDOUT FRAME 1
NOT REPRODUCIBLE
FOLDOUT FRAME
FOLDOUT FRAME 2

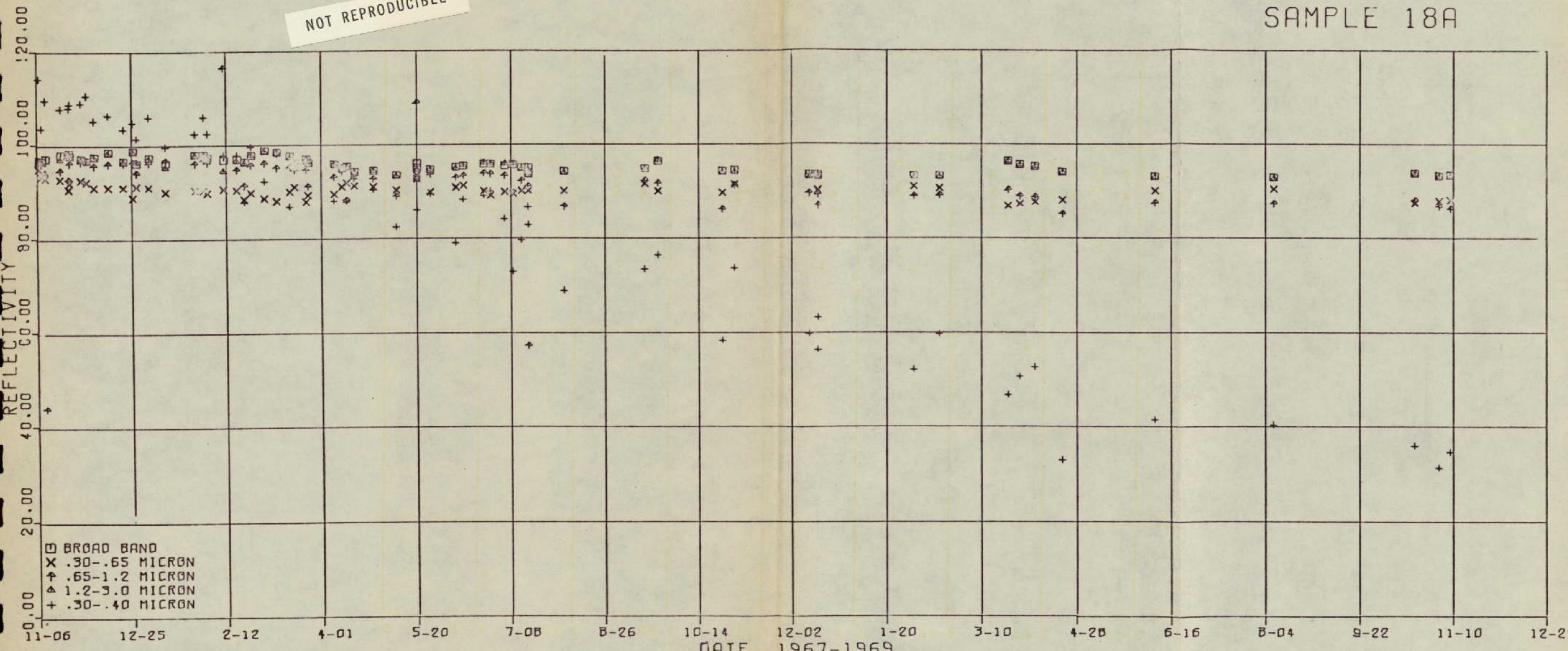

7003-Final

Figure 32. Sample 18A, Unshielded

FOLDOUT FRAME

NOT REPRODUCIBLE

FOLDOUT FRAME

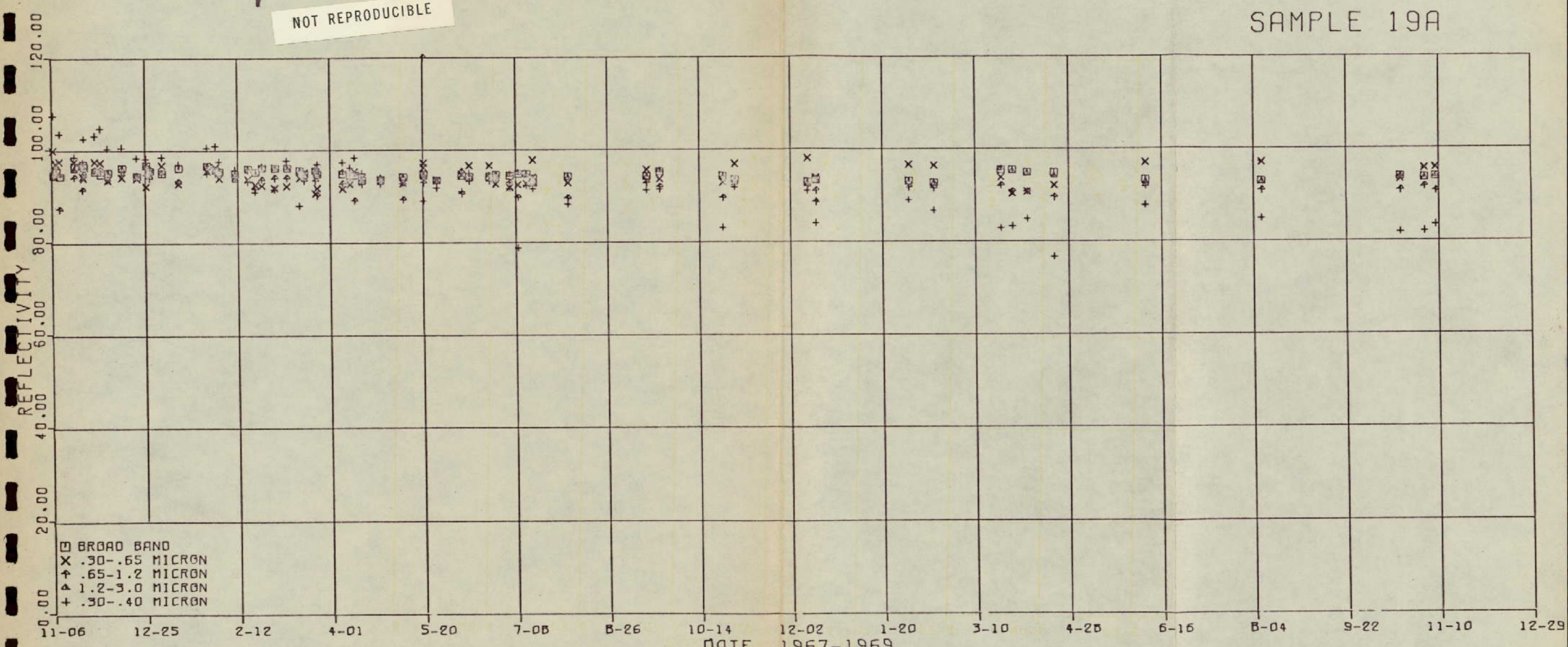

Figure 33. Sample 19A, Shielded

FOLDOUT FRAME 1

FOLDOUT FRAME 2

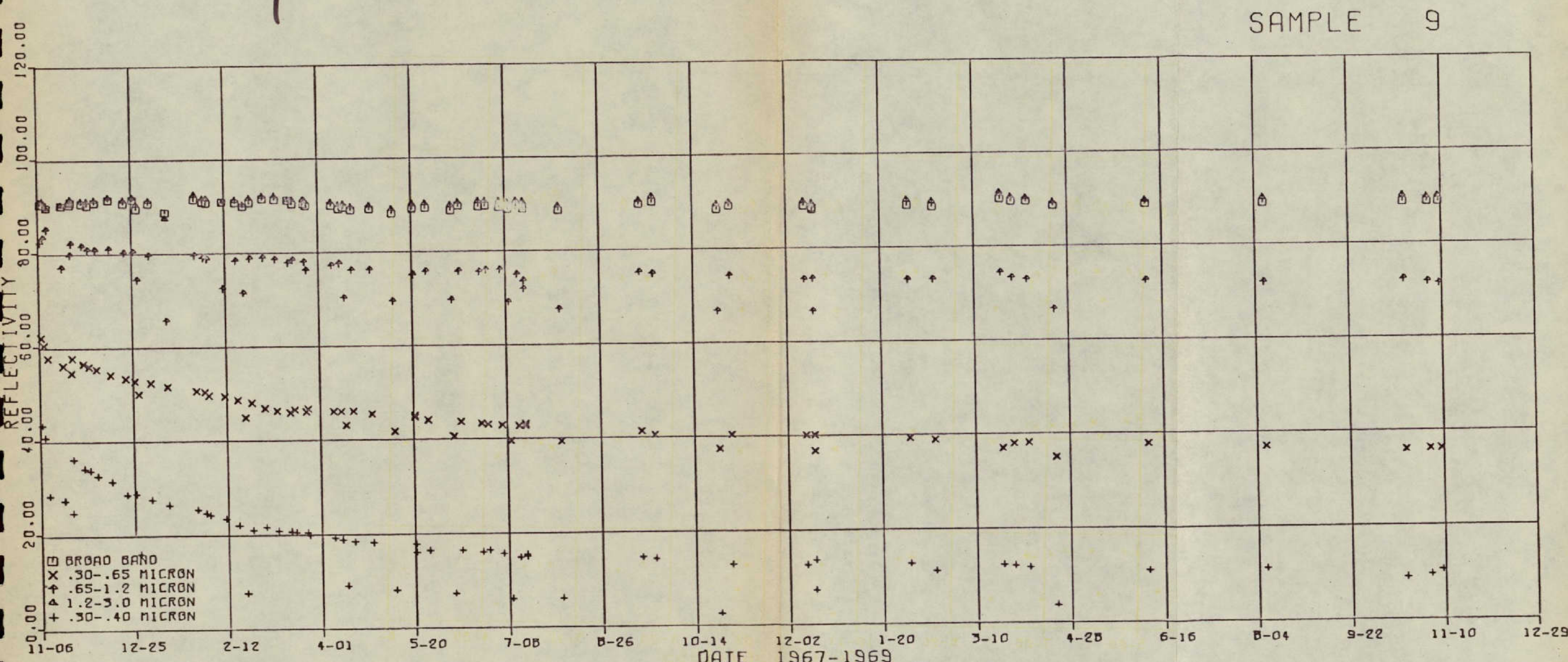

Figure 34. Sample 9, Shielded

FOLDOUT FRAME 1

FOLDOUT FRAME 2

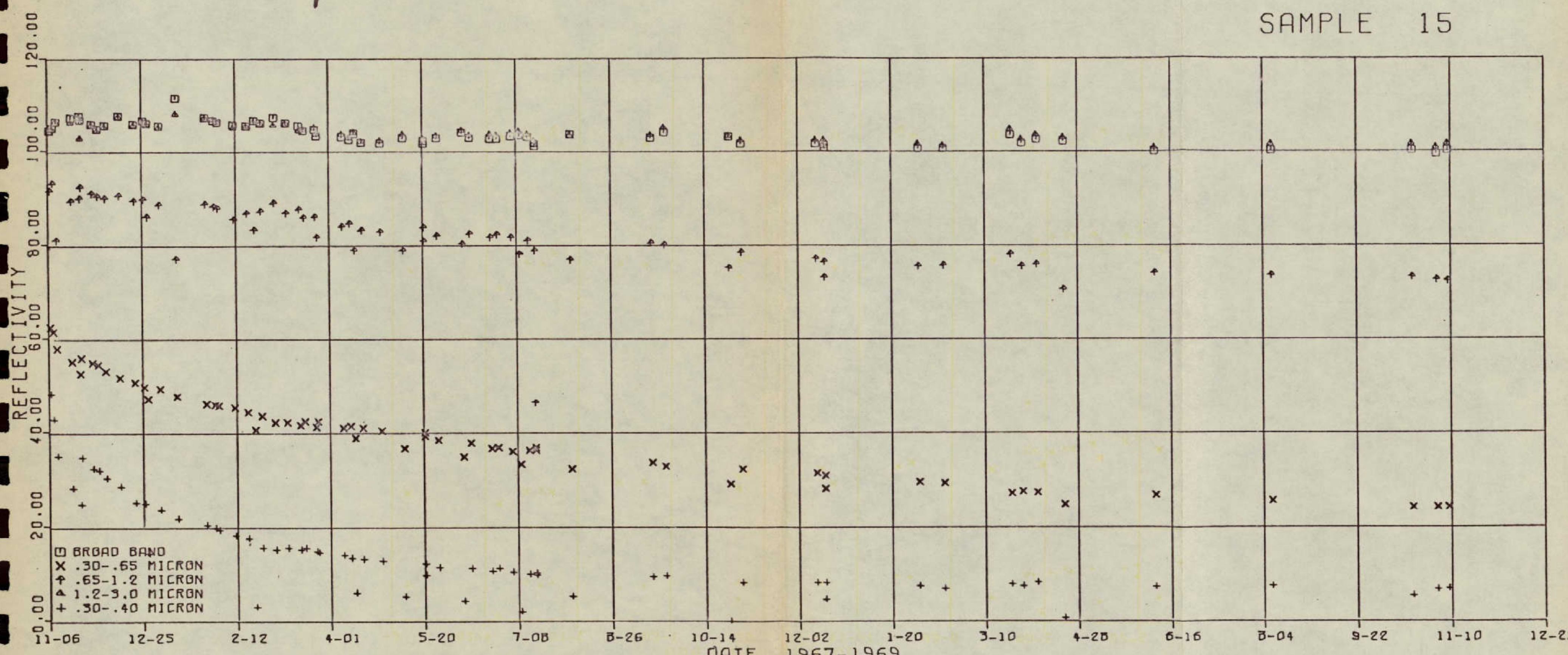

Figure 35. Sample 15, Unshielded

FOLDOUT FRAME 1

FOLDOUT FRAME 2

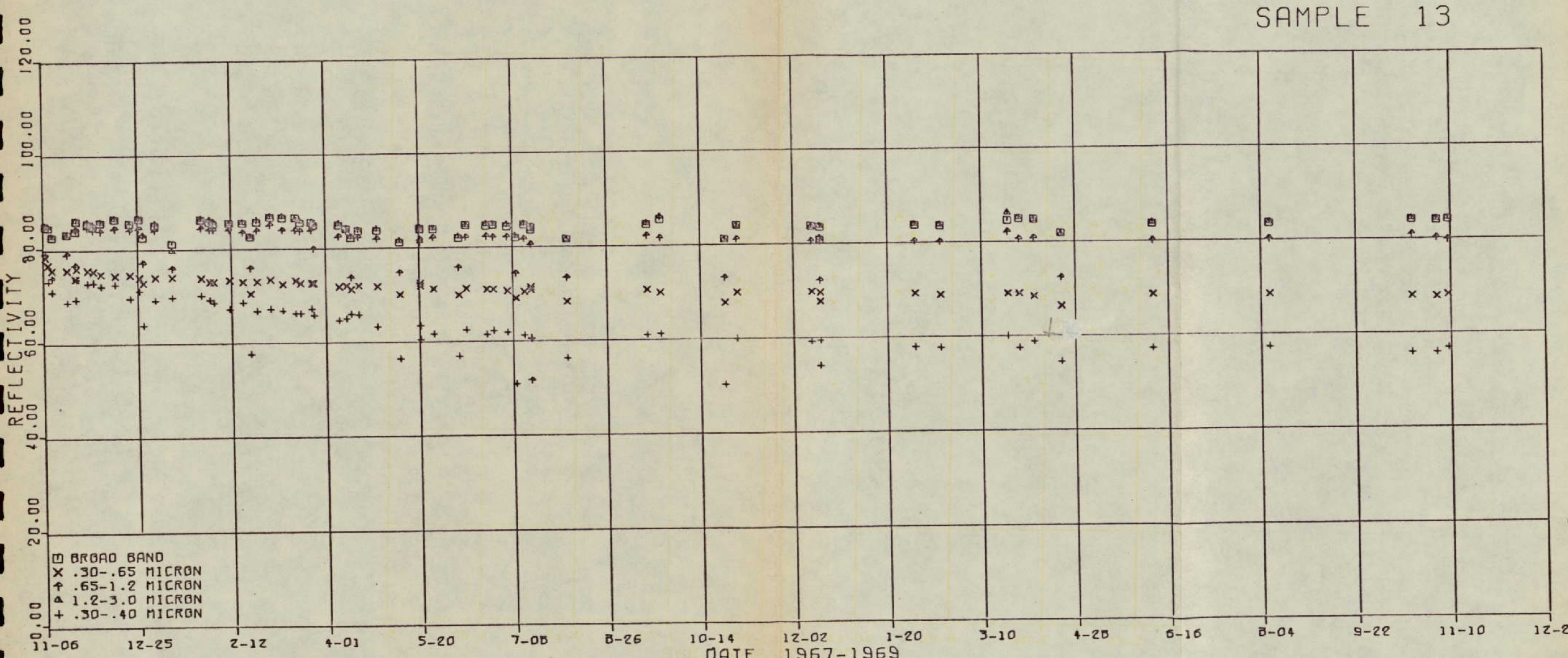

Figure 36. Sample 13, Shielded

FOLDOUT FRAME 1

FOLDOUT FRAME 2

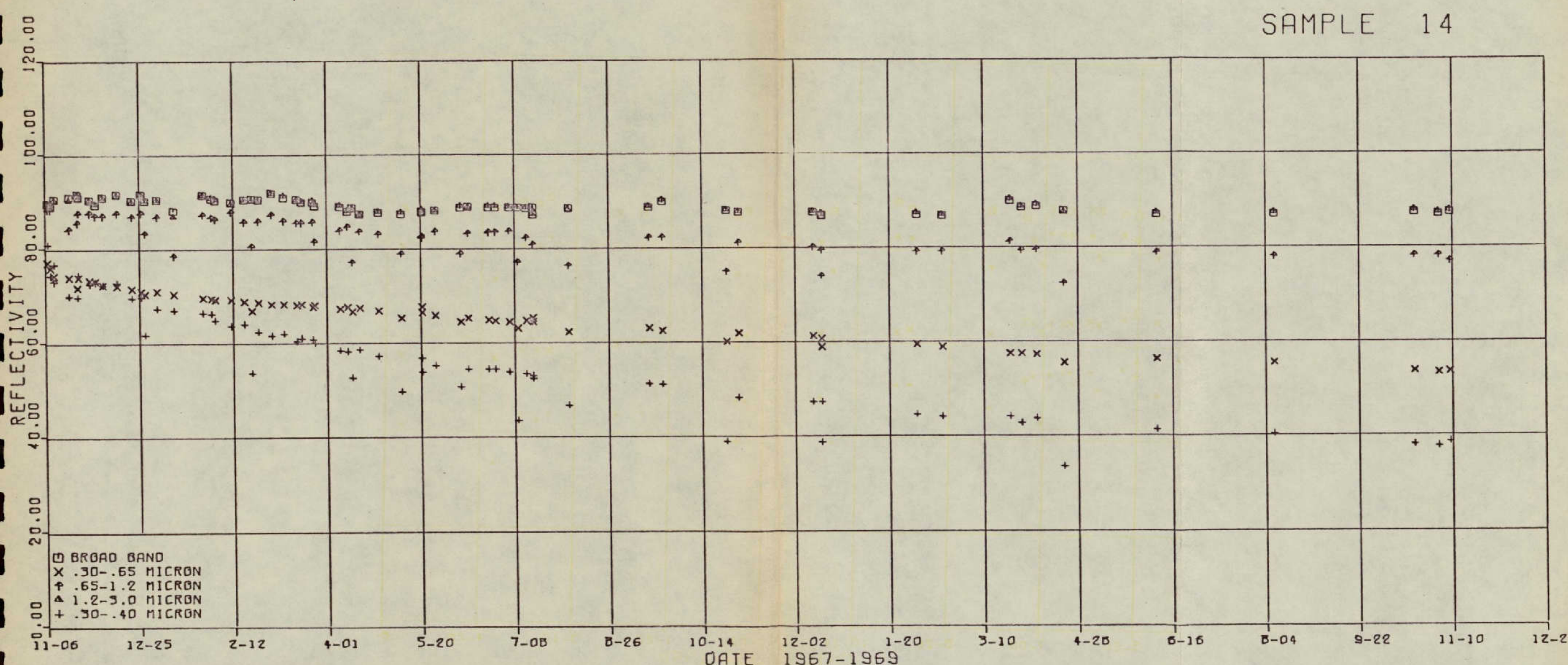

Figure 37. Sample 14, Unshielded

FOLDOUT FRAME 1

FOLDOUT FRAME 2

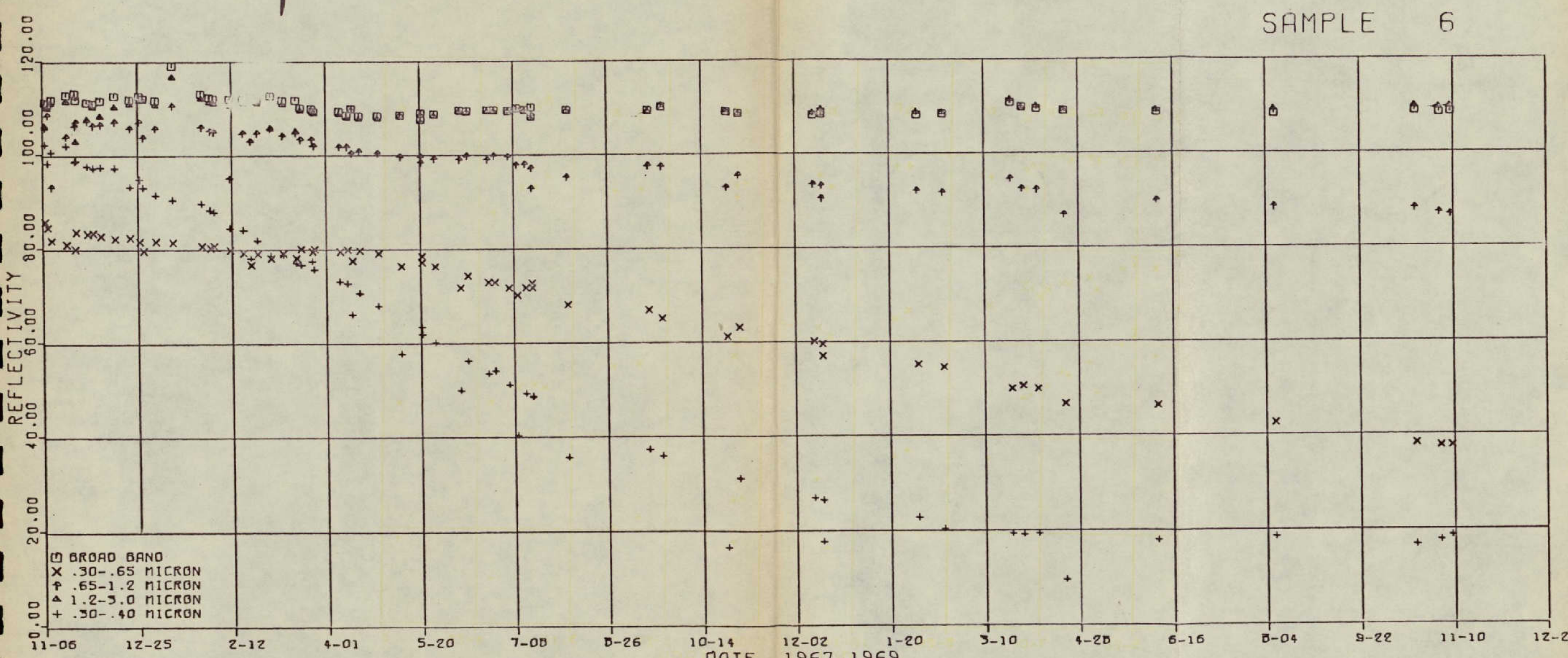

Figure 38. Sample 6, Unshielded

FOLDOUT FRAME 1

FOLDOUT FRAME 2

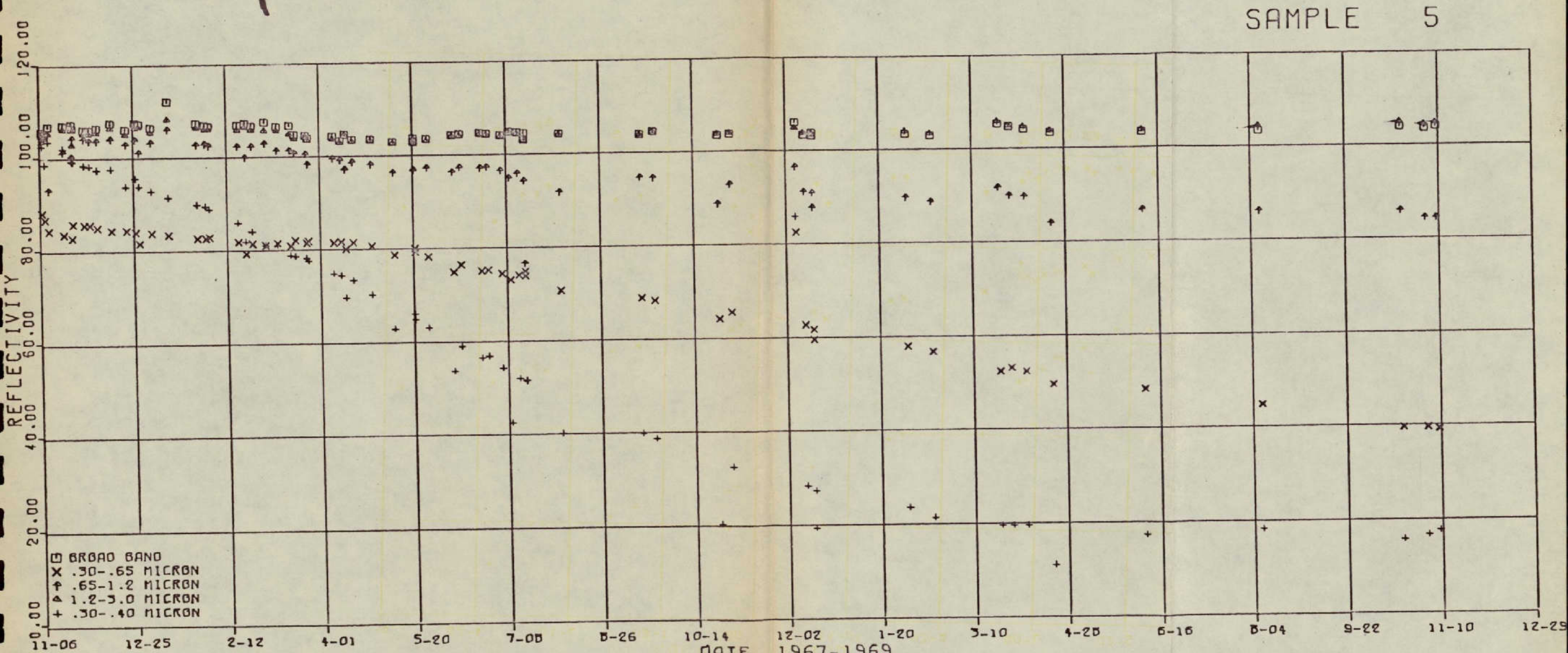

Figure 39. Sample 5, Unshielded

FOLDOUT FRAME 1

FOLDOUT FRAME 2

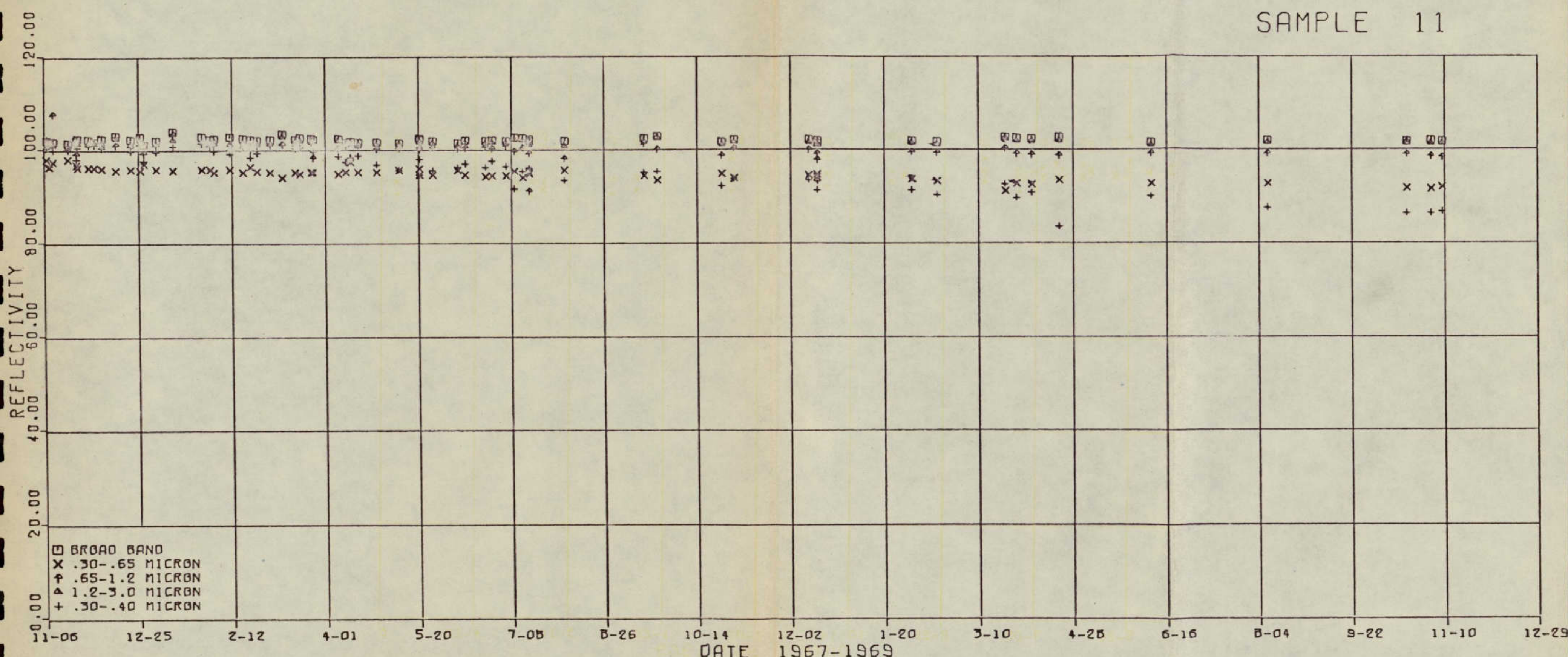

7003-Final

Figure 40. Sample 11, Shielded

FOLDOUT FRAME 1

FOLDOUT FRAME 2

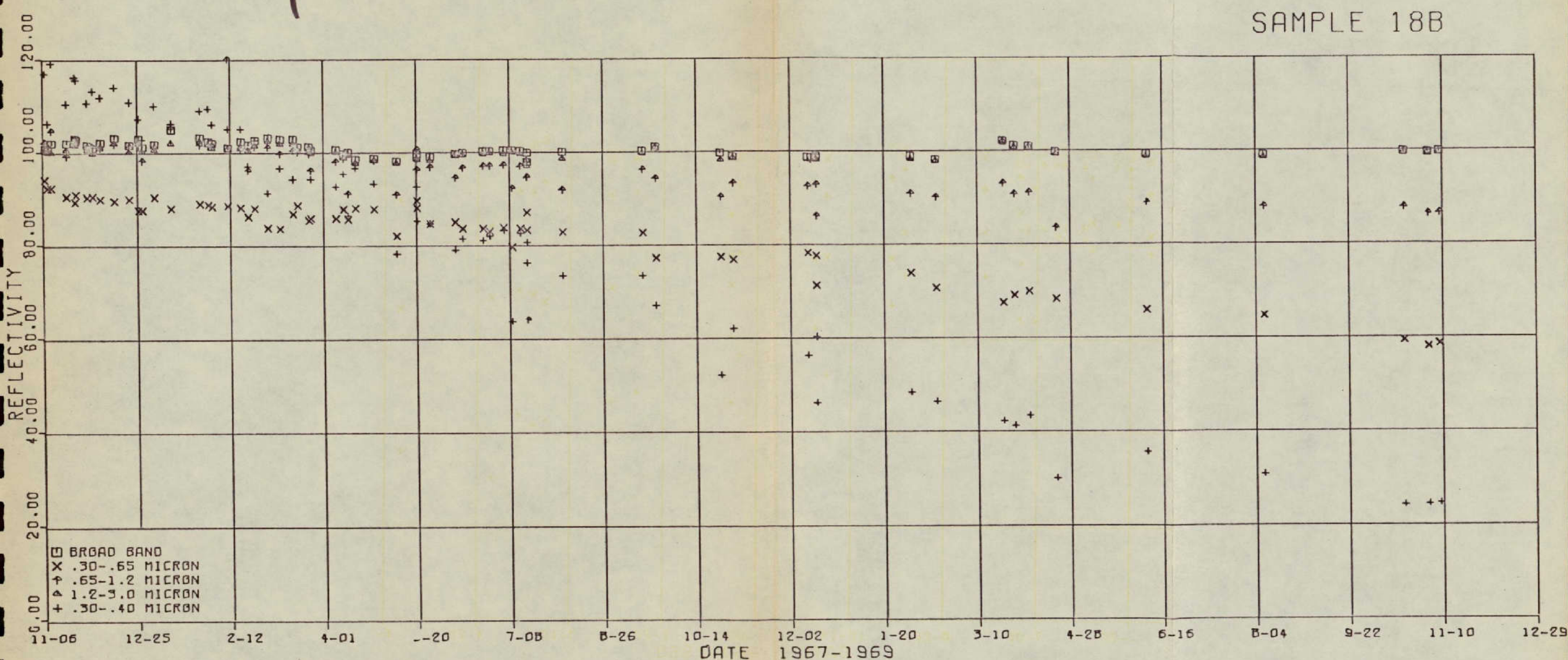

Figure 41. Sample 18B, Unshielded

FOLDOUT FRAME 1

FOLDOUT FRAME 2

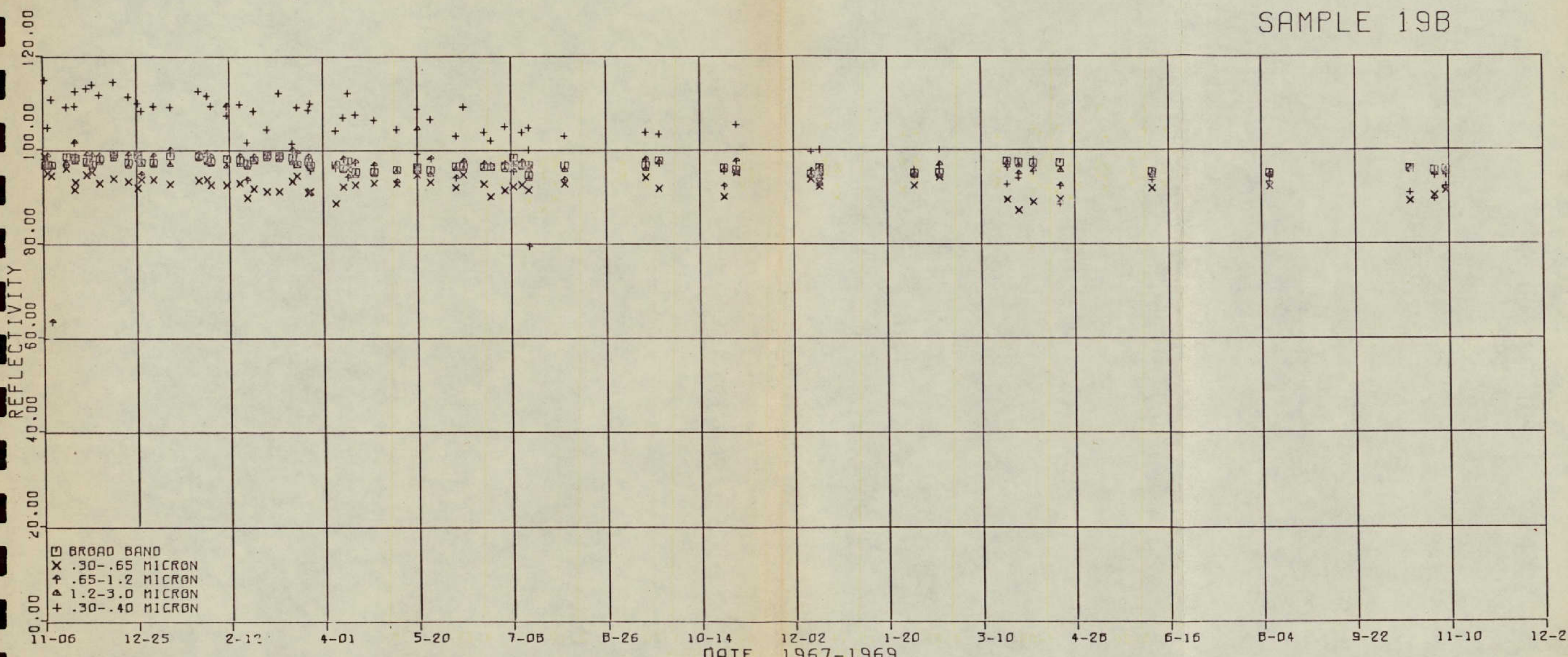

Figure 42. Sample 19B, Shielded

FOLDOUT FRAME 1

FOLDOUT FRAME 2

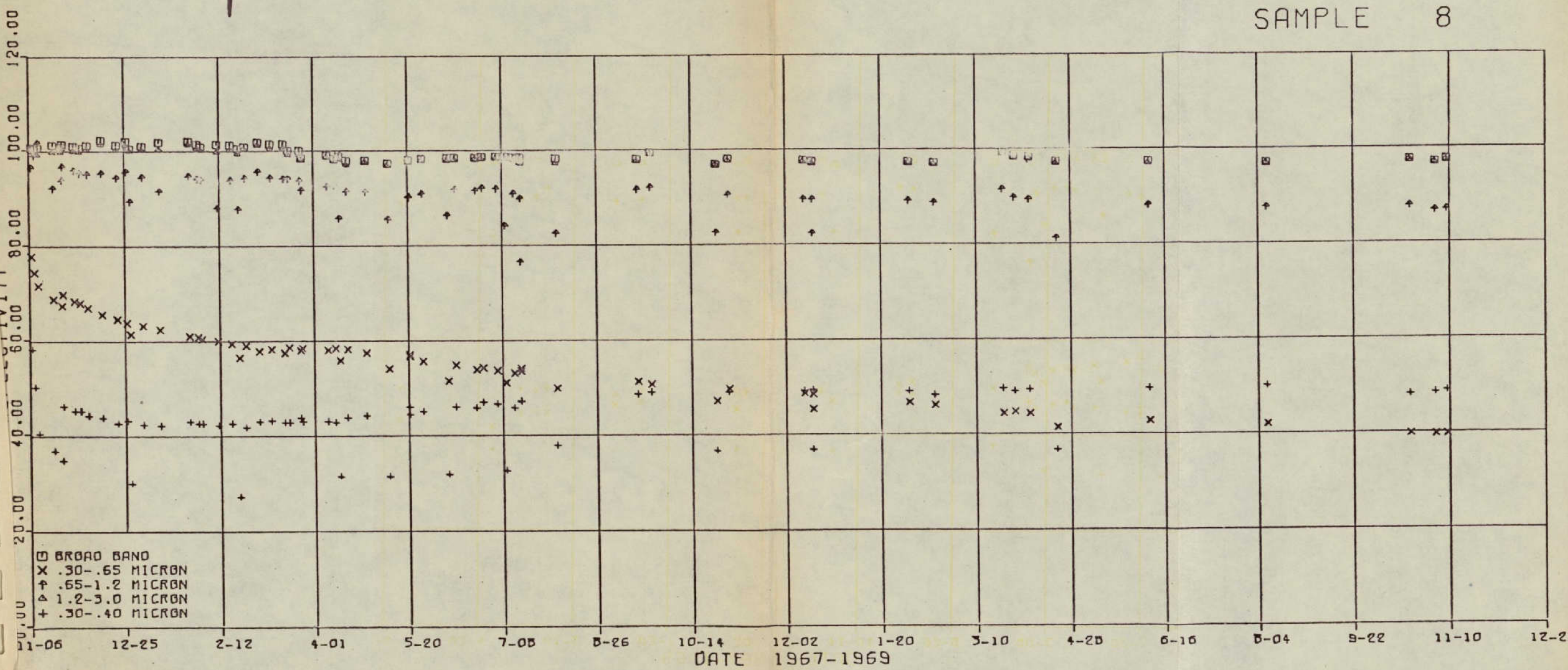

Figure 43. Sample 8, Unshielded

FOLDOUT FRAME 1

FOLDOUT FRAME 2

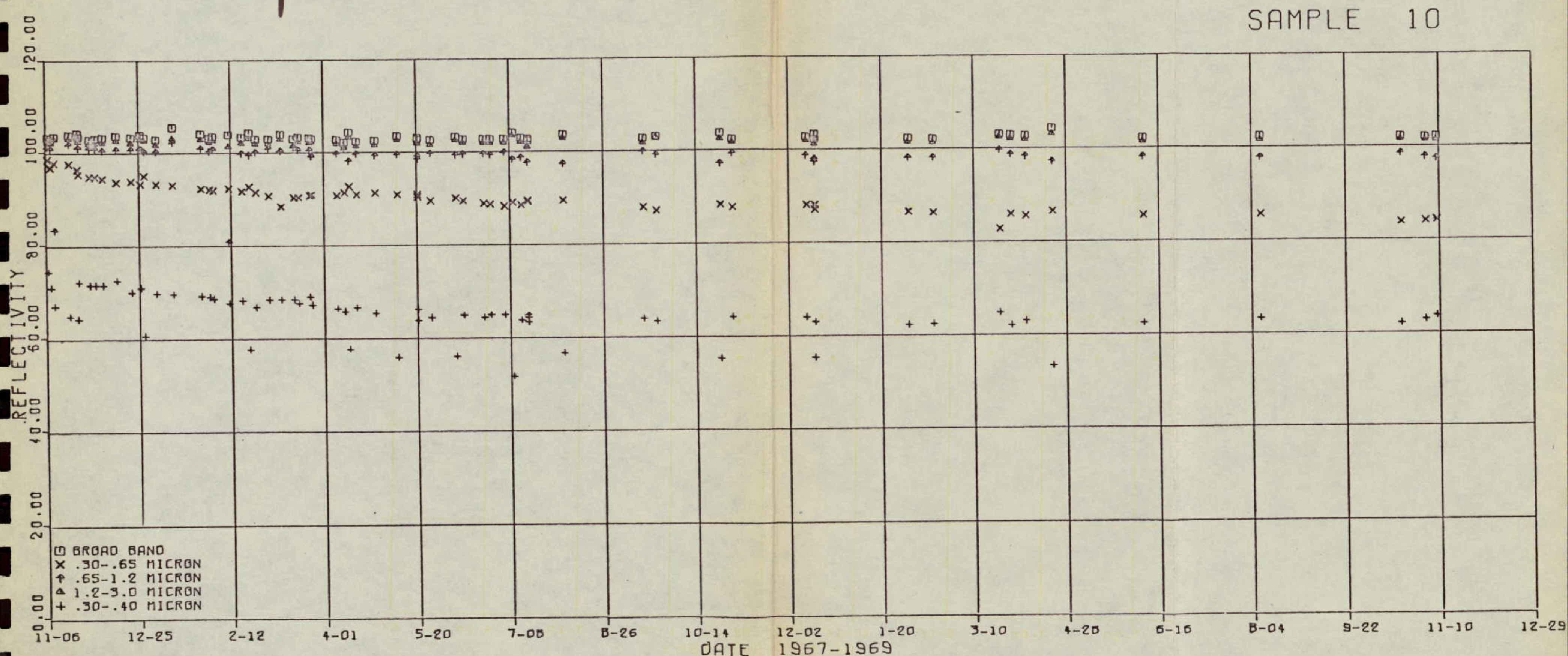

Figure 44. Sample 10, Shielded

Lamp B operation provided a signal approximately one-half as large as lamp A operation. Therefore, the low output signal due to lamp B in conjunction with the inherently low signal in the 0.3 to 0.65 micron range made the instrument susceptible to noise under these conditions.

5.4.2 GENERAL DEGRADATION CHARACTERISTICS

As was noted earlier the primary objective of this experiment was to determine the durability of selected specularly reflective surface materials in an actual space environment. This portion of the experiment was performed in order to provide directly applicable data for future design use. The results from the unshielded samples are of the greatest general use. The data from the shielded samples is more applicable for use under special conditions and for the development of scientific theories associated with the cause of degradation.

The broadband degradation of all of the samples was reasonably low and was consistent throughout the group of samples (see Table 5). The degradation of the unshielded samples in the broadband spectrum ranged from two percent to six percent on a normalized scale. Sample number 7 is the one exception. This sample showed a drastic change in reflectance near the end of the first year. The change was abrupt and was apparently due to a mechanical failure in the sample mounting or bonding. The mating sample in the shielded group showed no change of this nature throughout the test period. Examination of the raw data before and after the change did not reveal any major surface damage but did reveal a marked reduction in the reflected light level.

The 0.3 to 0.4 micron region of nearly all the unshielded samples showed a marked amount of degradation. These samples showed degradation as high as 86 percent using a normalized curve.

TABLE 5

PERCENTAGE OF REFLECTANCE AT END OF SECOND YEAR
(Normalized to Reflectance Value at Launch)

Sample No.	Broadband		0.3 to 0.4 Micron		0.3 to 0.65 Micron		0.65 to 1.2 Microns		1.2 to 3.0 Microns	
	(Unshielded)	(Shielded)	(Unshielded)	(Shielded)	(Unshielded)	(Shielded)	(Unshielded)	(Shielded)	(Unshielded)	(Shielded)
7, 12*	81	99	24	87	53	93	73	97	81	99
17, 20*	96	98	66	86	70	96	91	98	96	98
16	95	-	56	-	78	-	90	-	97	-
2*, 4	97	99	27	54	76	96	93	97	97	100
18A, 19A*	97	99	30	80	92	99	89	95	97	98
9*, 15	94	98	14	21	37	60	77	85	95	98
13*, 14	98	98	48	76	70	86	87	95	98	98
6	97	-	17	-	45	-	79	-	98	-
5, 11*	96	100	17	83	44	93	80	97	98	100
18B, 19B*	97	98	19	80	62	97	85	97	98	99
8, 10*	96	99	100	85	50	85	88	96	98	98
Average of Samples in Column	94.9	99.7	38.0	72.4	61.5	89.4	84.7	95.2	95.7	98.7

*Indicates samples that are shielded

The average degradation for the unshielded samples in the 0.3 to 0.4 micron range was 57 percent. This included one sample, sample 8, which at the end of two years had the same reflectivity as it did at launch. This sample exhibited a reduction in reflectance of approximately 16 percent by the end of the first three months after launch then started a slow increase in the reflectance for approximately the next nine months. The reflectance was constant after the end of the first year in space and had returned to the original reflectance value.

Table 5 shows the reflectance of each of the samples at the end of the second year in space. The values shown in the table are normalized to the reflectance at launch. The general trends indicated by the table show that the sample degradation at the longer wavelengths is not extremely high for either the shielded or unshielded samples, approximately 1 percent degradation for the shielded and approximately 5 percent for the totally exposed samples. The shorter wavelengths, however, degraded much more rapidly. The degradation in the 0.3 to 0.4 micron range was approximately 28 percent for the shielded samples and approximately 62 percent for the unshielded samples. The degradation for the intermediate wavelength ranges fell between the two extreme cases.

5.4.3 EXPLANATION OF DEGRADATION CAUSES

The ATS-3 reflectometer was designed to detect only specularly reflected light, commonly referred to as coherently scattered light. The degree to which light is scattered coherently or incoherently (diffuse) depends upon its wavelength and the roughness character of the reflecting surface. Consequently, the results of the experiment can be expected to be sensitive to any factors which might affect the roughness character of the sample surface.

Surface roughness causes the diffuse scattering of light and is particularly troublesome in the ultraviolet and vacuum ultraviolet regions of the spectrum. Figure 45 shows the optical scattering which occurs when light is reflected from a rough metal surface. Part of the incident beam is reflected in the specular direction, while the remainder is diffusely scattered around the specular direction. The fraction which is scattered depends on the ratio of the size of the irregularities to the wavelength. When the irregularities are large relative to the wavelength, they act as small mirrors reflecting light in various directions. Furthermore, the total reflectance of the surface may be smaller than that of a perfectly smooth surface of the same material because of multiple reflections between surface facets. Diffraction effects become important if the surface irregularities become comparable in magnitude to the wavelength.

The loss of specular (coherent) reflection due to surface roughness is demonstrated in Figure 46 as reported by Bennett and Bennett (Ref. 1). This shows the relative reflectance of an aluminized ground glass sample to that of a perfectly smooth surface of the same material. The relative reflectance is nearly zero when the rms height of the surface irregularities $\sigma = 0.2\lambda$, where λ is the wavelength. Thus, surfaces which have irregularities of the order of half a wavelength or more exhibit practically no specular reflection.

The theory relating surface roughness to specular reflectance when $\sigma \ll \lambda$ has been given by Bennett and Porteus (Ref. 2, 3, and 4). The ratio of the specular reflectance R from a given sample to the specular reflectance R_o from a perfectly smooth surface of the same material is

$$R/R_o = \exp[-(4\pi\sigma/\lambda)^2] + \text{incoherent term} \qquad (2)$$

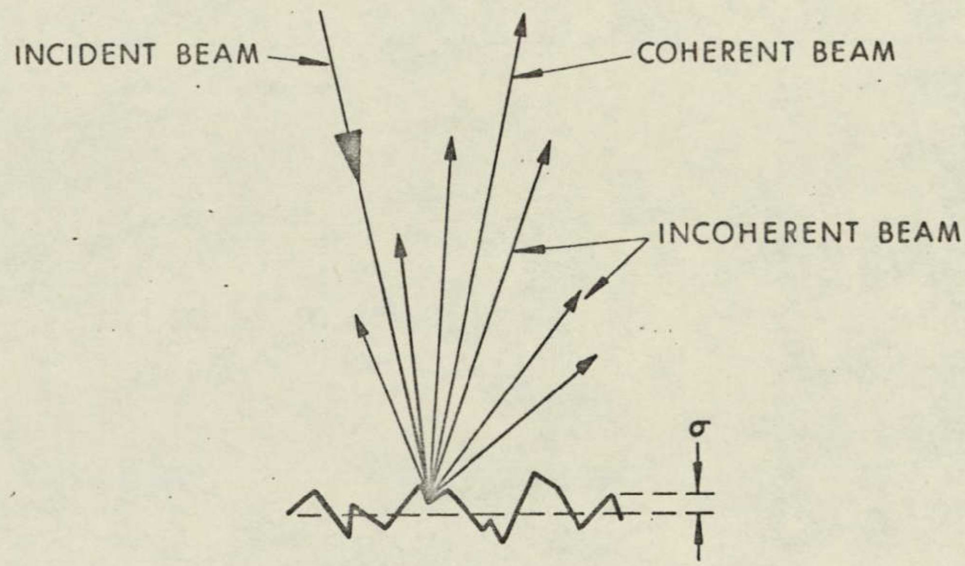

Figure 45. Schematic Representation of Reflectance from a Rough Surface

35279

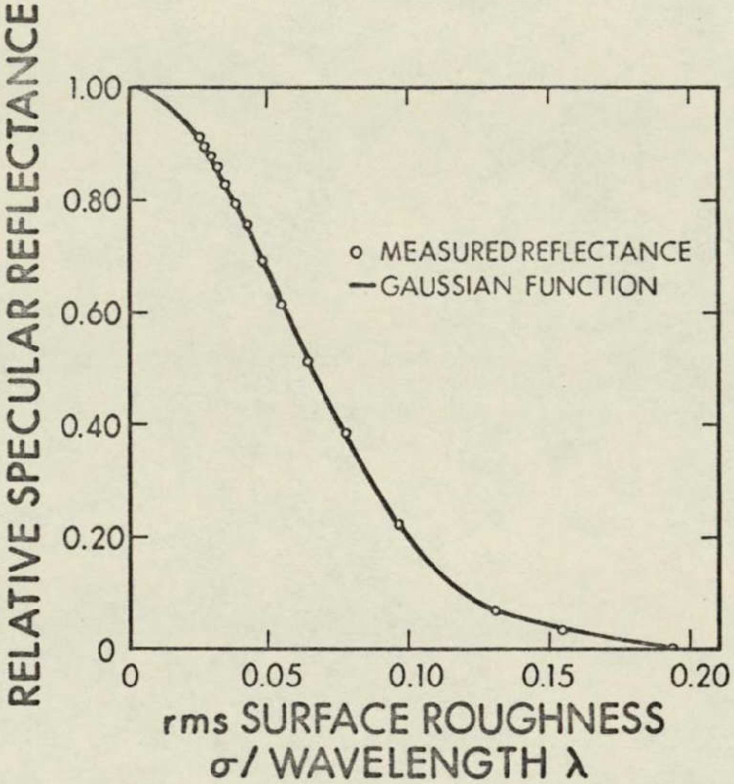

Figure 46. Relative Coherent Reflectance R/R_o versus σ/λ for Larger Values of Surface Roughness

35278

The first term on the right represents the specular or coherent scattering. The diffuse or incoherent term also contains an exponential function with, however, a $1/\lambda^4$ dependence which causes this term to decrease rapidly as the wavelength increases. The second term also decreases as the mean slope of the irregularities becomes steeper and as the acceptance angle of the instrument becomes smaller. In the ATS-3 Reflectometer experiment, light of normal incidence is specularly reflected off the sample, back along the path of incidence, through a system of mirrors and into an integrating sphere. Therefore, the acceptance angle of the instrument is small and the incoherent term of Eq. 1 can be considered equal to zero.

Since the ATS-3 Reflectometer only detects specularly reflected light, it follows that any loss of relative specular reflectance, as the result of changes in the sample surface which enhance diffuse scattering, would be interpreted as a degradation of reflectance. Also, designated identical surfaces which, however, have inadvertently been prepared with different roughness character would exhibit different initial values of relative specular reflectance (measured as R_s in the experiment), although values of total reflectance (not measured in the experiment) might conceivably be the same.

As will be shown here, the sample reflectance changes can be explained in terms of σ/λ, the surface roughness relative to wavelength. Since the data do not indicate the course of total reflectance, their interpretation in terms of development of an absorption band in the surface oxide layer is not possible without recourse to other data. A further discussion of the physical interpretation of the reflectance data is contained in a paper by Heaney (Ref. 5) which provides this comparison.

Bennett (Ref. 2) gives a curve of reflectance plotted against σ/λ, reproduced as Figure 46 of this report, which indicates that specular reflectance decreases to about 20% of the best obtainable value when

$\sigma/\lambda \approx 0.10$. As will be noted in the group I set of curves, the largest spectral, specular reflectance decrease occurs in the 0.3 to 0.4 micron band, corresponding to $\sigma = 0.035$ micron roughness for $\lambda = 0.35$ micron. It would appear that the surface oxide film effect is negligible for group I since Berning, Madden and Hass (Ref. 6) report naturally occurring Al_2O_3 films on aluminized mirror surfaces of about 0.0022 micron thickness at room temperature.

The effect on short wavelength reflectance stability due to substrate variations is indicated in group II samples. Comparing the reflectance curves of pair 7 and 12 with pair 17 and 20, little difference in rate of degradation of reflectance is seen indicating that the substrate material is not a prime factor in the degradation process.

Figure 47 was plotted from the data of Samples 2 and 4 which were SiO overcoated aluminum. The two plots are seen to vary with time raised to a power. The time dependence of these data attests an effect which is systematic although the cause cannot be conclusively determined from the available data. The functional dependence on the time suggests that this degradation on the wavelength range of 0.3 to 0.4 micron might be due to surface roughness which for small σ/λ (see Eq. 2) is expressed in the form

$$1 - R/R_o = (4\pi\sigma/\lambda)^2 \quad (3)$$

Equation 3 defines the diffusely scattered light $(1 - R/R_o)$. The ordinate of Figure 47 represents the difference between unity and the experimental values of relative spectral reflectance which is to be identified with the left-hand side of Eq. 3. In order for the ordinate of Figure 47 to vary with σ^2 as in Eq. 3, σ would have to vary with time raised to an appropriate power. For example, the data of Sample 4 would require for $\lambda = 0.35$ micron,

$$\sigma/\lambda = 0.03(t)^{0.15} \quad (4)$$

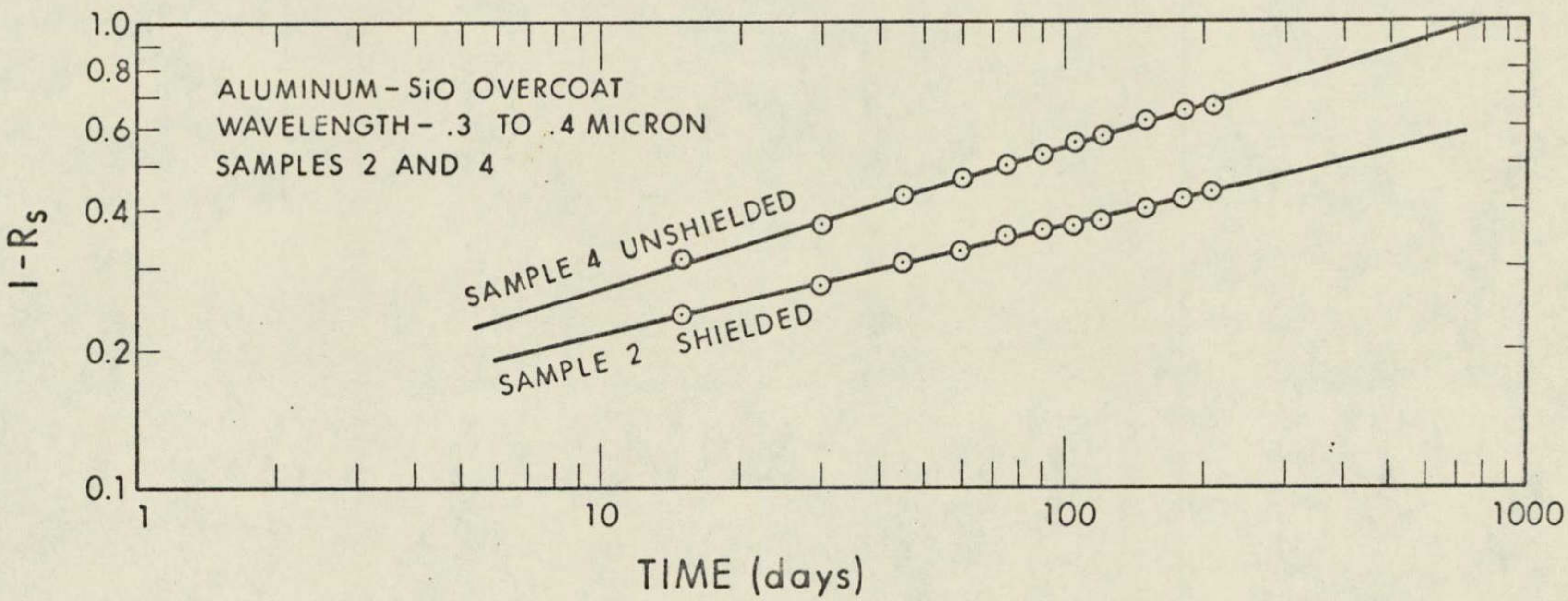

Figure 47. Decrease in Relative Spectral Scattering

where t is given in days. Equation 4 is plotted in Figure 48. Of course, Figure 48 is in the nature of pure supposition. It would require that the surface roughness factor increase relatively rapidly in the early days of the experiment and then begin tapering off. According to the analysis above, an rms value of surface irregularities of only 175Å would be required to cause the observed data. Pursuing the logic generated by the supposition, a rapid change in surface condition during the initial period of exposure to the vacuum of space suggests the possibility of vigorous outgassing. If the surfaces were prepared under conditions which permitted the formation of large crystallites and the trapping of significant amounts of residual gas molecules, it is conceivable that vacuum outgassing could proceed under the influence of activating ultraviolet irradiation such that a proous surface layer structure would develop, resulting in irregularities to an extent required to explain the data.

Again, referring to Figure 47, the lower rate of degradation of Sample 2 might be explained by the shield which would reduce the intensity of ultraviolet irradiation. On the other hand, an examination of the first (prelaunch) data points for the pair (2,4) strongly infers that the two samples were not identical although they were supposed to be the same. Initially, Sample 2 shows a mean relative reflectivity of about 95 percent whereas that of Sample 4 is closer to 85 percent.

The emphasis of the discussion above is that the very strong degradation effects observed in the data of the sample pair (2,4) were primarily due to an inherent nature of the surface which made them more vulnerable to the special environmental conditions. This latter statement seems valid upon examination of the data of the sample pair (18A, 19A) which are surfaces similar to those of (2,4). Examination of the data of (18A, 19A) shows only slight evidence of degradation.

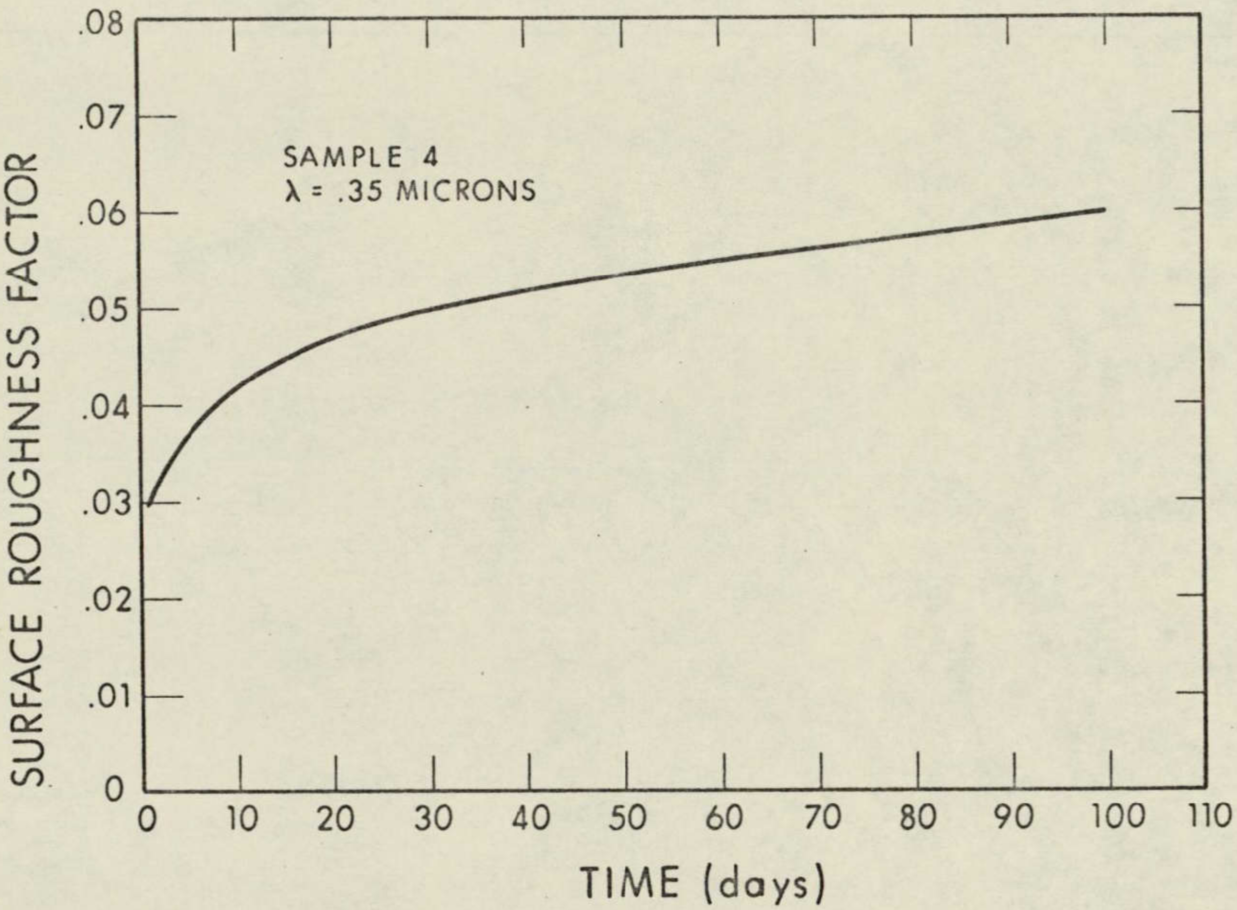

Figure 48. Plot of Equation (3)

35281

Another anomaly in the prelaunch data is seen in the 0.3 to 0.65 micron data of pair (5, 11) that are supposed to be identical. These prelaunch data points bear little resemblance, which precludes a meaningful comparative analysis. Sample 11 is identified as an aluminum reflecting surface with no overcoating. The behavior of Sample 11 is precisely that which would be expected from such a surface. The reflectivity is practically the same for all wavelengths which is the well known property of aluminum-oxide coated aluminum. Ordinarily, the presence of the oxide coating should not influence the optical properties above $\lambda = 0.2$ micron.

Samples 8 and 10, MgF_2-overcoated silver, show evidence in the 0.3 to 0.4 micron band of the sharp decrease in reflectance during the early part of the mission. This is a normal characteristic of silver at approximately 0.31 micron. Also, Sample 8 exhibits a pronounced degradation effect in the 0.30 to 0.65 micron band and, to a much lesser extent, in the 0.30 to 0.40 micron band. Studies (Ref. 7) have shown that MgF_2-protected aluminum mirrors retain their reflectance quality into the high vacuum ultraviolet during extended exposure to air, ultraviolet radiation, and bombardment by 1-Mev electrons and 5-Mev protons of flux intensities much greater than those encountered in space. Therefore, one is led to conclude that neither ultraviolet nor ion irradiations are directly responsible for the degradation shown by Sample 8.

In the 0.3 to 0.4 micron range, Sample 8 displayed an increase in reflectance after about three months in space. The sample degraded by approximately 16 percent by the end of the first three months then started a slow increase for approximately the next nine months. The reflectance at the end of the first year was back to the original launch value and remained constant through the second year. This indicates a sublimation of the coating with the coating reaching a

1/4 wavelength thickness at the end of the third month and being completely removed by the end of the first year. This trend was also becomming apparent in the shielded sample, Sample 10, and had reached a minimum by the middle of the second year. The trend was not grossly evident however because of the slowness of the cycle. This unusual reflectance characteristic enhances the theory that the coating did not withstand the space environment as was expected and that the degradation was enhanced by the presence of ultraviolet radiation.

Micro-meteorite bombardment does not appear to be a likely mechanism considering that the degradation proceeds much more rapidly during the early days of exposure rather than at a uniform rate as might otherwise be expected in such a case. Also, the effect of meteorite bombardment should be present to a similar degree in the data of all unshielded samples, and this has not been observed. Although lacking an explanation for the very first prelaunch 0.30 to 0.65 micron data points of Sample 8, the subsequent data after launch for that band can be explained in a similar manner to that of the (2,4) pair which has already been discussed in some detail.

The sample pair (9,15) shows very strong evidence of a reflectivity decreasing monotonically with wavelength. The prelaunch data for the shielded and unshielded samples are identical for the 0.30 to 0.40, 0.3 to 0.65, and 0.65 to 1.2 micron bands. The aforementioned disparity for this pair exists in the broad band data which, contrarily, exhibits a constant relative reflectivity of 105 percent for the unshielded sample and a lower value of 90 percent for the shielded sample. Subsequent degradation effects appear to be about the same for each wavelength band for each sample of the pair (9,15). That is, the shield apparently has no effect; this is one of the strongest bits of evidence against any erosion mechanism due to micro-meteorite or ion bombardment. This still allows the possibility that the degradation may be due to ultraviolet radiation, especially since the decreases in reflectivity proceed at a more uniform rate than that observed in some of the other cases, e.g., that of Sample 8.

In summary, the prelaunch data show in many instances that sample pairs were not identical, thus confusing the analysis of any subsequent degradation effects. However, it appears that micro-meteorite erosion and ion sputtering can be eliminated as causes of degradation. On the other hand, vacuum outgassing and/or chemical changes probably enhanced by ultraviolet radiation are suggested mechanisms responsible for the observed degradation. That is, a thoroughly degassed surface which is not subject to discoloration when exposed to ultraviolet would not be expected to demonstrate degradation effects in this experiment. In explaining shielded and unshielded sample data where obvious differences occur, it should be noted that the quartz shields transmit ultraviolet radiation but absorb the more energetic vacuum ultraviolet. Therefore, the exposure of the unshielded samples to vacuum ultraviolet radiation will greatly exceed that of the shielded samples. Finally, contamination does not appear to be a probable mechanism in the vacuum condition of space.

5.4.4 TEMPERATURE HISTORY

Figures 49, 50 and 51 indicate the case temperature, primary detector temperature, and secondary detector temperature histories, respectively. Temperatures throughout the instrument appear to be uniform, without appreciable gradient.

5.4.5 PRESSURE HISTORY

The housing pressure (Figure 52) was monitored throughout the data taking period. The initial pressure after temperature stabilization

FOLDOUT FRAME 1

FOLDOUT FRAME 2

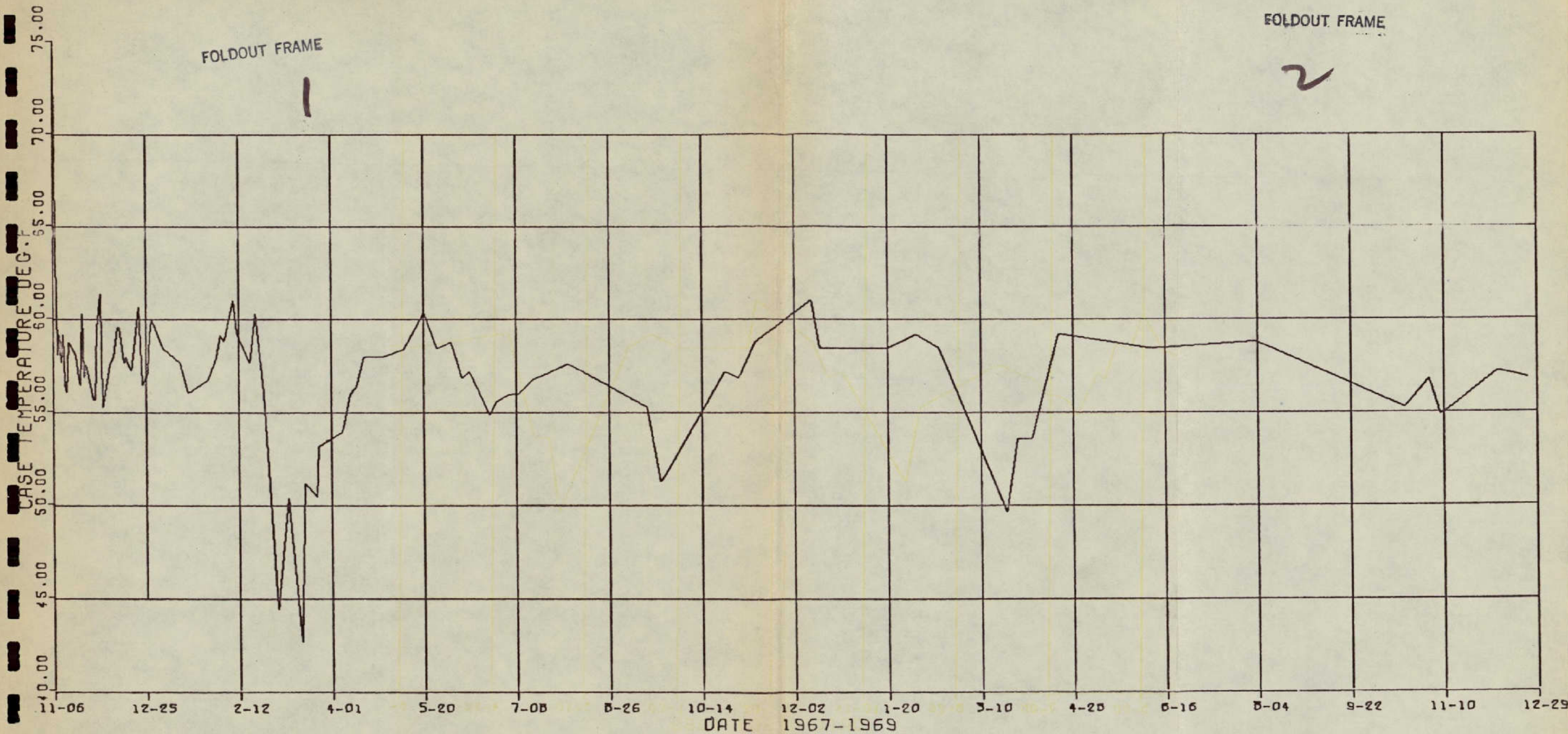

Figure 49. Case Temperature

FOLDOUT FRAME 1

FOLDOUT FRAME 2

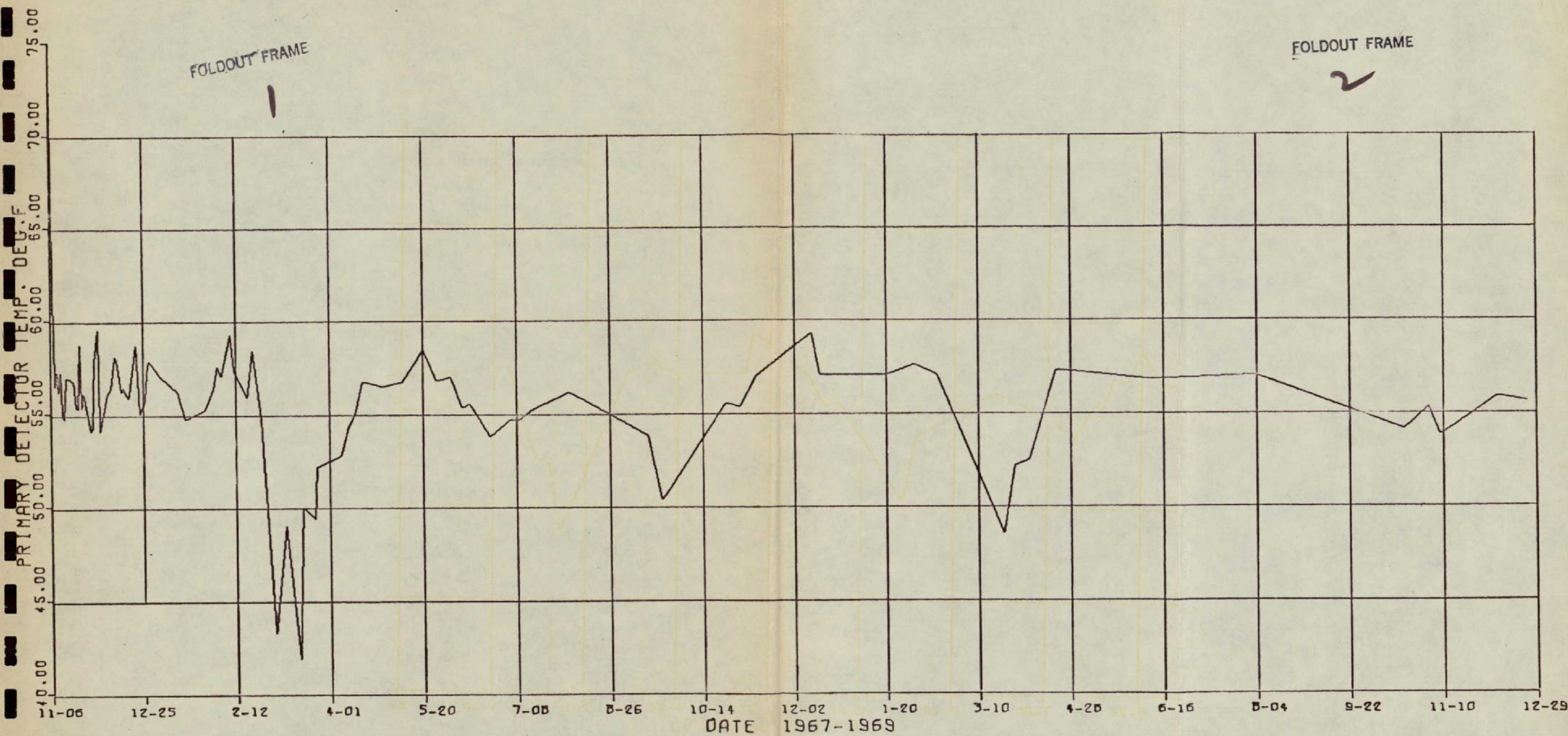

Figure 50. Detector Temperature, Primary

FOLDOUT FRAME

FOLDOUT FRAME

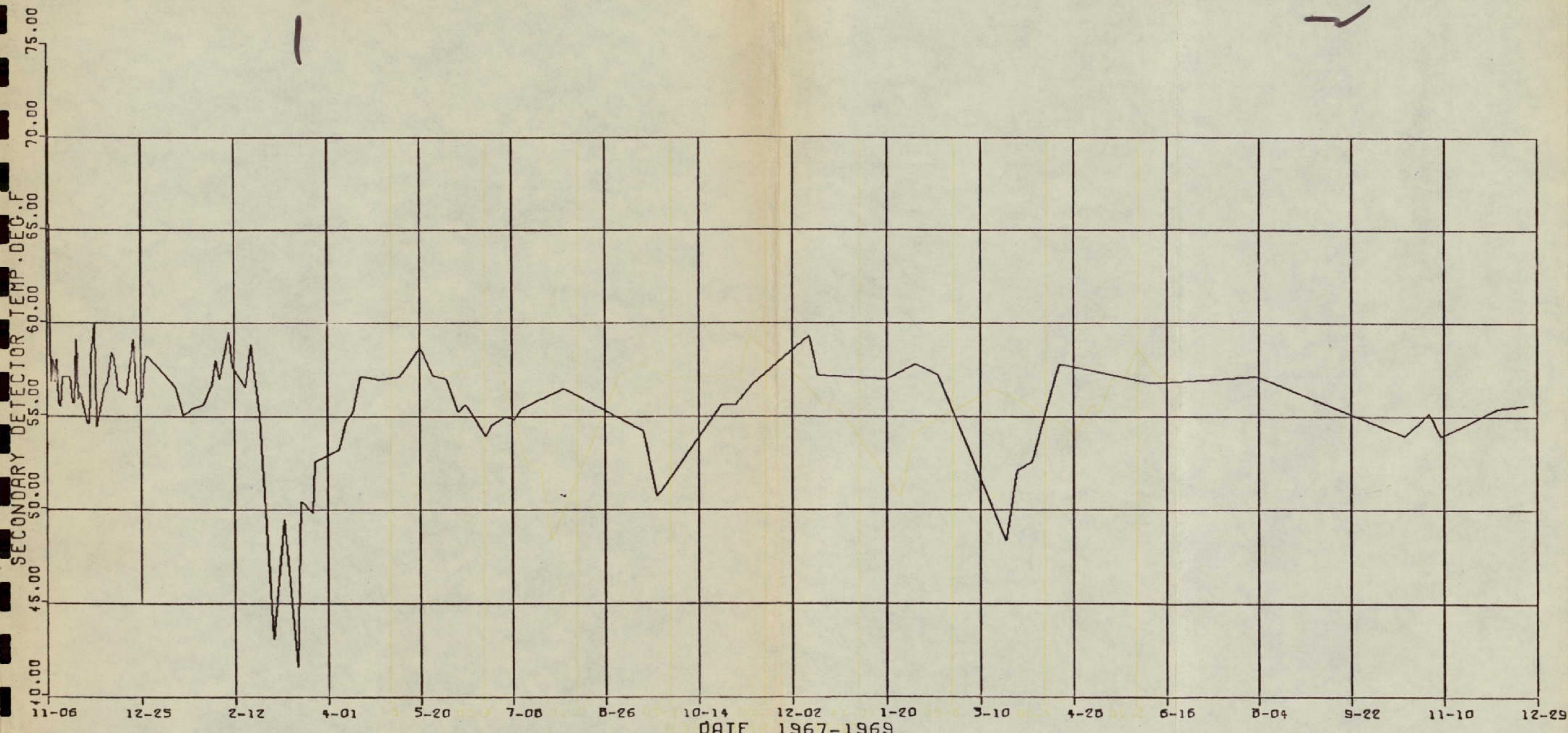

Figure 51. Detector Temperature, Secondary

FOLDOUT FRAME

FOLDOUT FRAME

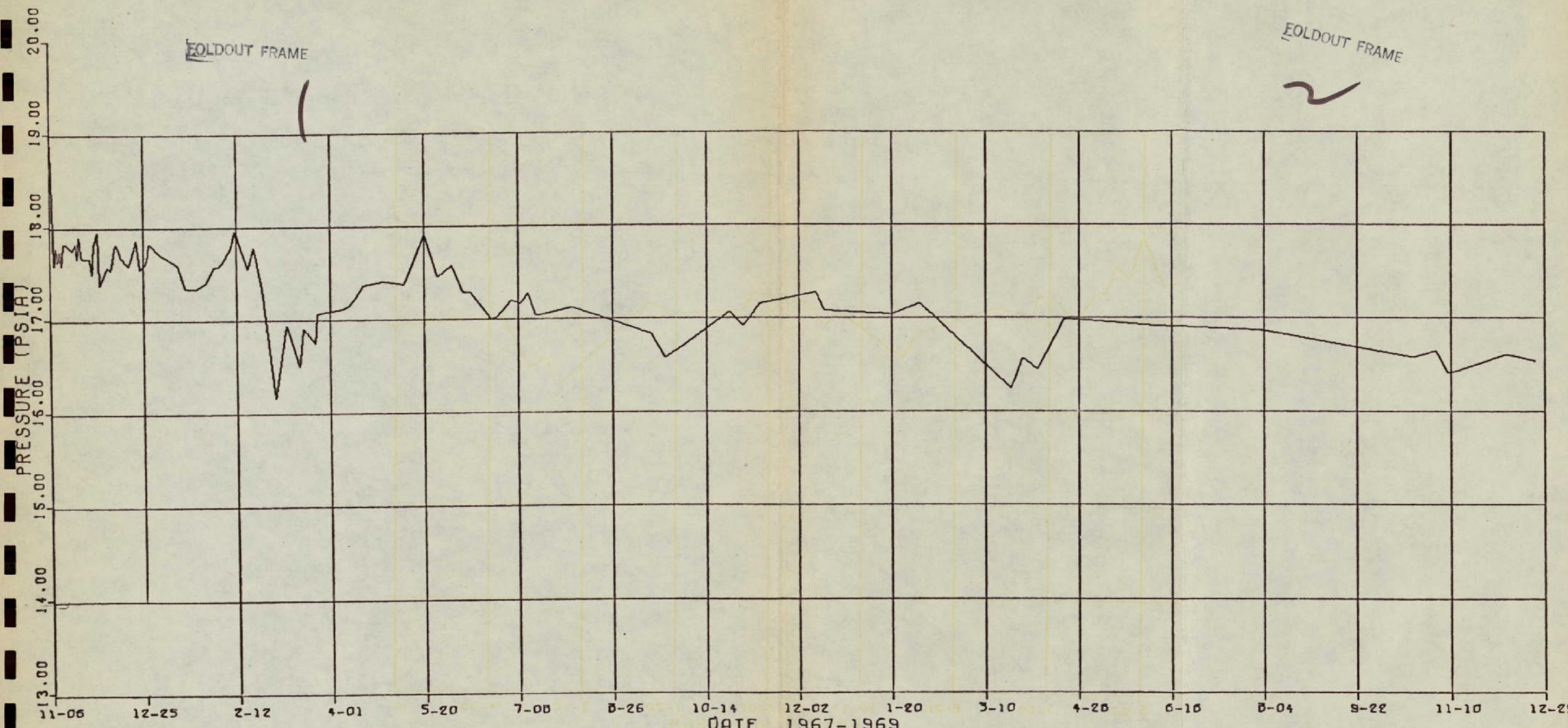

Figure 52. Enclosure Pressure (psia)

in space was approximately 17.75 psia and at the end of the second year had dropped to approximately 16.75 psia. These figures take into consideration temperature variations at each end point and provide an actual pressure loss of approximately 1/2 pound of enclosure pressure per year in space.

SECTION 6

NEW TECHNOLOGY

This instrument was designed and fabricated using components and techniques which were state of the art at the time of fabrication. No new technology was developed under this contract during the design development or fabrication of this instrument.

REFERENCES

1. H. E. Bennett and J. M. Bennett in "Physics of Thin Films" (G. Hass and R. E. Thun, eds.) 4, 1 (1967)
2. H. E. Bennett, J. Opt. Soc. Am., 53, 1389 (1963)
3. H. E. Bennett and J. O. Porteus, J. Opt. Soc. Am., 51, 123 (1961)
4. J. O. Porteus, J. Opt. Soc. Am., 53, 1394 (1963)
5. J. B. Heaney, AIAA Thermophysics Symposium, San Francisco, June 1969
6. P. H. Berning, G. Hass, and R. P. Madden, J. Opt. Soc. Am., 50, 586 (1960)
7. L. R. Canfield, G. Hass, and J. E. Waylonis, Appl. Opt., 5, 45 (1966)

APPENDIX I

BENCH CHECKOUT EQUIPMENT

APPENDIX I

BENCH CHECKOUT EQUIPMENT

The bench checkout equipment (BCOE) was designed to simulate spacecraft power and command subsystems and to record data from the reflectometer during testing (see Fig. 53). The BCOE is sufficiently adaptable to be used for early phases of instrument system-level developmental tests as well as all qualification and acceptance tests.

The BCOE consists of a Sanborn recording system model 958-5480A, control and display panel, a data patch panel, and power supplies (see Fig. 54). Signals are carried between the reflectometer and the BCOE by means of a single multiconductor cable. Data from the reflectometer is segregated at the data patch panel into telemetry A signals or telemetry B signals by means of a five-deck, two-position, six-pole rotary switch. Commands and power are transmitted to the reflectometer through a multiple-deck, two-position, single-pole rotary switch located on the control and display panel. Command subsystems A and B and spacecraft power are simulated through this switch. Simulated spacecraft power is provided by a -24V dc power supply.

The control and display panel contains manual switching circuits which simulate the function of the spacecraft power and command subsystems and a decoder which displays the scanner arm position. Pushbutton switches are provided to apply power (-24V dc bus) to the reflectometer, turn the motor on or off, turn the lamp on or off, select lamp A or B, and change gain on the lead sulfide and silicon detector channels. A "command enable" pushbutton switch is provided as protection against transmitting a command by accident. As mentioned previously

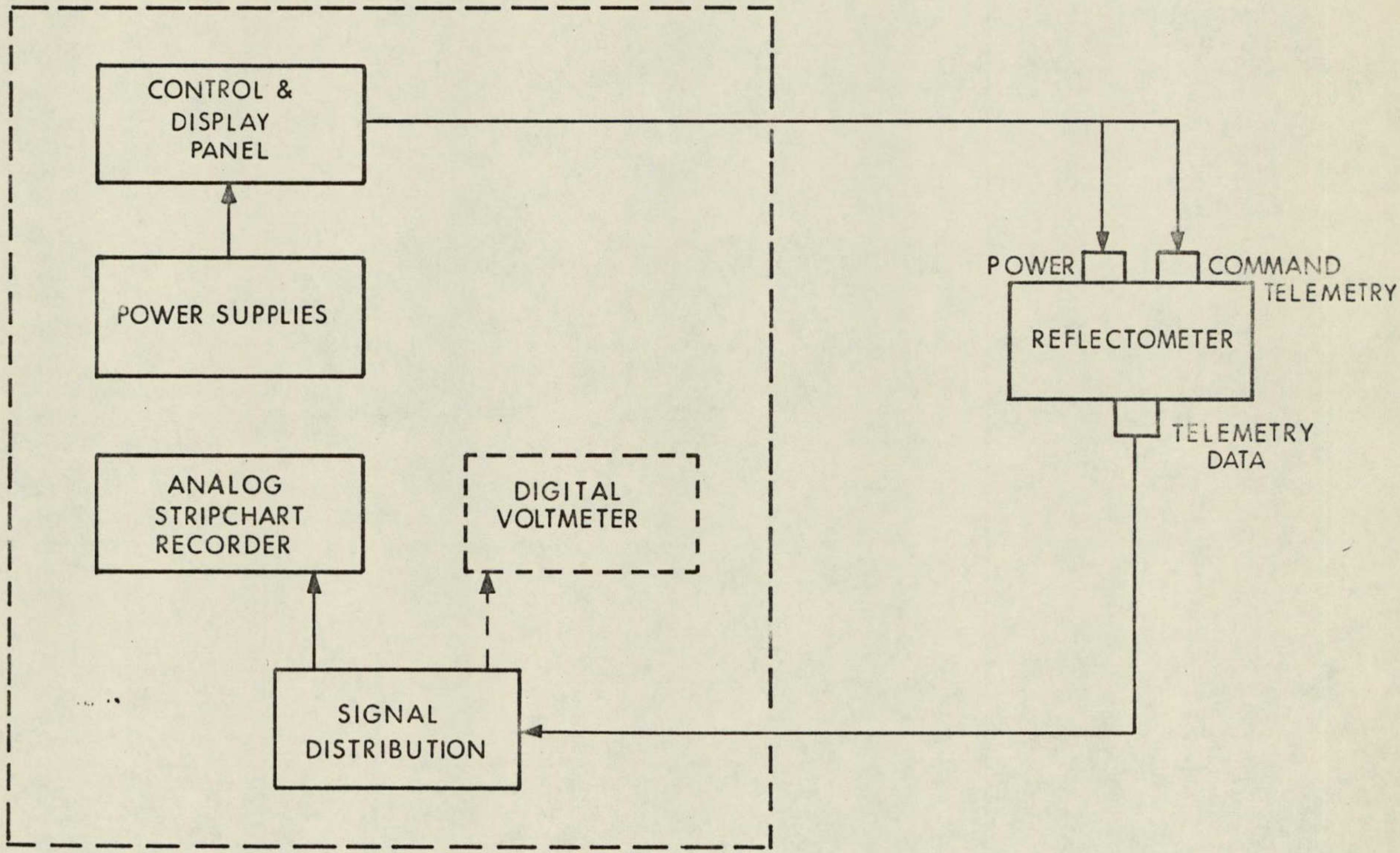

Figure 53. Bench Checkout Equipment Block Diagram

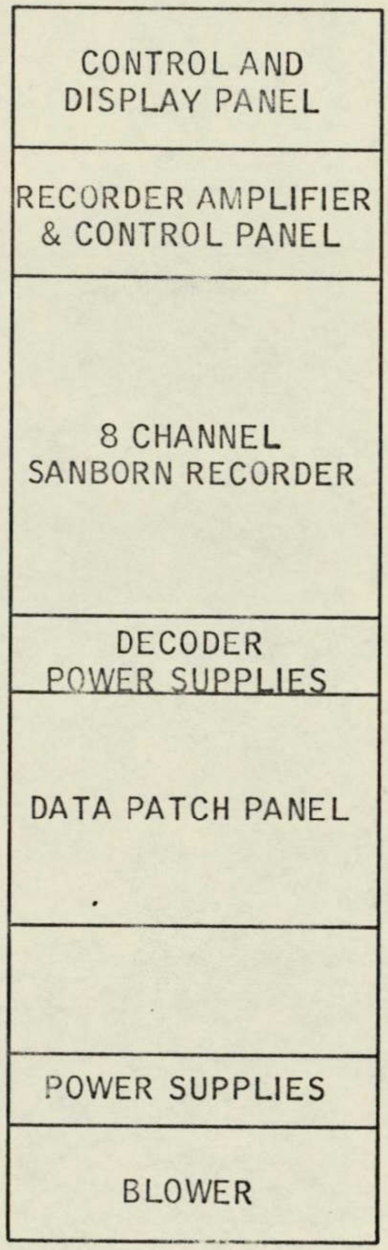

Figure 54. Bench Checkout Equipment

73628783

a rotary switch is supplied to allow A or B command subsystem simulation. Commands from the control panel are directed to the reflectometer through the same interface connectors which are used when the instrument is in the spacecraft.

The scanner arm position indicator is divided into three readouts as shown in Fig. 55.

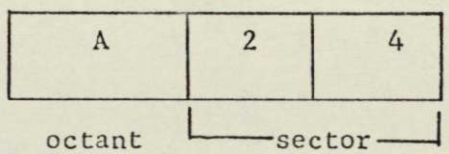

A = (first) octant

2 = (second) one-quarter of octant

4 = (fourth) one-eighth of quarter of octant

Figure 55. Scanner Arm Position Readout

The circle traveled by the arm is first divided into octants; the octants are divided into four sections, and the four sections of each octant are divided into eight sections. Therefore, 256 positions of the arm may be individually identified.

A special-purpose electronic decoder translates the Gray code output of the shaft position encoder into a useable readout signal for visual display. The encoder output can also be recorded on the strip chart recorder and monitored at the data patch panel.

All signals necessary for experimental data and instrument verification are to be telemetered. Therefore, the complete array of telemetry signals is fed to the BCOE through the normal telemetry interface connectors. A data patch panel is provided for switching or patching signals either to the stripchart recorder or to test terminals in the BCOE for use with auxiliary test equipment (e.g., oscilloscope, frequency counter, etc.). The A/B telemetry switch is used to select telemetry A or B output signals. A row of eight 24-position, single-pole switches is utilized to place any combination of eight signals simultaneously on the eight-channel recorder. Since there are more than 24 data signals, two decks were used on the 24-position switches. A row of eight 2-position, single-pole switches is used to select the deck to be displayed on the Sanborn recorder or to be made accessible to external monitoring.

A commutator is located on the data patch panel to provide automatic sampling of selected data signals. The commutator will read out the following signals on the selected recorder channel (in the order listed relative to each other):

a. Detector temperature primary
b. High voltage analog No. 1
c. Lamp voltage
d. High voltage analog No. 2
e. 0V dc
f. -2.5V dc
g. -5.0V dc
h. 0V dc
i. Detector temperature secondary
j. Bias voltage No. 2
k. Bias voltage No. 1
l. Detector bias voltage

The 0, -2.5, and -5.0V dc signals are reference signals provided by a voltage divider in the BCOE. The commutator speed may be varied by adjusting a potentiometer which is accessible at the front of the data patch panel. The reference voltages may be adjusted by turning a potentiometer which is accessible from the rear of the panel.

The data signals and switch positions required to display the data signals externally or on the strip chart are shown in Table 6. The telemetry switch used to select A or B telemetry signals is not listed in the table. All data signals are transferred through the telemetry switch prior to reaching the switches listed in Table 6.

There are four power supplies provided in the BCOE. One is a Sorenson QRC40-8A (0 to 40V dc, 0 to 8 amps) power supply used to supply the required -24V dc power to the reflectometer. The other three power supplies provide the voltages needed for proper operation of the decoder. These consist of one Sorenson QSA 12-2.1 (8 to 14V dc, 2.1 amps) and two Sorenson QSA 10-1.4 (0 to 10V dc, 1.4 amps) power supplies. The decoder requires -12V dc, -6V dc, and +6V dc voltages to convert digital Gray code encoder data into an alpha-numeric readout.

The BCOE was used to check out the reflectometer while in the lab and to calibrate reflectivity readings and other voltages. It was also used to operate the reflectometer and record data during environmental testing (qualification and acceptance tests).

TABLE 6

DATA PATCH PANEL SWITCH POSITIONS AND FUNCTIONS

Switch Position First Row	Switch Position Second Row	Function
A	1	Broadband reflectivity
↑	2	Spectral reflectivity (0.3 - 0.65μ)
	3	Spectral reflectivity (0.65 - 1.2μ)
	4	Spectral reflectivity (1.2 - 3.0μ)
	5	Spectral reflectivity (0.3 - 0.4μ)
	6	Detector temperature secondary
	7	Amplifier range
	8	Case temperature
	9	Space wire
	10	Detector temperature primary
	11	High voltage analog No. 1
	12	Detector bias voltage
	13	Bias voltage No. 1
	14	Bias voltage No. 2
	15	Internal pressure
	16	Lamp voltage
	17	High voltage analog No. 2
	18	T/M return A (B)
	19	Commutator output
	20	No wire
	21	No wire
↓	22	No wire
A	23	No wire

TABLE 6

DATA PATCH PANEL SWITCH POSITIONS AND FUNCTIONS (contd)

Switch Position First Row	Switch Position Second Row	Function
B	1	Encoder output E0
↑	2	Encoder output E1
	3	Encoder output E2
	4	Encoder output E3
	5	Encoder output E4
	6	Encoder output E5
	7	Encoder output E6
	8	Encoder output E7
	9	Home switch
	10	T/M Return A (B)
	11	Spare wire
	12	Spare wire
	13	Scanner octant position
	14	No wire
	15	No wire
	16	No wire
	17	No wire
	18	No wire
	19	No wire
	20	No wire
	21	No wire
↓	22	No wire
B	23	No wire

APPENDIX II

EOS REPORT 7003-TP-28-Rev. A

Flight Operational Test Procedure for the

REFLECTOMETER EXPERIMENT FOR APPLICATIONS TECHNOLOGY SATELLITE

Prepared for
National Aeronautics and Space Administration
Goddard Space Flight Center
Greenbelt, Maryland

EOS Report 7003-TP-28-Rev. A 29 September 1967

Prepared by

J Holloway

J. D. Holloway
Program Manager

Approved By

Duane D Erway

D. D. Erway, Manager
Optical Systems Division

ELECTRO-OPTICAL SYSTEMS, INC.
A XEROX COMPANY

FLIGHT OPERATION TEST PROCEDURE

1. GENERAL

The purpose of this test procedure is to outline the functional steps required to operate the reflectometer under orbital conditions.

The following procedures presume that the necessary spacecraft subsystems and ground support equipment are operating as required and available for use. Spacecraft system operational procedures and ground support and data systems functional specifications are considered beyond the scope of this document.

2. APPLICABLE DOCUMENTS

Unless otherwise specified herein notation as to spacecraft telemetry and command channel assignments refers to the following ATS program documents:

S2-0142-3	ATS-C (S/S_2) Spacecraft and Telemetry Measurements List (Rev. B, 8-17-66)
S2-0143-3	Spacecraft ATS-C (S/S_2) Command Assignment Specification (Rev. A, 7-27-66)

3. DATA ACQUISITION, RECORDING AND DISPLAY REQUIREMENTS

Unless otherwise specified herein the following data acquisition, recording and display functions shall be provided by NASA/GSFC or its designee:

a. Magnetic Tape Record — The telemetry channels listed in Table 7 shall be permanently recorded on magnetic tape. This data shall be made available in appropriate form and format to EOS for subsequent analysis.

b. Strip Chart Record — The telemetry channels listed in Table 8 shall be recorded in real-time at the spacecraft ground control station. These channels shall be recorded in analog format. This recording shall be employed as a real-time data monitor for "quick-look" evaluation of system performance and verifications of correct reflectometer scale factor setting.

c. <u>Ground Computer Class II Message</u> — The telemetry channels listed in Table 9 shall be evaluated by the NASA/GSFC computer facility and a Class II message generated regarding the status of the listed channels. Where required EOS will apply calibration data for temperature and pressure measurements to permit readout in appropriate engineering units.

4. TEST PROCEDURE

The following is the "Normal" mode of operation. For alternate procedures entailing non-normal scale-factors or other contingencies see Fig. 56.

a. Monitor and record the value of telemetered spacecraft power subsystem electrical load current and reflectometer Scanner/Home Switch Position (Channel L-7 and L-8. Ref: S2-0142-3).

b. Execute the following command:

   202 Regulator ON (Applies power to reflectometer.)

c. Monitor and record the value of telemetered spacecraft power subsystem electrical load current. The change in current between Step a. and Step c. shall be 450 mA ±100 mA.

d. Execute the following command:

   344 Scale Factor Select (Switches system gain to 5X range.)

e. Execute the following command:

   344 Scale Factor Select (Switches system gain to 25X range.)

NOTE

> The elapsed time between the execution of Step b. and Step e. should be minimized. However, the elapsed time between the execution of Step b. and Step f. should be not less than 90 seconds.

f. Execute the following command:

   261 Lamp ON/OFF (Applies power to the selected lamp)

g. Execute the following command:

   050 Motor ON/OFF (Applies power to the drive motor.)

NOTE

The elapsed time between the execution of Step f. and Step g. shall be an absolute minimum in order to enhance the useful life of the limited-duty lamps

h. Monitor the reflectivity data channels being displayed on the strip-chart recorder. Satisfactory operation of the reflectometer requires that each of the multirange channels operate wholly within the range 0 to -5.11 volts. If during the data acquisition cycle (approximately 8-minutes) any of these multirange channels exceeds this range, the cycle shall be repeated using a lower scale factor. Furthermore, if the maximum excursion of the three multirange channels, taken collectively, is less than -1 volt, the cycle shall be repeated using a higher scale factor. (For details see Section 5.0 Contingencies, below.)

   At the conclusion of one complete cycle of the reflectometer the scanner arm should automatically stop rotating and come to rest at its home position above the full-scale sample.

i. Execute the following command:

   327 Regulator OFF.

TABLE 7

MAGNETIC TAPE DATA

Channel	Title or Function	Item*
49	Broadband reflectivity	L2
50	Spectral reflectivity (0.3 - 0.65 micron)	L3
51	Spectral reflectivity (0.65 - 1.2 micron)	L4
52	Spectral reflectivity (1.2 - 3.0 micron)	L5
53	Spectral reflectivity (0.3 - 0.4 micron)	L6
14/2	Regulator ON/OFF	L1
17	Scanner position	L7-8
18	T/M Calibration reference	C27a
-	S/C Power system load current	-
62-32	Temperature detector (secondary)	L9
62-33	Amplifier range	L10
62-34	Temperature, case	L11
62-38	Bias voltage (-20V)	L14
62-40	Bias voltage (+15V)	L16
62-42	Bias voltage (-15V)	L17
62-43	Pressure, internal	L18
63-4	Temperature, detector (primary)	L13
63-5	High-voltage No. 1	L15
63-6	Lamp voltage	L19
63-14	High-voltage No. 2	L20

* Refers to "Item" column of S2-0142-3

Notes: 1) L12 not used
2) In addition to above data shall be included date, time, frame identification and other pertinent data as may be required or desirable.

0

TABLE 8

STRIP CHART DATA

Channel	Title or Function	Item*
49	Broadband reflectivity	L2
50	Spectral reflectivity (0.3 - 0.65 micron)	L3
51	Spectral reflectivity (0.65 - 1.2 micron)	L4
52	Spectral reflectivity (1.2 - 3.0 micron)	L5
53	Spectral reflectivity (0.3 - 0.4 micron)	L6

*Refers to "Item" column of S2-0142-3

TABLE 9

COMPUTER CLASS II MESSAGE DATA

Channel	Title or Function	Item*
62-32	Temperature, detector (secondary)	L9
62-34	Temperature, case	L11
63-4	Temperature, detector (primary)	L13
62-43	Pressure, internal	L18
63-5	High-voltage No. 1	L15
63-14	High-voltage No. 2	L20
63-6	Lamp voltage	L19
62-38	Bias voltage (-20V)	L14
62-40	Bias voltage (+15V)	L16
62-42	Bias voltage (-15V)	L17
62-33	Amplifier range	L10
18	T/M Calibration reference	C27a

* Refers to "Item" column of S2-0142-3

APPENDIX III

TECHNICAL DRAWING

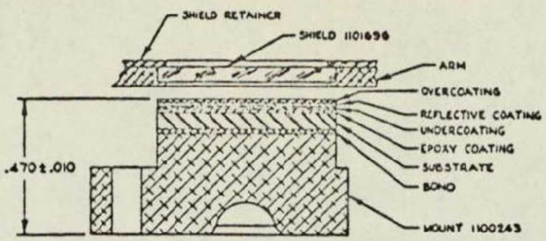

SECTION A-A
SAMPLE ASSEMBLY

NOTES:

1. In all coating operations, only the reflective surface shall be coated. All other areas of the mount shall be masked to prevent change in thermal properties. Masking shall be removed after final coating operation.

[illegible]

6. [illegible] 150°F. [illegible]

[illegible]

12. [illegible] Drawing Number 1100241, [illegible]

[illegible]

APPLICATION TECHNOLOGY SATELLITE REFLECTOMETER SAMPLE ARRANGEMENT										
SPECIMEN NO.	MOUNT DWG NO.	SUBSTRATE DWG NO.	SUBSTRATE PREPARATION	BOND		[illegible]	UNDERCOAT	REFLECTIVE COATING	OVERCOATING	SHIELD
1	1100243	1101236		[illegible]	[illegible]					
2	1100243	1100242-5		[illegible]	[illegible]	[illegible]	[illegible]	[illegible]	[illegible]	[illegible]
3	1101695									[illegible]
4	1100243	1100242-5		[illegible]	[illegible]	[illegible]	[illegible]	[illegible]	[illegible]	
5		-5				[illegible]	[illegible]	[illegible]		
6		-1						[illegible]		
7		-5				[illegible]	[illegible]	[illegible]	[illegible]	
8		-5				[illegible]		[illegible]	[illegible]	
9		-5	[illegible]				[illegible]	[illegible]	[illegible]	[illegible]
10		-5				[illegible]		[illegible]	[illegible]	[illegible]
11		-5				[illegible]	[illegible]	[illegible]		[illegible]
12		-5				[illegible]	[illegible]	[illegible]	[illegible]	[illegible]
13		-5						[illegible]		[illegible]
14		-5						[illegible]		
15		-5	[illegible]				[illegible]	[illegible]	[illegible]	
16		1100242-1				[illegible]			[illegible]	
17		1101696-3				[illegible]			[illegible]	
18		1100242-1	[illegible]						[illegible]	
19		1100242-1	[illegible]						[illegible]	[illegible]
20	1100243	1101696-3		[illegible]	[illegible]	[illegible]	[illegible]	[illegible]	[illegible]	[illegible]

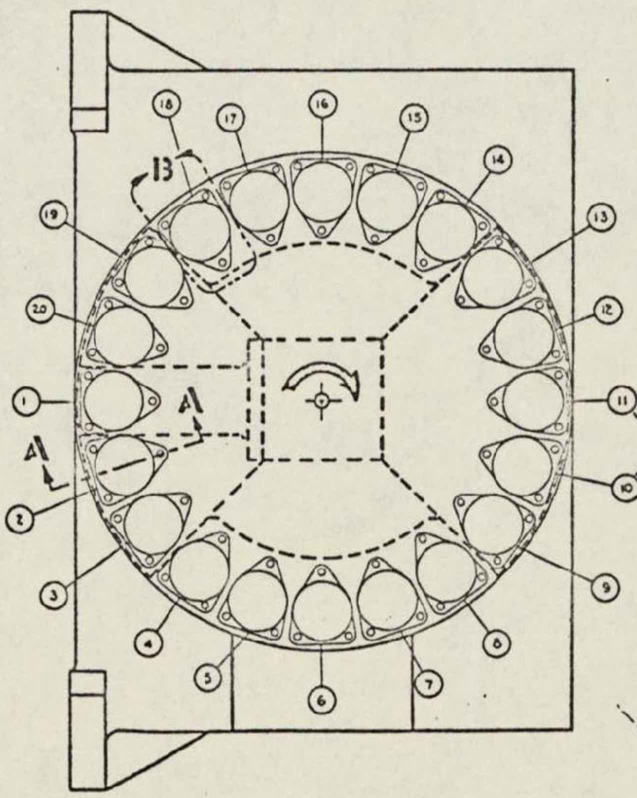

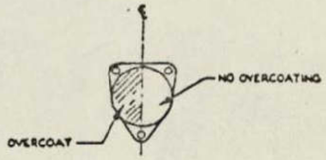

DETAIL B SPLIT OVERCOATING
(SPECIMENS 18 & 19 ONLY)

1100241 C

N/R			COATINGS		SEE NOTES & TABULATION BLOCK	
2		1101696-3	SUBSTRATE		FUSED SILICA	
8		1100242-5	SUBSTRATE		NICKEL, ELECTROFORMED	
2		1100242-3	SUBSTRATE		MAGNESIUM	
6		1100242-1	SUBSTRATE		ALUMINUM	
1		1101236	100% REFLECTOR		SEE APPLICABLE DWG	
1		1101698	0% ASSEMBLY		SEE APPLICABLE DWG	
19		1100243	MOUNT		SEE APPLICABLE DWG	

LIST OF MATERIALS

UNLESS OTHERWISE NOTED

ORIGINAL APPLICATION

ELECTRO-OPTICAL SYSTEMS, INC.

EXPERIMENT SAMPLE POSITIONING AND SAMPLE ASSEMBLY ARRANGEMENT-ATS REFLECTOMETER

UNCLASSIFIED | D | 1100241 | C

12705 | 7003 | NONE

NOT REPRODUCIBLE

III-1

ELECTRO-OPTICAL SYSTEMS

A XEROX COMPANY

PASADENA, CALIFORNIA 91107 · 213/351-2351